A Molecular Model for Cell Intercalation during Convergence and Extension: Interacting Cytoskeletal Elements and Myosin Regulation

Katherine Elizabeth Pfister
Falls Church, Virginia

Bachelor of Science with High Honors, University of Virginia, 2009

A Dissertation presented to the Graduate Faculty of the University of Virginia in Candidacy for the Degree of Doctor of Philosophy

Department of Cell Biology

University of Virginia
August, 2016

Table of Contents:

Abstract:

My doctoral research investigates the organization, behavior, force production, and regulation of the contractile actomyosin cytoskeleton and the dynamic adhesions underlying cell intercalation in the African clawed frog, *Xenopus laevis*. Cell intercalation is the process by which the cells of a tissue actively wedge themselves between one another (intercalate) along a specific dimension to produce a narrower, longer tissue, a process often called "convergence (narrowing) and extension (lengthening)" or CE.

CE in *Xenopus* occurs through progressive expression of Mediolateral Intercalation Behavior (MIB), a cycle of several iterated cell behaviors that drive the intercalation of the presumptive mesodermal cells on the dorsal lip of the blastopore. I examined the mechanism of MIB from the perspective of both the contractile cytoskeleton and dynamic cell adhesions. I have approached the question of the interaction and function of contractile actomyosin and cell adhesions by testing mechanisms of myosin regulation, tropomyosin activity, actin compartmentalization, and cadherin turnover based adhesions.

There is a role for a contractile actin cytoskeleton in both epithelial cell (Blankenship et al, 2006; Lavayer and Lecuit, 2012), and mesodermal cell rearrangement (Skoglund et al., 2008; Rolo et al., 2009; Kim et al, 2010). Myosin II function in the "node and cable" cytoskeletal network (NCN) in *Xenopus* mesodermal cells is critical for CE of both mesodermal and neural tissue (Skoglund et al, 2008). In Chapter 2 of this dissertation, I show that regulation of myosin contractility through phosphorylation of Serine-19 on the Myosin Regulatory Light Chain (MRLC) is necessary for organization of the NCN, for cell bipolarity and for cell intercalation. Additionally, cell intercalation is dependent on cadherin cell adhesions and I present a working model of how tension generated by myosin contractility is transmitted through cadherin plaques on the mediolateral surfaces of mesodermal cells to generate tissue-scale tension in this axis. Removing regulation of intracellular C-Cadherin through expression of a constitutively active C-Cadherin resulted in rearrangements of the actin cytoskeleton and failure of CE.

I present evidence that a nonmuscle isoform of the actin-binding protein Tropomyosin (XTm5) is present and necessary for the NCN. Tm5 has been shown to enhance myosin association and activity with the cytoskeleton in mammalian cells (Bryce et al, 2003). Consistent with this hypothesis, Morpholino-knockdown of XTm5 results in loss of the NCN and in CE defects. I posit that XTm5 plays a critical role in the endogenous myosin-actin interaction during MIB in *Xenopus*.

Using Total Internal Reflection Fluorescence Microscopy (TIRFM) on the mesodermal cells exhibiting MIB, I show that there is an additional actin cytoskeleton between the plasma membrane and the NCN, that I term the TIRF-Imaged Cortical Actin Network (TCAN). The TCAN movement is significantly different than the NCN oscillations and the movement is regulated by actin polymerization and less so by myosin activity. I present possible functions for this cytoskeleton, including spatial regulation of membrane proteins.

In the first chapter, I will summarize the current state of knowledge about CE and cell intercalation, with focus on the pertinent topics relating to my work.

Dedication/Acknowledgements:

Graduate school is only half about what your experiments demonstrate; the other half is how people demonstrate their support for you. I'd primarily like to dedicate this dissertation to my two greatest Science teachers: my mentor, Dr. Raymond E Keller, and my father, Dr. Albert J Pfister. My dad first piqued my interest in science and never let me give up on my dream to succeed. His caring, attention, and wisdom has undoubtedly shaped all my future endeavors.

Ray Keller has been kind enough to take me in as his final graduate student and teach me some of all he knows. I aspire to his amazing memory of each major experiment, meeting, or conversation in his career and his invigorating excitement about new experiments! We've had amazingly formative conversations over the years about both the biophysical implications of a certain experiment and my ideas for a career in science. He has put in long hours of editing and movie watching at my behest and I have only just begun to feel the impact of these lessons and advice.

The final product of my dissertation could not have happened without the support and patience of my first reader, Dr. Dorothy Schafer. Dr. Schafer taught a class in my undergraduate career at UVA that first opened my eyes to the wonder of research, and the critical thinking involved in reading the primary literature. As a graduate student, she has gone above and beyond the call of duty as a first reader and I cannot thank her enough.

Two of the biggest interests of mine in doing this graduate work has been both the choreography of Xenopus development, and trying to image it. I have to send a big thank you to my mentor Ray for allowing me to pursue as many imaging opportunities as I could find, including visits to: Janelia Farms Research Campus, Cold Spring Harbor Laboratories, and the Marine Biological Laboratory at Wood's Hole. Additionally, Dr. Paul Skoglund was the postdoctoral researcher who first got me excited about imaging live cytoskeleton movements and the idea has stuck ever since. The Keck Center for Cellular Imaging at UVA has been a second lab-home to me. Dr. Ammassi Periasamy and the staff at the KCCI have been helping me image *Xenopus* embryos for far longer than any job description would dictate. The facilities and the education I received at the KCCI has increased my understanding of science and physics, and even gave me a nostalgic parallel in the lenses and filters I used in my previous theatre electrics jobs.

The support of my peers and most importantly my family was critical for my success in graduate school. I'd like to thank the patience, love, and endurance from my mother, my brothers, my sister and my partner as I learned clumsily how to describe what it is I actually do all day. My classmates and friends have been the lifeline I needed to not feel isolated in lab, and to sympathize, reminding me that my particular vexing problems are not unique.

I have learned much more than what you will read in these pages about actin and myosin, and it's my hope to bring this same level of education/advice/self-discovery to any students I'm lucky enough to teach.

Chapter 1: The Emergence of Cell Intercalation Mechanisms for Convergence and Extension

"The germ is a unit, in space and in time. What we are interested in is its formative activity, it's fascinating struggle in escaping from the sphericity or similar state imposed by banal physiocochemical conditions and in building up an organized embryo that will be soon capable of dominating its environment."[1]

[1] Dalcq, AM. Form and Causality in Early Development (1938) Cambridge University Press, Gr. Britain

I: Universality of Shape Change and Pattern Formation

Many natural processes result in pattern formation. Wind shapes sand dunes, trees and vines twist in helical shapes, and organisms grow and move according to heredity and adaptation. As embryologists, we take advantage of the rapid development and large cell size in embryos to study the patterns emerging from cell activity. We observe shape changes during embryo development (morphogenesis) and apply external perturbations to understand the mechanisms that have proved most advantageous through evolution. There are several approaches to experimentation: focus on the genetic code, biochemistry, the cellular protein levels, and the biomechanical forces generated and maintained. It has been my aim in the course of my doctoral research to use facets of genetics, biochemistry, and cell biology while maintaining a primary role as an observer of the "big picture" of embryo development to answer some of the big questions currently debated in the field. Following centuries of great embryo observers, my work adds a molecular component to the natural phenomena of morphogenesis and will hopefully raise questions for future researchers. In the words of my advisor's advisor J.P. Trinkaus, this work "will have succeeded if it accelerates its already burgeoning obsolescence".[2]

II: Cell Intercalation as a Mechanism for Tissue Shape Change

Historical observations of morphogenesis were facilitated by use of invertebrate and vertebrate organisms that develop externally. Frogs, fish, and tunicates have served

[2] Trinkaus, J.P. Cells into Organs. The Forces that Shape the Embryo. Prentice-Hall, Englewood Cliffs, N. J., 1969.

this role due to the ease of obtaining eggs and the rapidity of tissue development. Highly detailed visual descriptions of specific stages in the development of amphibians, fish, ascidians, and mammals are still referenced by current developmental biologists parsing out the mechanisms of embryo development (Keller, 2000). Though most of the historical narratives of embryogenesis included antiquated ideas, the suggestion of an active role for cells in morphogenesis was evoked by use of words like “wedged” or “pushed” in these narratives. In my studies as a modern developmental biologist I have addressed the same questions of how cells interact with the environment and how a tissue can generate measureable physical forces deforming the embryo.

Organism (whole embryo) morphogenic changes are a result of genetic regulation, protein expression, and cell movement. One necessary morphogenic movement in vertebrate development is Convergence and Extension (CE). CE is a term to describe any large scale shape change involving narrowing (convergence) in one axis and elongation (extension) in the perpendicular axis (Fig 1). CE encompasses several coordinated cell behaviors and is not exclusive to embryos. In many vertebrates, tissue elongation occurs with minimal contribution from cell divisions, cell death, or cell growth. Instead, cell

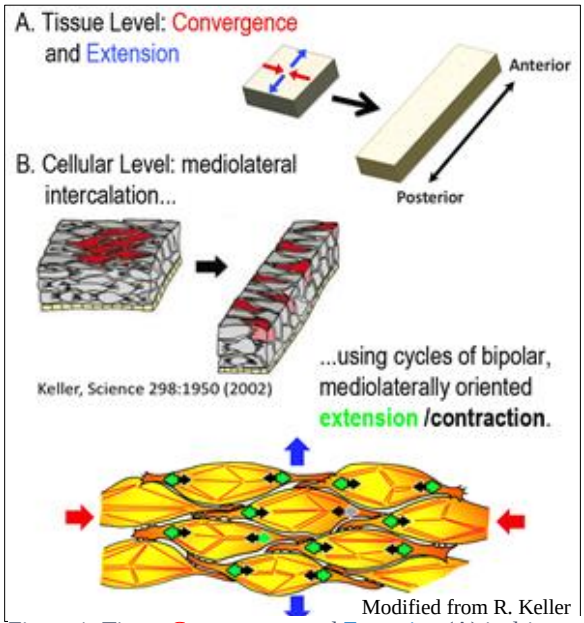

Figure 1: Tissue Convergence and Extension (A) is driven by Cellular Mediolateral Intercalation Behavior in the Frog (B). Intercalation of the mesodermal tissue in *Xenopus* requires active cytoskeletal rearrangements (orange) and cycles of protrusion extension and contraction.

intercalation is the driving force. In *Xenopus,* cells move between one another in the mediolateral axis, are constrained from thickening by neighboring tissues (Keller, 2002) , and as a result are displaced in the anterior-posterior axis. Despite differences in tissue type and cell size, the mechanism of axial elongation by intercalation is conserved in multiple invertebrate and vertebrate phyla. I will describe different mechanisms of intercalation: Mediolateral Intercalation Behavior (MIB), Junctional Remodeling, and Basolateral Protrusive Activity during CE in several model organisms.

Mediolateral Intercalation Behavior:

Several variations of the general phenomenon of MIB evolved in different species and in different tissues of the same species. Here I will discuss the form of MIB found in the mesenchymal cells of Xenopus embryos.

MIB begins in the mesoderm at about St. 10.5 (approximately 11 hours post fertilization) and persists through St. 18. MIB begins with the formation of the vegetal alignment zone (VAZ) forms. The VAZ is a localized arc of expression of MIB that spans the anterior somitic/notochordal region and the dorsal

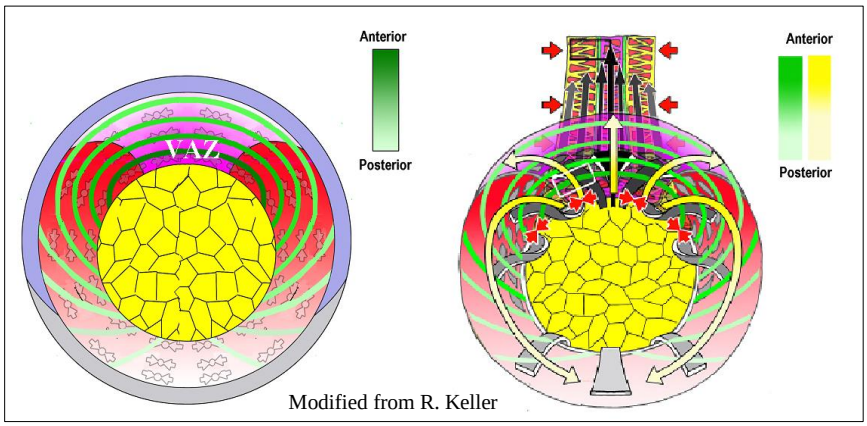

Figure 2: MIB in *Xenopus* embryos is first expressed in the Vegetal Alignment Zone, shown in the left figure. This creates hoops of tension around the blastopore as shown in green. MIB (yellow arrows) and involution (gray arrows) begins at the dorsal lip which will become the future anterior end of the embryo.

lip of the blastopore with its lateral ends anchored in the vegetal endoderm (Shih, Keller 1992b) (Figure 2). Initially unpolarized cells in the presumptive VAZ make lamellipodia that adhere to adjacent cells, and exert traction on the neighboring, "substrate" cells as the cell body contracts (Shih, Keller 1992b). These iterated cycles of extension, attachment of protrusions, and contraction of the cell body result in traction force that progressively elongates and aligns MIB-expressing cells, and actively pulls the cells between one another (intercalation), which produces a longer and narrower array (CE) (Shih and Keller, 1992a)

MIB of the mesodermal cells results in both CE of the tissue and blastopore closure while the overlying *Xenopus* neural plate undergoes parallel CE movements using a different mode of MIB. In the neural tissue, cells show medially biased protrusive activity and intercalate as they directionally migrate towards the neural midline (Fig 3). This type of MIB involves spatially different rates of movement of intercalating cells, medially to laterally. The program of directional intercalation is similar to the movement of the ventrolateral cells of the zebrafish mesoderm towards the dorsal area. The zebrafish cells then transition into the type of MIB shown in *Xenopus* mesoderm (Glickman et al, 2003; Solnica-Krezel et al, 2012; Elul and Keller, 2000).

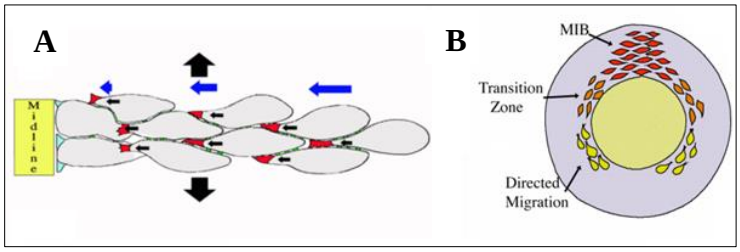

Figure 3: CE of *Xenopus* Neural (A) and Zebrafish Axial Tissue (B) occurs through a directed migration behavior similar to MIB. Modified from R Keller

Epithelial Cell Intercalation by Junctional Remodeling:

Epithelial tissues undergo cell intercalation while maintaining impermeable tight junctions. *Drosophila* morphogenesis involves elongation of the germband epithelial tissue by a type of cell intercalation that occurs through junctional rearrangements. The blastoderm of the embryo is patterned along the anterior-posterior axis by a toll-like receptor code (Pare et al, 2014) to which the germband cells respond by localizing myosin II and Rho to the anterior-posterior facing sides of the cells, and Par3 to the orthogonal surfaces (Simoes et al, 2010). The anterior/posterior boundaries undergo a myosin-driven contraction thereby bringing dorso-ventral cells into contact at an unstable four-cell junction, which is resolved by separation of anterior-posterior neighbors (Type I neighbor exchange, Fig 4) (Bertet, 2004). The contraction can also extend across several neighbor changes simultaneously (Rosette Type neighbor exchange, Fig 5) (Blankenship et al, 2006). Although myosin localization to anterior and posterior faces of the cells has been emphasized (Blankenship et al, 2006), its apparent localization there may be dynamic due to a uniform contraction of an actomyosin network of alternating strong and weak anchorages at the anterior and posterior boundaries of the cells. Cytoskeletal contraction results in alternate

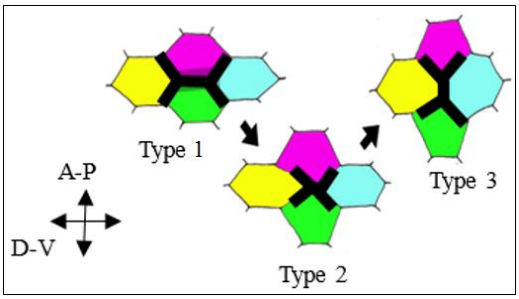

Figure 4: Epithelial Junctional Remodeling using the Type 1, 2, 3 Rearrangements, changing junctions marked in **bold** (modified from A Sutherland, R Keller)

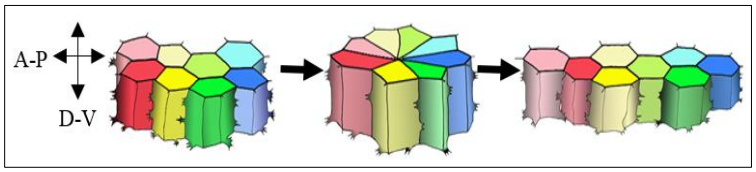

Figure 5: Epithelial Junctional Remodeling using the Rosette Rearrangements (modified from A. Sutherland, R. Keller)

sweeps of the network towards the anterior or posterior vertical cell boundaries, due to alternating increases of E-Cadherin endocytosis on the anterior and posterior faces and weakening one of the anchoring junctions relative to its neighbor (Levayer and Lecuit, 2012). Only the apical side of *Drosophila* germband cells have been examined so far, and thus we do not know if the deeper basal surfaces also contribute to CE.

Epithelial Cell Intercalation by Basolateral Protrusive Activity:

A third mechanism for intercalation involves biased basolateral protrusive activity of epithelial cells. CE in *C. elegans* (Williams-Masson, 1998), and more recently in mouse neural tube elongation (Yen 2009, Williams 2014), involve both polarized remodeling of the apical junctions, polarized protrusive activity, and cell traction. In *C. elegans*, protrusions extend and make adhesions predominantly in the axis of convergence, a process initiated by basal and progressively apical protrusion and junction remodeling (Fig 6A) (Williams et al 2014). In the mouse, both apical junctional remodeling and biased basal protrusive activity occur. This raises the question of how much each of these processes contribute to the intercalation of the cells. In fact, the number of times that

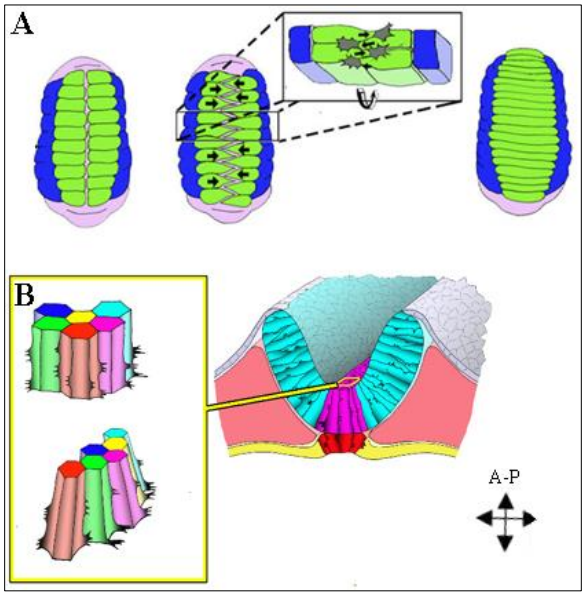

Figure 6: Basolateral protrusive activity in *C Elegans* (A) dorsal hypodermis and in mouse neural plate extension (B). Cells exhibit mediolaterally biased protrusions on the basal ends and resolve apically to elongate the tissue.
Modified from A. Sutherland, R. Keller

exchange of neighboring cells (intercalation) occurs at the apical end first and the number of times it occurs at the basal end first is about the same (Fig 6B; Williams et al, 2014). Here, as is in *Drosophila*, epithelial sheets retain a planar cell polarity as well as an apical-basal polarity. In addition to junctional rearrangement and biased basolateral protrusive activity, oriented cell division has been implicated in neurulation of several species, including the teleost fish (Gong et al, 2004), the chick (Wei et al, 2000; Firmino et al, 2016), and the mouse (Sulik et al, 1994). This suggests that in higher vertebrate organisms there are many cellular modalities for CE, which is evidence of plasticity and redundancies in cell intercalation mechanisms. The specifics of the cellular movements vary, but the overall tissue change is similar. One highly conserved aspect of intercalation is the fact that the global signaling systems that regulate the orientation of cell intercalation act perpendicular to the axis of cell intercalation and parallel to the axis of extension despite the fact that the molecular aspects of these signaling systems vary (Keller, 2006). The examples provided in this section do not represent an all-encompassing list of every type of intercalation during tissue CE.

III: Molecular Components of Cell Movement

Here I discuss the role of the actin cytoskeleton networks of individual cells and the inter-cell connections that enable coordinated movement.

The Actin Cytoskeleton is Associated with Force Production:

There are several filamentous components of the cytoskeleton, including but not limited to microtubules, intermediate filaments, and actin microfilaments. Perturbations of microtubules (Lane and Keller, 1997) and intermediate filaments (Weber et al, 2012) have not yet shown as pronounced effects on CE in *Xenopus* mesodermal cell intercalation as interdictions in the actin cytoskeleton (Lane and Keller, 1997; Weber et al, 2012). A normal MIB-expressing cell consists of two major domains of actin: contractile bundled filaments in stress-fiber-like structures and dynamic branched and cross-linked filaments of lamellipodial protrusions. The bipolar shape of the intercalating cell is defined by restriction of lamellipodial protrusions to the medial and lateral sides of the elongated cell, with the larger arcs of bundled actin microfilaments restricting protrusive activity on the anterior and posterior surfaces of the cell (Katsumi et al, 2002; Kolega, 1986). Understanding the regulation of movement and organization of these intracellular actin compartments can link the known behavior of the cells during MIB to the force produced by the tissue in CE.

Cell movements require changes in cytoskeletal structure to deform the cell from one state to another. Quantification of actin-mediated contractive forces with Traction Force Microscopy (TFM) links cytoskeletal organization to force production. For example, TFM of uni-directional migration defines a lamellipodial leading edge with both a protrusive pushing force as the cell membrane is stretched away from the cell body, and traction forces as the protrusion adheres to the substrate (Vincente-Manzanares et al, 2007; Danuser et al, 2006; Harris et al, 1980; Hind et al, 2015). The retrograde flow

of actin in protrusions towards the proximal lamellar region strengthens the adhesion and traction force, seen as a displacement of the flexible substrate. Lamellar actin is bundled in arcs and has a high association with myosin motors. The increased contractile ability of actomyosin matures adhesions into larger plaques, creating a trailing edge, which establishes a threshold of force necessary to de-adhere the trailing edge from the substrate, promoting forward movement (Vicente-Manzanares et al, 2007). In the case of *Xenopus* intercalating cells, they are bipolar, and there are lamellipodial "leading edges" on both the medial and lateral faces of the cell, and the cells adhere to both a substrate (extracellular matrix) and to each other at both ends. This level of complexity presents a challenge to our understanding of how actin organization is related to cell movements *in vivo.* Based on my observations of these actin networks, and on my observations of the dynamics of cell-cell adhesions I present a working model for the cytoskeletal rearrangements during CE that generate force in both *ex vivo* preps of tissue and in the whole embryo.

Non-Muscle Myosin is required during CE:

The motility of MIB-expressing cells in *Xenopus* involves, to a first approximation, a double-ended lamellipodial "migration" which results in bipolar traction and thus intercalation. Deep mesodermal cells are initially round, displaying unpolarized protrusions. Over the course of several hours, the cells change shape by re-organization of actin filaments. MIB-expressing cells limit protrusive activity to the medial and lateral ends. Tensile and stiff actin arcs form along the anterior-posterior surfaces between the

two traction-generating ends, a tension which represses protrusive activity along these surfaces, much as in fibroblasts *in vitro* (Kolega, 1986; Parsons et al, 2010). This change in local actin behavior in each cell generates the traction forces produced and thereby the intercalation of the cells.

With this model in mind, it is useful to consider mechanisms for how cell movements in a tissue are integrated to autonomously generate force outside the context of the whole organism. The force produced by the tissue can and has been measured, but it has not been possible to directly measure those produced by single cells. Studies of the cell-level regulation of contractile force has focused on the non-muscle myosin II family, which is expressed during CE. Although the myosin IIA isoform has major functions early in *Xenopus*, these have not been characterized in detail. Myosin IIB is upregulated during gastrulation, specifically in tissues undergoing CE (Bhatia-Dey et al, 1998) and it is critical for CE in both neural and mesodermal tissue in *Xenopus* (Skoglund et al, 2008; Rolo et al, 2009). These studies included time-lapse imaging of cells in the *ex vivo* prep of converging and extending tissues, which produce CE similar to that seen *in vivo* (Keller et al, 1989; Shih and Keller, 1992a, b; Elul and Keller, 2000). Live fluorescence microscopy of the actomyosin cytoskeleton in mesodermal cells show the dependence of the cortical "node and cable" cytoskeletal structure and movement on total myosin IIB levels. Also, Morpholino knockdown of myosin IIB results in dose-dependent failure of CE and blastopore closure, as well as loss of adhesion (Skoglund et al, 2008). I have extended these investigations with studies of myosin regulatory light chain (MRLC),

which document changes in cytoskeletal functions after MRLC reduction and correlate these changes to differences in the magnitude of tissue forces.

Phosphorylation of Myosin Regulatory Light Chain Regulates Contractility

Myosin II regulates the organization and behavior of the cytoskeleton in two ways: through its contractility and its cross-linking function (Ostrow et al, 1994). I examined the role of myosin contractility on the cytoskeleton separate from its role in crosslinking actin by focusing on the myosin regulatory light chain (MRLC), a component of the myosin II complex. Normally, ATP association with the myosin head domain induces a conformational change to promote actin binding. As ATP is hydrolyzed, another conformational change occurs exposing MRLC. The dissociation of the resulting ADP causes the "power stroke" in which the myosin contracts into the rigor state.

MII has multiple phosphorylation sites on both the heavy chain and light chains that promote or prevent contractile activity, but the strength of contraction of myosin bundles is attributed to the phosphorylation state of MRLC. The Serine 19 residue on MRLC is the major activating residue for myosin contractility (Somlyo et al, 2003), but an additional phosphorylation on the Threonine 18 residue stabilizes contractile bundles, like those seen in stress fibers (Mizutani et al, 2006). From my experiments with a single phosphonull mutation on S19 of MRLC, I show that Myosin II can still assemble and function in cytokinesis in the absence of a phosphorylatable MRLC, but force production during the power stroke is significantly decreased (Pfister 2016). Multiple kinases are

capable of phosphorylating MRLC S-19 including but not limited to Rho Kinase, Myosin Light Chain Kinase, Citron Kinase, and Rac/Pak Kinase (Bresnick, 1999; Yamashiro et al, 2003). The dephosphorylation of MRLC has consistently been attributed to the activity of Myosin Phosphatase (MP) (Ito et al, 1998). In chapter 2 I present the data showing the significant decrease in tissue force during CE when a phosphonull MRLC is expressed, and in these cells the actin cytoskeleton does not form the bipolar node and cable array.

Tropomyosins are Regulators of Myosin Contractility and Cell Behavior:

The progressive development of MIB in *Xenopus* embryos, described above, requires spatial and temporal regulation of cell behaviors that undoubtedly involve cytoskeletal regulators other than myosin II, and one category of known regulators of the actin cytoskeleton is the tropomyosin family.

The separation of distinct pools of actin in the cell is maintained by the localization and behavior of actin binding proteins. The branched actin organization of lamellipodial actin is initiated and maintained by association with the Arp 2/3 complex (Welch et al, 1997). Conversely, formin proteins promote nucleation of linear bundles of actin. The structure of actin can be rapidly remodeled by the activities of capping proteins, depolymerizing factors, or myosin (Blanchoin et al, 2000). The transition of lamellipodial actin to lamellar actin is defined by increased association of myosin, which is promoted by local expression of a tropomyosin isoform (Gupton et al, 2005). Mammalian tropomyosin 3 associates with treadmilling actin bundles and Tm3

association with actin promotes actin depolymerization and rapid turnover and sustained lamellipodial behavior. Conversely, Tm5 association with actin filaments prevents Actin Depolymerizing Factor (ADF) binding thereby promoting MII associating with actin filaments. In this way, tropomyosins have been described as the "divining rods for actin cytoskeletal function" (Gunning et al, 2005). Modulation of tropomyosin isoform expression changes the behavior of the actin cytoskeleton without affecting the level of motor protein. Interestingly, although fibroblasts can still migrate after tropomyosin depletion the traction forces are significantly different, demonstrating that tropomyosins influence force generation and transmission to the substrate (Waterman et al, 2005). Without distinct domains of protrusive behavior and contractile behavior, the morphogenic machinery lacks a level of regulation. I show that knockdown of the *Xenopus* equivalent of Tm5 prevents the formation of the node and cable network. This is a similar phenotype to the phosphonull MRLC, consistent with my hypothesis that the structure and formation of the node and cable network, in addition to Myosin contractility, is necessary for cell intercalation during CE.

IV: **Cell-Matrix Adhesions vs Cell-Cell Adhesions in CE:**

As mentioned earlier, cell intercalation requires coordinated cell movement, which means that actomyosin contractions within a cell must be transmitted across the tissue. The cells involved in *Xenopus* CE must exchange neighbors to intercalate, which implies dynamic adhesions must exist. However, the cells must also maintain sufficient tissue cohesion to maintain the mechanical properties of compressive forces (Moore et al,

1995) and tensile stiffness (Shook et al, unpublished data) required to generate the tissue-scale forces underlying the shape changes of CE (Keller et al, 2000). To address this paradox, studies have focused on integrin-mediated cell affinity for extracellular matrix and intercellular junctions formed by cadherin homodimers.

Signaling and Mechanical Roles for FN-integrin interactions during CE

In *Xenopus* CE, mesodermal cells appear to make adhesions with and crawl on their neighbors to intercalate (see Keller et al, 1989; Keller, 2000), but they are also surrounded by extracellular matrix and therefore could also crawl on this matrix. The extracellular matrix molecule fibronectin (FN) and its receptor, Integrin α5β1, are essential for the bipolarization of the deep mesodermal cells during MIB and for their intercalation (Davidson et al 2006). As CE progresses, fibronectin is secreted by cells and assembled into a progressively denser mesh in a manner dependent on the cytoskeleton and FN-integrin activity (Marsden et al, 2006; Davidson et al, 2008). Inhibition of FN-integrin interactions by a function-blocking antibody results in increased, multipolar protrusive activity, suggesting that FN-integrin signaling is essential for suppression of protrusive activity at the anterior and posterior faces of the cell. Conversely, superactivation of integrins with manganese suppresses protrusive activity, but the cells maintain bipolarity and elongated shape (Marsden et al, 2006). The results of these studies suggest a signaling role for the FN-integrin interaction in polarization during MIB. However, the fact that adhesion to substrate-attached molecular fibronectin retards CE, and the observation that FN fibrils twitch in response to the protrusive activity

suggests that cells exert traction forces on the FN matrix as they intercalate (Davidson et al, 2004). Thus the FN fibrils could serve both a signaling and a mechanical role in CE.

To investigate the role of FN as a mechanical tether between cells, Rosario and others (Rosario et al, 2009) expressed a 70kD fragment of FN that contains the multimerization domain. Normally, mechanical stretch of FN fibrils exposes the multimerization domain, promoting fibrillogenesis, resulting in the dense mesh seen late in CE (Ohashi and Erickson, 2005; Davidson et al, 2008). Expression of the 70kD fragment provides a dominant-negative inhibitor of FN fibrillogenesis, while maintaining the molecular signaling role of FN. The absence of FN fibrils did not have a substantial effect on CE in these experiments, although the cells endogenous capacity to produce FN and dilute the effect of either the dominant-negative or a FN-specific Morpholino may underestimate the mechanical role of FN fibrils.

Cell on Cell Traction: the Role of C-Cadherin in MIB

The finding that integrin mediated traction on FN probably plays a lesser role in *Xenopus* MIB turns attention to cell-cell traction as the dominant model for cell intercalation. C-Cadherin is the major cadherin expressed in early *Xenopus* mesoderm (Gumbiner et al, 2005). While the level of C-Cadherin remains constant throughout gastrulation, its activity is down-regulated during CE (Zhong et al, 1999). In the cell-cell traction model (Keller et al, 2000), cells extend lamellipodia, make and strengthen adhesions, and then detach the adhesions to “get a new grip” on the neighboring cells. Therefore, C-Cadherin activity must be regulated in order to anchor a force-producing

contraction and then disengage it during each iteration of extension, adhesion, contraction and relaxation the cells undergo. The alternative model of how cell-on-cell adhesion could be involved in cell intercalation is the "cortical tractor" model (Jacobsen et al, 1986) in which the underlying actin cortex treadmills directionally, and carries with it the attached cell adhesion proteins (in this case C-Cadherin), thereby forming a directional tractor. This model could potentially work in *Xenopus* CE, however it assumes a bidirectional tractor in a single cell predicting incremental intercalations because the tractive forces would be zero once a cell has intercalated between two neighbors (see Figure 7). This pattern of intercalation cannot explain the group dynamics or promiscuous intercalation seen during direct observations of cell intercalation in *Xenopus* explants (Shih and Keller 1992b).

The cell-on-cell traction model proposed by Keller and others suggests that cells extend lamellipodial protrusions onto neighbors, form nascent adhesions which strengthen as the cell contracts, before disengaging and undergoing another round. This serves to continually wedge the cells together while maintaining a dynamic regulation of the activity of the "stiffening adhesion". While the original work did not provide a definitive candidate for the "stiffening adhesion", I propose this role is filled by C-Cadherin. I present evidence that C-Cadherin is dynamic during intercalation (Chapter 2) and show that adhesion dynamics are necessary for CE by expressing a C-Cadherin mutant that cannot detach from neighboring cells (Chapter 3a).

V: Advances in Live Imaging Cell Behaviors:

The presence of yolk in every cell of *Xenopus* embryos has historically inhibited live-imaging of developing embryos. By using explants and advances in the light microscopy and post-image processing fields, I have made significant advances in producing high resolution fluorescent images of live *Xenopus* cells during CE. The Laser Scanning Confocal Microscopes (LSCMs) used in my imaging studies have sensitive detectors that decrease the laser power needed for imaging fluorescently-tagged proteins. Thus I imaged explants for longer periods of time with less phototoxicity and fluorophore bleaching compared to older LSCM technology. I used Total Internal Reflection Fluorescence Microscopy (TIRFM) to detect novel cortical cytoskeletal structures in cells undergoing CE. Similarly, Lattice Light Sheet technology separates the illuminating and detecting objectives to increase resolution beyond the Rayleigh Criterion; this system allowed me to simultaneously image separate layers of cortical cytoskeleton. In Chapter 3 I discuss the shortcomings of traditional microscopy techniques for imaging developing *Xenopus* embryos and recommend integrated use of multiple systems to image embryonic dynamics in a near *in vivo* state.

Chapter 2: Molecular Model for Force Production and Transmission during Vertebrate Gastrulation

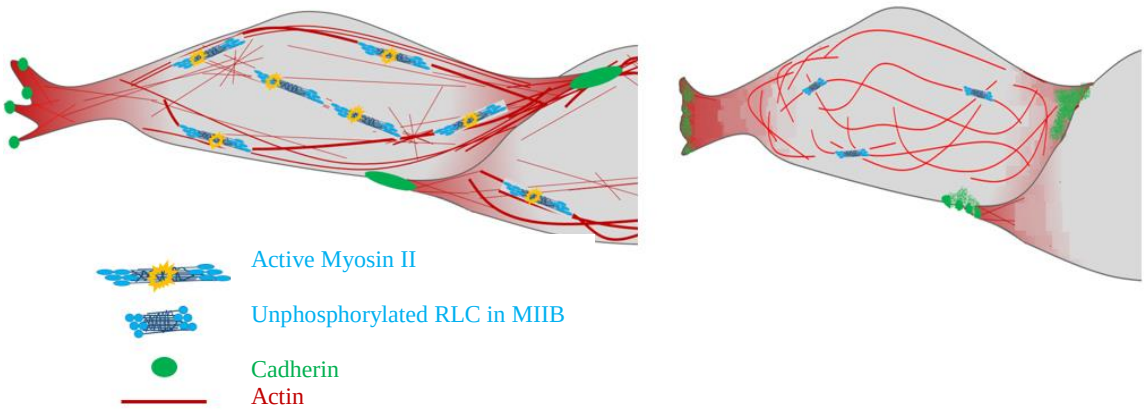

Figure Legend: Intercalating mesodermal cells in *Xenopus* laevis express Mediolateral Intercalation Behavior (MIB): lamellipodial protrusions are restricted to the mediolateral ends of the cell (left-right in the diagram above) causing an elongated shape in that axis. Cell intercalation requires active myosin II and the Node and Cable Network (NCN) of F-Actin. Myosin contractions on the NCN produce force that is transmitted throughout the tissue via C-Cadherin adhesions. When myosin II activity is reduced using a Myosin Regulatory Light Chain Morpholino (MRLC MO), the NCN fails to form, and large C-Cadherin adhesions do not form, instead clouds of smaller C-Cadherin puncta are seen on the mediolateral ends. Protrusive activity is unchanged in MRLC MO cells, but the cell shape is closer to round instead of the elongated shape of wild type cells.

This is a modified version of the published work Pfister et al. Molecular Model for Force Production and Transmission during Vertebrate Gastrulation (2016). Development: 143 (4): 715-727

ABSTRACT:

Vertebrate embryos undergo dramatic shape changes at gastrulation that require locally produced and anisotropically applied forces, yet how these forces are produced and transmitted across tissues remains unclear. We show that depletion of Myosin Regulatory Light Chain (RLC) levels in the embryo blocks force generation at gastrulation through two distinct mechanisms: destabilizing the Myosin II (MII) hexameric complex and inhibiting MII contractility. Molecular dissection of these two mechanisms demonstrates that normal convergence force generation requires MII contractility, and we identify a set of molecular phenotypes correlated with both this failure of convergence force generation in explants and of blastopore closure in whole embryos. These include reduced rates of actin movement, alterations in C-Cadherin dynamics and a reduction in the number of polarized lamellipodia on intercalating cells. By examining the spatial relationship between C-Cadherin and actomyosin we also find evidence for formation of transcellular linear arrays incorporating these proteins that could transmit mediolaterally-oriented tensional forces. These data combine to suggest a multistep model to explain how cell intercalation can occur against a force gradient to generate axial extension forces. First, polarized lamellipodia extend mediolaterally and make new C-Cadherin based contacts with neighboring mesodermal cell bodies. Second, lamellipodial flow of actin coalesces into a tension-bearing, MII-contractility dependent, node and cable actin network in the cell body cortex. And third, this actomyosin network contracts to generate mediolateral convergence forces in the context of these transcellular arrays.

INTRODUCTION:

Gastrulation and elongation of the body axis are key events in shaping vertebrate embryos, but the molecular basis for how the mechanical forces are produced, regulated, and propagated across the tissues undergoing this morphogenesis remains incompletely understood. In all vertebrates examined, including frogs (Keller et al., 2000; Keller et al., 1992), fish (Glickman et al., 2003; Solnica-Krezel and Sepich, 2012) and mice (Williams et al., 2014; Yen et al., 2009), the dorsal posterior mesodermal and neural anlage undergo convergence and extension (CE), a narrowing and lengthening of the tissue that occurs by cell intercalation. CE can operate in the context of both mesenchymal and epithelial tissues, and has also been described in developing invertebrate systems including several distinct regions of the *Drosophila* embryo (Keller, 2006).

In vertebrates, the major cellular process driving CE is Mediolateral Intercalation Behavior (MIB). Initially defined in *Xenopus* (Keller et al., 2000; Shih and Keller, 1992a; Shih and Keller, 1992b; Wilson and Keller, 1991), MIB-expressing cells become polarized, elongate along the mediolateral axis, and extend large lamelliform and filiform protrusions biased along the mediolateral axis. These protrusions attach to and apply tractional forces to neighboring cells as the cell shortens, pulling cells between one another in support of intercalation. As the cells wedge between one another they generate an extension force of between 0.6 and 5μN as measured in smaller dorsal tissue isolates or larger whole axial/paraxial explants, respectively (Moore, 1994; Moore et al., 1995; Zhou et al., 2015). The forces generated during *Xenopus* CE are tissue autonomous and internally generated (Keller and Danilchik, 1988). Unlike cells migrating in culture

that crawl on a stable substrate, intercalating mesodermal cells act both as force producers and as substrates upon which neighboring cells apply tractional forces. The tensile convergence forces pulling the cells together is thought to be generated by cortical actomyosin structures, either a “node and cable” cytoskeleton or its precursor; this network exhibits contractile oscillations coincident with cycles of cell elongation and shortening (Kim and Davidson, 2011; Rolo et al., 2009; Skoglund et al., 2008). Similar iterated contractile events are associated with a number of morphogenetic processes, including *Caenorhabditis elegans* oocyte polarization (Munro et al., 2004), and in *Drosophila* gastrulation (He et al., 2014; Martin et al., 2009), dorsal closure (Sawyer et al., 2009), germband extension (Fernandez-Gonzalez and Zallen, 2011; Rauzi et al., 2010; Sawyer et al., 2009) and oocyte elongation (He et al., 2010).

Investigations into the molecular basis for embryonic tensional force generation during CE have focused on non-muscle myosin II (MII). MII is a hexameric protein complex consisting of pairs of heavy chains (MIIHC), regulatory light chains (RLC) and essential light chains, with three different heavy chains providing MII isoform diversity (Wang et al., 2011). MII complexes exhibit two distinct activities: 1) crosslinking actin filaments to stabilize actomyosin structures and 2) regulated actin- and ATP-dependent contractile activity that slides actin filaments between one another, and that when attached to cellular structures exerts tension (Vicente-Manzanares et al., 2009). Depletion of MIIB in *Xenopus* results in defects in CE, blastopore closure, and development of the node and cable actomyosin structures (Rolo et al., 2009; Skoglund et al., 2008), while depleting MIIA does not alter CE (Buisson et al., 2014). In the *Xenopus* embryo, MII

contractility is likely the source of force production in tissues undergoing CE as indicated from: characterization of polarized actomyosin structures in these tissues, the presence of mediolateral but not anterior-posterior tension in intercalating cells, and small molecule inhibition of MII (Shindo and Wallingford, 2014; Zhou et al., 2009). However, how MII action generates convergence forces, what cellular structures or anchors in the cell are involved in this tension, and how these elements function in the context of a force-producing intercalation of cells is currently unknown.

During the process of tissue-level convergence, mediolateral tensile forces exerted by intercalating cells during MIB must be transmitted either from cell to cell or through an extracellular matrix (ECM) to form a large scale, tensile convergence machine stretching across the dorsal, axial mesodermal tissue. Cells exhibiting MIB are surrounded by ECM *in vivo*, and MIB is dependent on fibrillin (Skoglund and Keller, 2007), the PCP-dependent deposition of fibronectin at tissue interfaces (Goto et al., 2005), and signaling through the integrin α5β1 receptor (Davidson et al., 2006). Live imaging of fibronectin fibrils reveals remodeling by intercalating cell motility suggesting that fibronectin fibrils could be used as tractional "tethers" to transmit tensile force between intercalating cells (Davidson et al., 2004). However, blocking fibronectin fibrillogenesis while leaving the essential fibronectin/integrin signaling intact failed to retard CE (Rozario et al., 2009), suggesting that cell traction on fibronectin fibrils adds little to the force generated by MIB. An alternate idea is that cell intercalation occurs by cell-on-cell traction (Keller et al., 2000; Keller et al., 1992), and this traction could be mediated by calcium-dependent cadherin adhesion (Lee and Gumbiner, 1995). C-

Cadherin is the predominate cadherin in *Xenopus* tissues undergoing CE, and its activity has been shown to be modulated during both CE and mesendoderm migration (Bjerke et al., 2014; Brieher and Gumbiner, 1994; Schwartz and DeSimone, 2008; Zhong et al., 1999).

Here we examine the consequences of reducing MII contractile activity in the developing embryo. Direct measurements show that convergence force is reduced in explants of the marginal zone, and this reduction correlates with failure of blastopore closure in intact embryos. We examine the molecular phenotypes exhibited by intercalating cells experiencing reduced MII contractility, finding defects in both specific actomyosin structures and in the localization of membrane associated C-Cadherin that correlate with this reduction in force production. Observations of the normal dynamics of C-Cadherin and actomyosin in cells undergoing CE suggests the hypothesis that they function together to generate and transmit force across the intercalating tissue. These data combine to suggest a model for how actomyosin structures and dynamic cell-cell adhesions can collaborate to generate convergence forces during vertebrate gastrulation.

RESULTS:

Development of Cadherin Adhesions Coincides with Morphological Progression of Actin Structures

Mediolateral Intercalation Behavior (MIB) in *Xenopus* deep mesodermal cells is characterized by bipolar protrusive activity and progressive increase of length-to-width ratio with respect to the mediolateral axis. We examined the organization and relative

localization of actin and C-Cadherin during this process, distinguishing four distinct phases defined by the morphology and dynamics of both cortical actin networks and C-Cadherin adhesion structures.

Phase 1 is characterized by an isodiametric cell shape, and lamellipodia that are unpolarized with respect to the embryonic axis. C-Cadherin and cortical actin are evenly distributed with C-Cadherin as a circumferential signal on the cell membrane and actin as a basket around the periphery of the cell (Fig 1A, E, I). Cells enter Phase 2 when they break isodiametric symmetry, first occurring at developmental St. 10.5 by either exhibiting a single large lamellipodial protrusion or extending three or four filopodia in different directions, without respect to the embryonic axis (Fig 1B, F, J). After 20-30 minutes in Phase 2, the cells adopt the bipolar morphology characterizing Phase 3. Cells extend lamellipodia primarily in the medial and lateral directions as they begin to intercalate between neighboring cells. F-actin flowing rearward within lamellipodia coalesces into distal actin structures we call “proto-nodes” (arrowhead Fig.1C) (Fig. 1C, G, K), and linear clusters of C-Cadherin aligned parallel to the axis of protrusion that co-localize with actin in a similar pattern (20/25 phase 3 cells exhibit both) (Fig.1G, K (arrowheads)). Several hours later, at St. 12.5, cells begin to exhibit hallmarks of Phase 4. Transient proto-nodes stabilize into definitive nodes, and thick actin cables link the nodes throughout the cortex (21/ 23 cells) (Fig. 1D, H, L), and these stages are diagrammed (M). Actin cables appear organized as a linear array that spans two neighboring intercalating cells (Fig 1N).

To investigate the function of proto-node contractions (Fig 1O, O’), we examined

the hypothesis that proto-nodes and C-Cadherin in the membrane are a mechanical element linking the actin networks of neighboring cells. We quantified the relative mediolateral movement between the proto-nodes and C-Cadherin at the membrane under three conditions: 1) when one cell contracts locally and its neighbor undergoes a corresponding local relaxation; 2) when two adjacent cells each contract; and 3) when two adjacent cells each relax. We find that the C-Cadherin exhibits the fastest rate of displacement (Fig 1P), and spends the largest percent of time moving (Fig 1Q) when one cell locally contracts and its neighbor relaxes. This displacement occurs predominantly towards, rather than away from, a local contraction only when the neighboring cell relaxes (Fig1R) suggesting a mechanical cooperation between neighboring cells to drive cell intercalation and CE. An example with one cell contracting (arrowhead) and a paired relaxation (asterisks) is shown (Fig1S, S'), and a pair of cells exhibiting contractions (Fig.1T, T").

These results indicate that the location and appearance of both actomyosin structures and C-Cadherin dynamics are developmentally regulated during CE. Moreover, co-localization of C-Cadherin and actomyosin in nascent linear arrays suggests they may function together during MIB.

RLC Phosphorylation is required to Establish Notochordal Cell Polarity

In order to evaluate the role of myosin II contractility in the cellular transitions exhibited during MIB we depleted Myosin Regulatory Light Chain (RLC) from developing *Xenopus* embryos. Morpholino-mediated knockdown (MO) resulted in 50%

depletion of RLC protein as compared to either control Morpholino (COMO)-injected or uninjected embryos (Fig 2A). To determine if depleting RLC has functional consequences in the intact embryo, we examined the morphology of mosaically morphant axial cells coinjected with fluorescent dextran. We found that morphant mesodermal cells appeared disorganized and displayed irregular morphologies as compared to COMO injected cells (Fig 2B,B'), indicating that normal cell morphology depends on normal levels of endogenous RLC in intact embryos. Because this cell shape phenotype is similar to that observed in *Xenopus* notochordal cells morphant for MHC-IIB (Skoglund et al., 2008), we examined the levels of MHC-IIB in RLC morphant embryos. We found that MHC-IIB exhibited RLC Morpholino-dose dependent degradation to generate faster migrating MHC-IIB fragments when assayed by western blotting (arrowheads-Fig 2C). In order to rescue this effect, we expressed either a wild type RLC (wtRLC) or a phosphonull mutant of RLC (T18A; S19A) (pnRLC) in embryos, both tagged with mCherry (Fig 2D). Immunofluorescence of cultured axial explants revealed that ~ 50% of both MHC-IIB and RLC are depleted in RLC morphant explants, and that this effect could be rescued by expression of either wtRLC or pnRLC (Fig2E). This result was also confirmed in whole embryos by using western blotting, with either wtRLC or pnRLC expression restoring MHC-IIB levels in RLC-depleted morphant embryos (Fig 2F). RLC morphants also exhibit an increased average cell surface area in explants, similar to the whole embryo phenotypes in panel B, and this phenotype can be rescued by expression of either wtRLC or pnRLC (Fig 2G). While wtRLC or pnRLC expression rescues both MHCIIB levels in RLC morphants and cell surface area phenotypes, we conclude that

any differences between these two rescue phenotypes allow for direct examination of the role of RLC phosphorylation in the context of the MII complex during CE.

The average length-width ratio of control intercalating cells in late stage CE is ~3. Scatter-injected RLC morphant cells in the context of a wild type explant displayed an average aspect ratio of <2:1(Fig 2H). This cell shape phenotype was rescued by expressing wtRLC, but not pnRLC, indicating that full expression of cell shape polarization during MIB requires normal levels of phosphorylation of RLC on T18/S19 (Fig 2I).

RLC Phosphorylation is required to Generate Convergence Force in Explants and for Morphogenesis in Intact Embryos

To directly test the hypothesis that RLC phosphorylation is required to generate the forces that drive convergence and extension of dorsal mesoderm, we utilized a biomechanical measuring device termed the "Tractor Pull" (Fig3A). This device measures the cumulative tensional convergence forces developed by pairs of control or morphant marginal zone explants in a "giant sandwich" configuration (Poznanski and Keller, 1997). We found that explants derived from RLC morphant embryos converge with about 500 nN less force than control explants by the end of gastrulation (Fig3B). These tensile pulling forces can be rescued in explants made from RLC morphants rescued with wtRLC, but not by expression of pnRLC, demonstrating that normal convergence forces require the presence of an RLC that can be phosphorylated (Fig3C).

We next examined whether reduced force production in RLC morphant embryos

had any overt effect on embryo morphology by measuring embryo length. At control stage 30, RLC morphant embryos are about half the length of control uninjected sibling embryos, and 30% shorter than COMO injected siblings (Fig3D). This defect in axial (anterior-posterior) extension can be rescued by wtRLC expression but not pnRLC expression, indicating that axial length in the embryo correlates with the magnitude of tensional convergence forces generated in the dorsal axis during gastrulation. Moreover, both axial elongation and tensile convergence forces depend on phosphorylatable RLC. We also found that blastopore closure was delayed or blocked in RLC morphant embryos (Fig3E, F) and that this effect can also be rescued by expression of wtRLC but not pnRLC (Fig3G, H). We rule out the presence of neomorphic activity arising from expression of pnRLC that might result in failure to rescue morphogenesis because COMO injected embryos expressing pnRLC closed their blastopores similar to control embryos (Fig3H).

Actin Movement in Cell Body Nodes and Proto-nodes Depends on RLC Phosphorylation

The progressive maturation of the cortical actin cytoskeleton from isodiametric to a polarized and contractile node and cable system is inhibited in RLC depleted embryos. Although RLC morphant cells maintain a cross-linked actin network throughout this time, they displayed less than one node per cell, compared to control cells that display more than three nodes (Fig 4A, B). The number of dynamic nodes per cell is partially rescued by wtRLC expression but not by pnRLC expression (Fig4C, D, and E). Actin

nodes were previously shown to exhibit mediolaterally polarized movement (Fig4F) (Kim and Davidson, 2011; Skoglund et al., 2008), and we show here that this movement also depends on normal RLC levels (Fig 4G). Though the lifetime of nodes appears similar in morphant and control cells, the rate of mediolateral movement of nodes in RLC morphant cells was decreased and node movement was partially rescued by expression of wtRLC but not pnRLC (Fig4H).

We next analyzed the rate of actin flow in control or RLC morphant cells in these explants. A depiction of the kymograph measurements is shown in Figure 4I. We separated actin flow into two regions of the cell: the lamellipodial protrusions and the cell body cortex containing proto-nodes. Lamellipodial actin rates were measured transverse to rearward flow, while the radial proto-node condensation actin rates were averaged across two axes (red lines on Fig 4I). RLC depletion significantly decreased the rate of actin flow during condensation of proto-nodes, and expression of wtRLC, but not pnRLC, restored normal actin network flow rates (Fig4J). In contrast, RLC depletion did not affect the rate of lamellipodial F-actin flow (Fig 4K). However, the number of lamellipodia on these MIB expressing cells was significantly reduced upon RLC depletion, a phenotype that depends on phosphorylatable RLC (Fig4L).

Relationships between transcellular cable components

Double labeling of RLC and actin in intercalating cells showed them to be co-localized with each other, and analysis of their relative fluorescent intensities indicates that RLC is evenly distributed across the node and cable structure of this actomyosin

network (Fig 5A, B). In whole mount immunostaining for both myosin IIB heavy chain (MIIB) and phosphorylated RLC both MIIB and pnRLC localize to the cell cortex (Fig5C).RLC morphant explants exhibit both reduced MIIB and RLC-P staining ((Fig5D), which are both rescued by wtRLC expression (Fig5E) while only MIIB levels are rescued by pnRLC expression (Fig 5F).

C-Cadherin Protein Dynamics and Localization Depend on RLC Phosphorylation

Because we hypothesized that C-Cadherin likely serves as the intercellular adhesion protein supporting transcellular tension across the tissue we examined C-Cadherin dynamics in intercalating cells. Immunostaining experiments utilizing a C-Cadherin antibody in explants reveals that the intensity of C-Cadherin staining in puncta is reduced in RLC morphant explants at both St. 10(Fig5G,H), and at St.12(Fig5I,J). Live imaging of both red (tdTomato) and green (GFP) tagged C-Cadherin in neighboring cells in explants reveals that they co-localize at the cell membrane, consistent with a role for C-Cadherin in adhesion during gastrulation (Fig5K-L)(Lee and Gumbiner, 1995).

Polarized lamellipodia exhibit C-Cadherin that becomes dynamically associated with active actin extension and rearward flow (Fig 6A). We found more mature C-Cadherin adhesion plaques at the cell boundaries, specifically between linear actomyosin filaments in both cells (Fig 6B-asterisk). These adhesions move in concert with actin movements in both cells, and occasionally undergo rapid release and retraction at regions where cells contact one another suggesting they are under tension (Fig6D). We found 92 % ± 26 % incidence of these large C-Cadherin adhesion plaques per cell in one confocal

section, lasting an average of 220 ± 71.75 seconds (n = 23 cells). In contrast, C-Cadherin signal remained diffuse in lamellipodia of RLC morphant explants and did not often mature into clusters of cadherin plaques (Fig 6C). There was a 23 % ± 8% incidence per cell of these adhesions which were on average 70% smaller and lasted on average 18 ± 5.5 seconds (n = 61 cells). The dynamic behavior of C-Cadherin at presumptive sites of cell-cell contact differed in RLC morphants compared to that in COMO-treated and untreated cells, for example C-Cad signal remained diffuse in extending RLC morphant lamellipodia and did not mature into clusters of cadherin plaques (Fig 6C). Imaging of scattered morphant cells (blue cell) in a wild-type background showed that the depletion of RLC lead to a decreased interaction between morphant and non-morphant cells (Fig 6E). Wild-type cells extending lamellipodia onto a morphant neighbor failed to establish discrete C-Cad puncta, even while the C-Cad signal between that same cell and a neighboring wild-type cell increased. This reveals that RLC morphant cells are defective in both generating and supporting the generation of de novo C-Cad adhesions. A difference in C–Cad dynamics is also seen between control and pnRLC expressing morphant cells, but with a markedly different phenotype than that exhibited by RLC morphant cells (Fig 6F). These cells in explants exhibit their characteristic reduced length-width ratio, have established contact with one another with through stable C-Cad structures and exhibit very little protrusive activity or adhesion remodeling.

These data support the hypothesis that MII contractility-dependent remodeling of C-Cad dynamics is required for CE, and our observation of transcellular arrays of

actomyosin networks linked by plaques of C-Cad at the cell membranes suggests that such structures are responsible for the transmittal of tensile force across intercalating tissue.

Discussion:

Several lines of evidence indicate that trans-cellular molecular complexes produce, transmit and spatially remodel the tensional convergence forces required for *Xenopus* CE. First is the identification of mechanically linked complexes of actomyosin and C-Cadherin capable of generating and transmitting tension between cells and through intercalating tissue. These complexes appear to be under tension and mature as convergence forces rise. We propose these complexes act as dynamic but coherent tension-bearing elements that are required for convergence to be translated into extension during CE. Second, myosin contractility supports the assembly and functioning of these complexes, generates convergence forces in explants, and inhibits progress of two convergence –driven processes: blastopore closure and axial elongation in the intact embryo. These data indicate that force generated from MII contractility is required for CE. Third, C-Cadherin is in position to transmit mediolateral tension, and visualization of the complex by time-lapse microscopy suggest a cooperative role in transmitting tension. These data allow us to identify a molecular mechanism that promotes cell intercalation up a force gradient. In this mechanism, lamellipodia extending medially or laterally in the tissue form nascent C-Cad-based adhesions with neighboring cells. Analogous to focal adhesions, the nascent adhesions then mature and engage the cortical actin networks,

creating a continuous linkage between actomyosin networks in neighboring cells. Contractile activity then shortens the distance between mature adhesions and the midbody of the cell to power cell intercalation. This work reveals a molecular mechanism by which a combination of dynamic MII contractility and cell adhesion are transduced into extension forces by cell intercalation, as proposed previously at the cellular level (Keller et al., 2000; Keller et al., 1992).

RLC Molecular Phenotypes show that MII Contractility is Essential for Development of Convergence Forces

Depleting either RLC or MIIB blocks gastrulation, thus both interdictions may function by destabilizing the MIIB complex (Shindo and Wallingford, 2014; Skoglund et al., 2008). To avoid this MII degradation phenotype and focus specifically on the role of T18/S19 phosphorylation in axial morphogenesis we rescue MIIB complex stability by expressing wtRLC or pnRLC proteins. These rescues reveal that one important function for RLC is to stabilize the MII complex, that this role does not depend on the phosphorylation state of the RLC, and that both the wtRLC and pnRLC rescue proteins we express can function in the context of this complex.

In addition to protecting MII complexes from degradation, RLC proteins also regulate their contractile function through phosphorylation. Phosphorylation of RLC on Serine 19, and subsequently Threonine 18 (T18-P; S19-P), upregulates MII complex contractility by 60-1000 fold in various assays and can increase assembly of MII complexes into mini-filaments, thereby regulating production of force and modulating

actin crosslinking activity (Aad et al., 2015; Sellers, 1985; Sellers, 1991; Somlyo and Somlyo, 2003; Trybus, 1989; Vasquez et al., 2014; Wendt et al., 2001). While both wtRLC and pnRLC rescued morphants exhibit stabilization of the MII complex, only wtRLC rescues blastopore closure and convergence force production, indicating a strong dependence of these force-production events on RLC phosphorylation. We exclude a neomorphic role for the pnRLC mutant protein because embryos injected with both control Morpholino and pnRLC close their blastopores normally, and exclude the hypothesis pnRLC does not function because it rescues both MII complex levels and cell surface areas in explants. The most parsimonious explanation is that pnRLC-rescued MII complexes are compromised for force-generating MII contractility, because wtRLC but not pnRLC rescued morphants can both close their blastopores as whole embryos and generate normal convergence forces as explants. However, these experiments do not rule out a contribution of a second direct negative effect on the MII complex by pnRLC expression that is distinct from inhibiting contractility. Moreover, these experiments do not separate the relative roles for tension generation by MII contractility in direct generation of convergence forces as opposed to a secondary role in the establishment and maintenance of cortical actin and C-Cadherin containing networks, as has been seen with E-Cadherin (Liu, 2010). In fact, we see such molecular phenotypes in pnRLC-rescued intercalating cells, and further suggest that these elements combine into a tension-dependent transcellular molecular array responsible for the generation and propagation of convergence forces.

We interpret our findings in the following manner, 1) the morphant RLC

depletion phenotype arises from a combination of MII complex destabilization and inhibition of MII complex contractility; because complex degradation occurs with a time lag of several hours (Park et al., 2011) this phenotype transitions from an initial loss of contractility towards phenocopying the loss of MIIB, 2) pnRLC rescued RLC depletion provides significant actin crosslinking activity but lacks contractile activity, and 3) expression of wild-type RLC fully restores force generation by restoring both crosslinking activity and MII contractility in RLC morphants. Actin phenotypes resulting from perturbing RLC phosphorylation include the reduction in the frequency and rates of actin movement in condensing proto-nodes, reduction in the number of nodes, and rates of node movement in the node and cable actin network. These results strongly suggest that contractility operating in the context of these actomyosin structures supplies both convergence forces and the molecular machinery required for their propagation.

Spatial Regulation of C-Cadherin Function is Critical for Cell Intercalation

Xenopus embryos develop arcs of convergence force across the dorsal mesodermal tissues beginning at mid-gastrulation that function to close the blastopore, are associated with bipolar mesodermal cells, and require tension to be transmitted across the multicellular tissue (Keller, 2002; Shih and Keller, 1992a; Shih and Keller, 1992b). The mediolaterally polarized protrusions on intercalating cells are the sites at which new adhesions are made, and these then become the anchor points that link to the cytoskeleton and generate traction forces on neighboring cells. This suggests that the mediolateral polarization of actomyosin structures could arise as a direct consequence of the presence

of mediolaterally polarized lamellipodia (Kim and Davidson, 2011; Shih and Keller, 1992b; Skoglund et al., 2008), and both actin polarization and mediolateral cell elongation share a common dependence on the vertebrate non-canonical Wnt planar cell polarity (PCP) pathway (Goto and Keller, 2002; Kim and Davidson, 2011; Wallingford et al., 2000). Although protrusive activity does not itself generate traction forces, in its role of "getting a new grip" it is universally associated with a subsequent traction force in traction-force microscopy of both single cells, and groups of cells (Beningo et al., 2001; Beningo et al., 2006; Harris et al., 1980; Hind et al., 2015; Lo et al., 2004; Lo et al., 2000). While integrin-mediated traction forces have received most experimental attention, C-Cadherin adhesion also functions in force transduction in *Xenopus* (Bjerke et al., 2014; Schwartz and DeSimone, 2008), and E-Cadherin mediated cell traction forces have also been seen during *Drosophila* border cell migration (Cai et al., 2014; Fulga and Rorth, 2002; Geisbrecht and Montell, 2002; Rauzi et al., 2010).

We hypothesize that actomyosin cables are mechanically linked across plasma membranes by C-Cadherin plaques to form transcellular arrays. C- Cadherin has been shown to be required for gastrulation (Lee and Gumbiner, 1995) and its adhesion activity is tightly regulated during CE, with activity decreasing without altering protein levels on the surface of intercalating cells (Brieher and Gumbiner, 1994; Zhong et al., 1999). The findings that *Xenopus* C-Cadherin from two neighboring cells localizes to plaques in the context of transcellular arrays support our contention that C-Cadherin and actomyosin are components of a molecular machine capable of producing and transmitting tension during gastrulation. Such locally mediated cellular regulation has been shown to support

assembly of distinct actomyosin structures in different regions of individual cells (Scott, 2006), and we have previously shown that perturbing the cortical actin network during CE by targeting myosin IIB heavy chain also reduces C-Cadherin-based adhesion activity without altering receptor levels on the cell surface (Skoglund et al., 2008). *Xenopus* C-Cadherin can either be diffusely distributed or localized to puncta on the cell membrane, and we find that this localization within the membrane, formation of puncta on the cell body, as well as the formation of new puncta on lamellipodia, are dependent on MII contractility. This is consistent with the idea that local tensional state of cytoskeleton regulates C-Cadherin dynamics, as has been described in cell culture (Liu, 2010).

Summary of the Role of Myosin II Contractility and Dynamic C-Cadherin Distribution in CE

To summarize the molecular machinery proposed to drive CE, initially unpolarized deep mesodermal cells become polarized and form large, mediolaterally oriented lamelliform protrusions that participate in an iterated cycle of motility, adhesion, and contraction. As these lamellipodia preferentially extend in the mediolateral axis, they elongate the cell, extend its “reach “ onto neighboring cell bodies, and establish adhesions to these neighboring cells in the form of nascent C-Cadherin puncta between their cell bodies and the lamellipodia (Fig. 7A). As the actin filament cytoskeleton of the lamella undergoes retrograde flow towards the cell body, it forms interlocking arcs, or “protonodes”, which subsequently mature to form the definitive “node and cable” cytoskeleton of the cell body. The proto-node/node and cable undergoes cycles of

contraction and relaxation linked to these mediolaterally biased anchor points, and generation of mediolaterally polarized, repetitive traction forces, which are invariably associated with these types of protrusions. The nascent C-Cadherin puncta mature into larger, linear C-Cadherin adhesion plaques, which become linked to the actin cytoskeleton and connect the contractile activity in individual cells in a tensile array spanning the mediolateral aspect of the tissue. The formation of the characteristic node and cable actin cytoskeleton, the maturation of the C-Cadherin adhesions, and the emergence of mediolateral polarity, are all dependent on RLC (Fig. 7C). The C-Cadherin-adhesions link the intracellular contractile node and cable cytoskeletal systems in each cell into a large, transcellular, tensile array. Because these adhesions are both modulated as the cells intercalate and eventually turn over, the exact path of tensile forces through the tissue varies but it is always present and intact.

Acknowledgements
The 6B6 antibody was procured from the DSHB, and concentrated in the Wiley lab. We thank Dr. Dorothy Schafer and Dr. Ammasi Periasamy for comments, advice and discussions. We cite the following instrumentation grants; RR021202, ODO16446. K. P. was partially funded by the training grant GM008136. This work was supported by NIH grants HD069297 to C. C., MERIT Award R37 HD025594 and related supplement HD025594-S1ARRA GM099108 to R. K., and GM099108 to P. S. We thank the Institutes of Child Health and General Medicine at the NIH.

MATERIALS AND METHODS:

Embryos and manipulations

Xenopus laevis embryos and explants were generated (Skoglund et al., 2008), and MO and mRNA injections were into both cells at the 2-cell stage or dorsally targeted into single blastomeres at 32-cell stage (Lee and Gumbiner, 1995), as described. Final concentrations of MO were 1-15 µM, mRNA was 1-2 ng/embryo equivalent, and Ruby-labelled dextran was at 1-2µg/embryo equivalent in the injected cell. The tractor pull experiments consist of measuring the convergence forces generated by sandwich marginal zone explants by monitoring the deflection of a mechanically coupled fiber optic probe with a known spring constant. Further details are online.

Morpholinos and expression plasmids

A Morpholino directed against RLC from Myl-12B (5-GGTCTTTGCTCTTTTGCTGGACATC-3) was produced (Gene Tools, Philomath, OR). wtRLC and pnRLC constructs were made with a MO insensitive N terminal end from Myl-12B sequences, adding a C-terminal mCherry tag. Moesin-GFP was as described (Skoglund et al., 2008). LifeAct-mCherry was made in pCS2+, while C-Cadherin-GFP, C-Cadherin-tomato was made in pCS105. Capped RNA was from the mMessage mMachine Kit (Ambion, Austin, TX). A Morpholino and control Morpholino (varied at five nucleotides) oligonucleotide (MO and COMO) directed against RLC from Myl-12B (5-GGTCTTTGCTCTTTTGCTGGACATC-3); (COMO-5-GGTGTTAGCTCATTAGCTGGAGATC-3) were produced (Gene Tools, Philomath, OR). This RLC Morpholino varies at three locations from another RLC Morpholino

derived from Myl-9 (Shindo and Wallingford, 2014), however both experiments use the same set of antibodies to assay RLC depletion. Both wtRLC-GFP and pnRLC-GFP were generated from Myl-12 sequences with the following modifications near the translation start site to make them insensitive to Morpholino: ATG TCC AGC AAA AGA GCA AAG ACC AAG was changed to ATG agC tcC AAg cGg GCg AAa ACg AAG, however these changes did not affect the coding sequence of MSSKRAKTK. A linker sequence consisting of CGA ATT CTG CAG TCG ACG GTA CCG CGG GCC CGG GAT CCA CCG GTC GCC ACC was inserted between RLC sequences and mCherry sequences in both constructs. pnRLC was also modified internally by changing the coding sequence of Myl12B, changing ACA TCC to GCC GCC; this had the effect of changing the amino acid sequence of the resulting translation product from 16-RATSNV-21 to 16-RAAASV-21. C-Cad-GFP was generated by PCR of C-Cad sequence followed by its digestion with EcoRI/KpnI and ligation with KpnI/NotI fragment of pEGFP-N2 plasmid (from Clontech). The ligation product was inserted into the EcoRI/NotI digested pCS105 vector. C-Cad-tdTomato was constructed by replacing the GFP sequence of C-Cad-GFP with tdTomato sequence via ligation of the PCR product from pRSET-B-tdTomato plasmid (kindly provided by Dr. Roger Tsien).

Whole-mount immunohistochemistry and Western Blotting

Embryo lysates were generated (Stukenberg et al., 1997), and run (Skoglund and Keller, 2007) as described, except 4-20% gradient gels and the Odyssey-LiCor imaging system was used. Explants for whole-mount IHC were fixed in two stages modified from

(Becker, 2006; Luther, 1989). Explants or embryos were fixed in two stages, first in a 0.45% Formaldehyde, 75mM cyclohexylamine solution, pH 6.5, for 45 min at room temperature, then in a MEMFA solution (3.7% Formaldehyde, 0.25% Glutaraldehyde, 5% DMSO solution, pH 7.8) for 1 hour. Blocking solution was 10% FBS, 1% BSA, 5% DMSO, and 0.1% TritonX-100. Antibodies were anti-RLC (sc15370@1:200) from Santa Cruz Biotechnology, anti- RLC Ser19P (Cell Signalling#3675@1:500), anti-C-Cadherin (6B6@1:250) from DSHB, and anti-MHCIIB@1:2000) from Sigma (M7939).

Imaging and Analysis

Low magnification images were taken using an Olympus SZX16 stereoscope with a DP72 camera. Blastopore closure images were taken on an Olympus IX70 with a Hamamatsu C4742 camera and collected using Metamorph software at a rate of 1frame/3min for 12 hours. Zeiss 510Meta and 780 confocal microscopes were used for imaging of live and fixed explants, using 25x or 63x objectives and line averaging. Time lapses had a 5-15 second framing rate, and Z-stacks had 1µm or 0.1µm steps. Foci tracking and kymographs were done using the Manual Tracker or Multiple Kymograph plugins for Image J software, and the angle and length of kymograph lines measured in ImageJ.

Figure 1: Actin and C-Cadherin dynamics during MIB.

Representative images of actin organization (A-D), C-Cadherin distribution (E-H) and double-labeling (red-actin; green-C-Cad) (I-L) in cells in dorsal marginal zone explants during the four phases of MIB (M). Scale bar in I is 20 μM. Linear arrays of actin spanning multiple cells are seen in a late stage dorsal marginal explant (N). Node condensation is represented by an increase in fluorescent intensity in an ROI, O' is 30 seconds after O. Quantification of rate of mediolateral displacement (P) and time C-Cad is displaced (Q) in cases where one cell contracts and the neighbor relaxes, when both cells contract, or when both cells relax. Proportion of displacement towards a node contraction in the specific cases where one cell contracts and the neighbor relaxes compared to contraction events regardless of the neighbor cell's behavior (R). n for P, Q and R is a minimum of 12 events from 6 cell pairs. Both a contraction (arrow)/relaxation (asterisk) pair (Fig 1S, S'), and a contraction/contraction pair (arrows) are shown (Fig 1T, T').

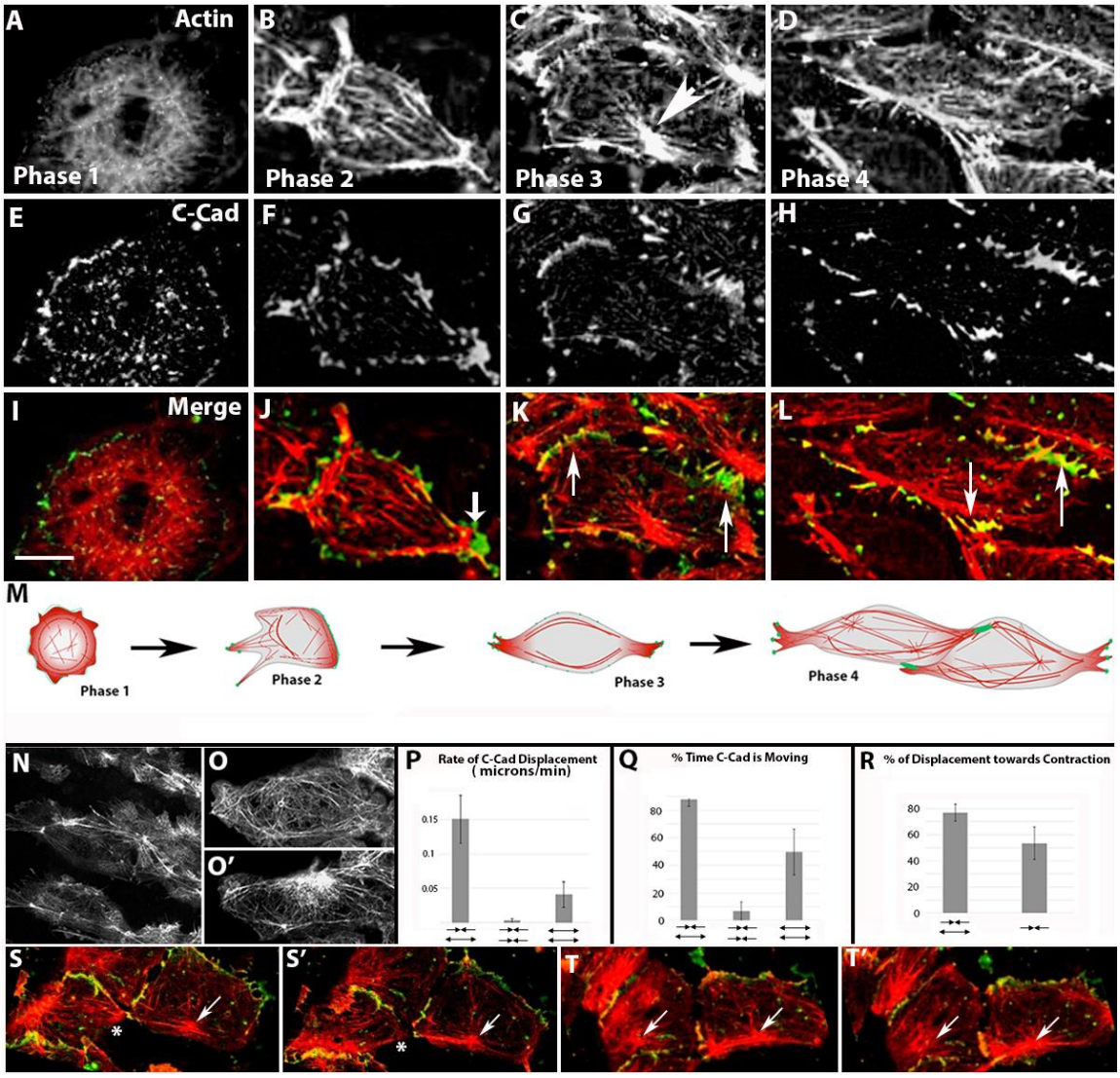
A
Actin
Phase 1
B
Phase 2
C
Phase 3
D
Phase 4
E
C-Cad
F
G
H
I
Merge
J
K
L
M
Phase 1
Phase 2
Phase 3
Phase 4
N
O
O′
P
Rate of C-Cad Displacement
(microns/min)
0.15
0.1
0.05
Q
% Time C-Cad is Moving
80
60
40
20
0
R
% of Displacement towards Contraction
80
60
40
20
0
S
S′
T
T′

Figure 2: RLC Molecular and Cellular Phenotypes

Western blotting reveals RLC protein decreases in a Morpholino dose-dependent manner compared to COMO (A; n=13 gels). Scattered COMO (B) or RLC morphant (B') cells in intact St. 17 embryos visualized in 15μm Z projections of stacks by means of co-injected fluorescent rhodamine dextran reveals a cell shape dependence on RLC levels. Myosin IIB heavy chain levels exhibit an RLC Morpholino dose-dependent decrease associated with an increase in proteolytic degradation (C). Injecting wtRLC-mCherry or pnRLC-mCherry mRNA into developing embryos leads to protein expression as detected by anti-mCherry antibody (D) Two methodologies show that wtRLC and pnRLC expression rescues MHCIIB stability; quantification of RLC and Myosin IIB immunofluorescence levels in RLC morphant dorsal marginal zones explants (E; n= 7 explants/condition), and western blotting analysis of Myosin IIB heavy chain levels in RLC MO embryos (F). RLC morphant cells have a larger surface area than control cells in explants, and this phenotype can be rescued by either wtRLC or pnRLC expression (G; n= at least 52 cells/condition). However, RLC morphant cells have a reduced Length-to-Width ratio, and wtRLC but not pnRLC expression substantially rescued this cell shape phenotype (H; n= at least 14 cells/condition). Morphant cells expressing pnRLC labeled with rhodamine dextran (red) display lower length-width ratios than corresponding control cells (green)(I).Error bars represent S.E.M.

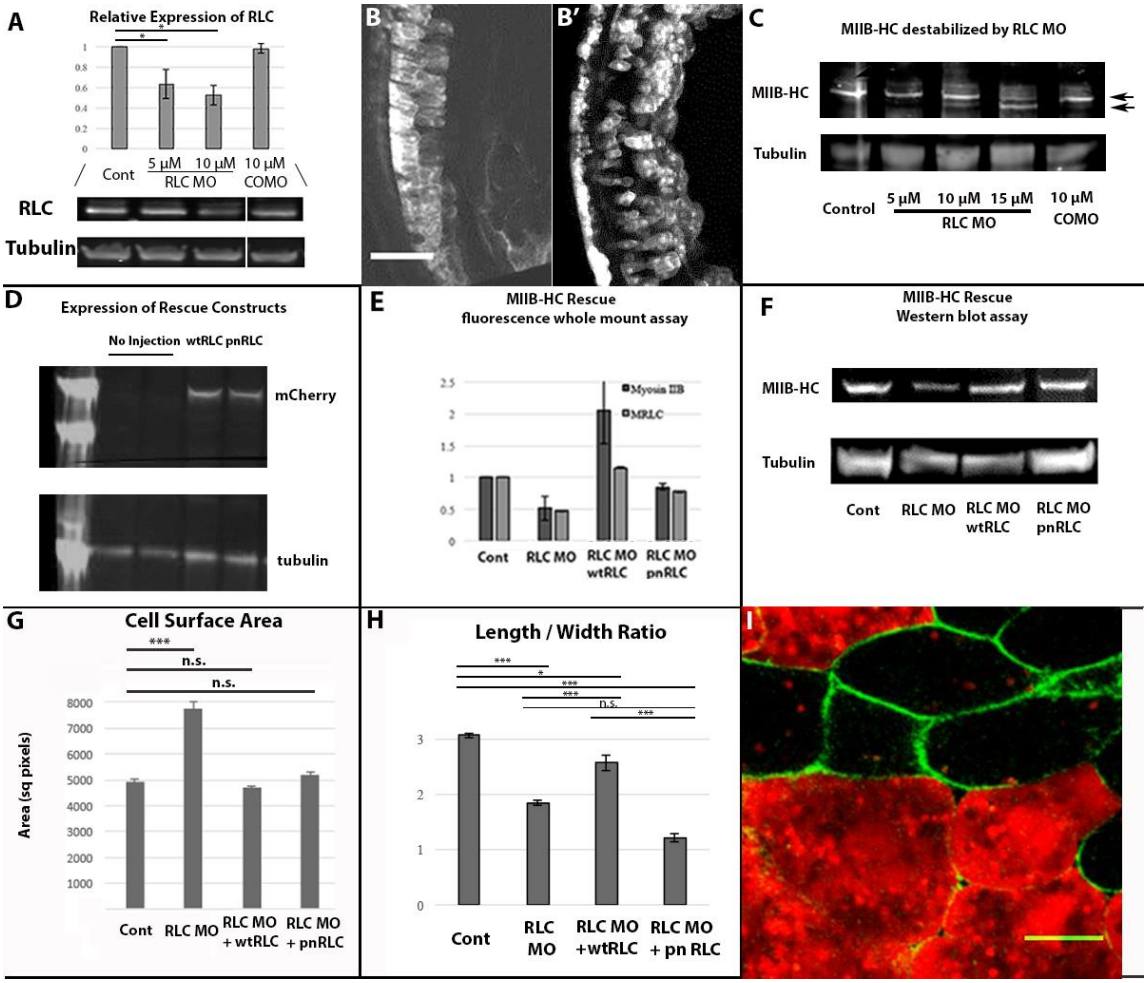
A
Relative Expression of RLC
Cont
5 μM RLC MO
10 μM RLC MO
10 μM COMO
RLC
Tubulin
B
B′
C
MIIB-HC destabilized by RLC MO
MIIB-HC
Tubulin
Control
5 μM
10 μM
15 μM
RLC MO
10 μM COMO
D
Expression of Rescue Constructs
No Injection
wtRLC
pnRLC
mCherry
tubulin
E
MIIB-HC Rescue
fluorescence whole mount assay
Myosin IIB
MRLC
Cont
RLC MO
RLC MO wtRLC
RLC MO pnRLC
F
MIIB-HC Rescue
Western blot assay
MIIB-HC
Tubulin
Cont
RLC MO
RLC MO wtRLC
RLC MO pnRLC
G
Cell Surface Area
Area (sq pixels)
***
n.s.
n.s.
Cont
RLC MO
RLC MO + wtRLC
RLC MO + pnRLC
H
Length / Width Ratio
Cont
RLC MO
RLC MO +wtRLC
RLC MO + pn RLC
I

Figure 3: Reduced Convergence Forces affect Whole Embryo Morphology

A schematic of the "Tractor Pull" device to measure convergence forces is shown (A). Explants made from RLC morphant embryos generate less pulling force than controls (B), and co-expressing wtRLC but not pnRLC rescues these pulling forces (C) as measured in sandwich explants at 4 and 6 hours after the onset of gastrulation (n= 6 axes/condition). The length of tailbud stage embryos is reduced in RLC morphants; this effect is rescued by wtRLC but not pnRLC co-expression (D, n= at least 9 embryos/condition). Time-lapse movies show normal blastopore closure (E), delayed blastopore closure in an RLC morphant (F), and rescue by expressing wtRLC (G). This delay is not rescued by expression of pnRLC (H), although an embryo co-injected with pnRLC and COMO gastrulates normally (I). Times indicate hours post St.10, and dorsal is up in E-I.

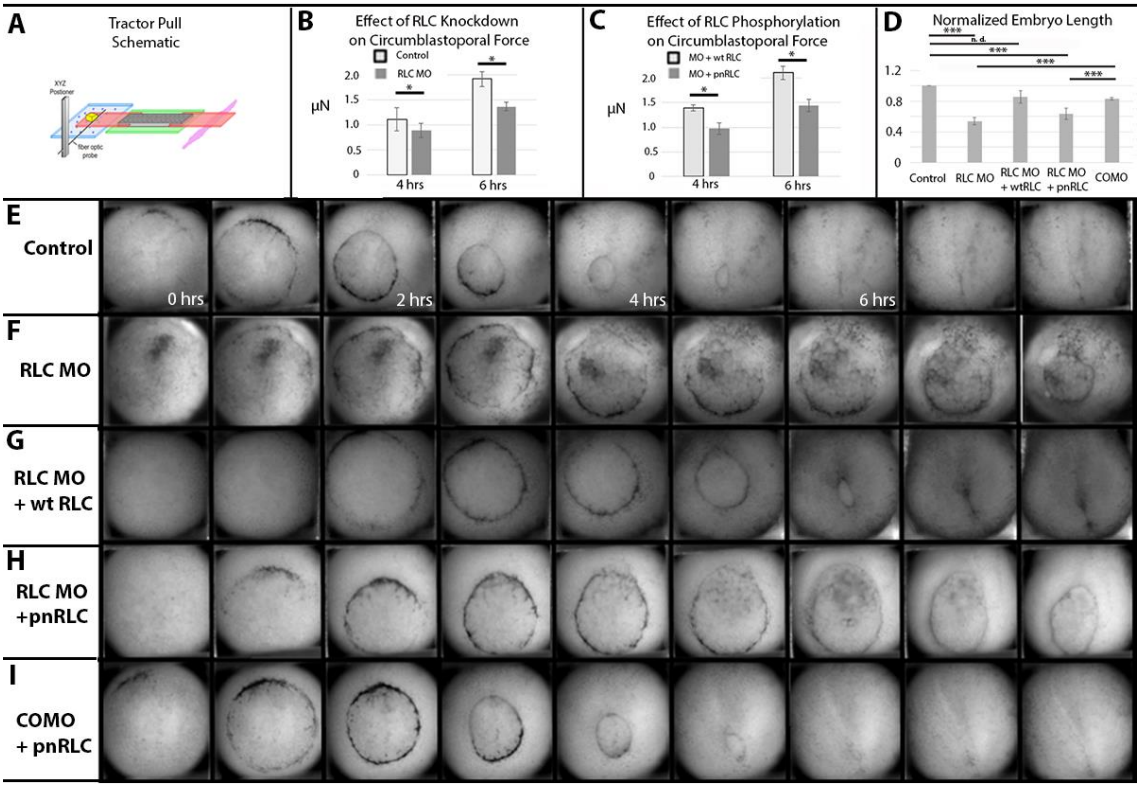
A
Tractor Pull
Schematic
XYZ
Positioner
fiber optic
probe
B
Effect of RLC Knockdown
on Circumblastoporal Force
Control
RLC MO
μN
2.0
1.5
1.0
0.5
0
*
*
4 hrs
6 hrs
C
Effect of RLC Phosphorylation
on Circumblastoporal Force
MO + wt RLC
MO + pnRLC
μN
2.0
1.5
1.0
0.5
0
*
*
4 hrs
6 hrs
D
Normalized Embryo Length
***
n.d.
***
***
***
1.2
0.8
0.4
0
Control
RLC MO
RLC MO
+ wtRLC
RLC MO
+ pnRLC
COMO
E
Control
0 hrs
2 hrs
4 hrs
6 hrs
F
RLC MO
G
RLC MO
+ wt RLC
H
RLC MO
+pnRLC
I
COMO
+ pnRLC

Figure 4: Actin Structures depend on RLC Phosphorylation

Imaging of the cortical actin structures in control cells reveals a normal cortical actin structure (A), while an RLC morphant cell exhibits a reorganization of this actin (B). This effect is partially rescued by wtRLC expression (C), but not pnRLC expression (D). These differences are quantified by comparing the number of node structures per cell (E; n= at least 22 cells assayed/condition). Dots represent the starting point of the node and the lines represent the node displacement for a control cell (F) and RLC morphant cell (G) are shown. Rate of node movement is quantitated (H; at least 9 nodes assayed per condition). Quantification of kymograph analysis of cortical actin in the regions shown (I), shows a reduction in the rate of actin movement during node formation that depends on RLC phosphorylation (J). In contrast, actin movement in lamellipodia is not sensitive to RLC depletion (K). For J-K, at least 48 kymographs were averaged for each condition. The number of new lamellipodia per cell also depends on RLC phosphorylation (L; n is at least 31 lamellipodia for each condition). All morphants are at 10 μM. Scale bars represent 20um, error bars represent S.E.M.

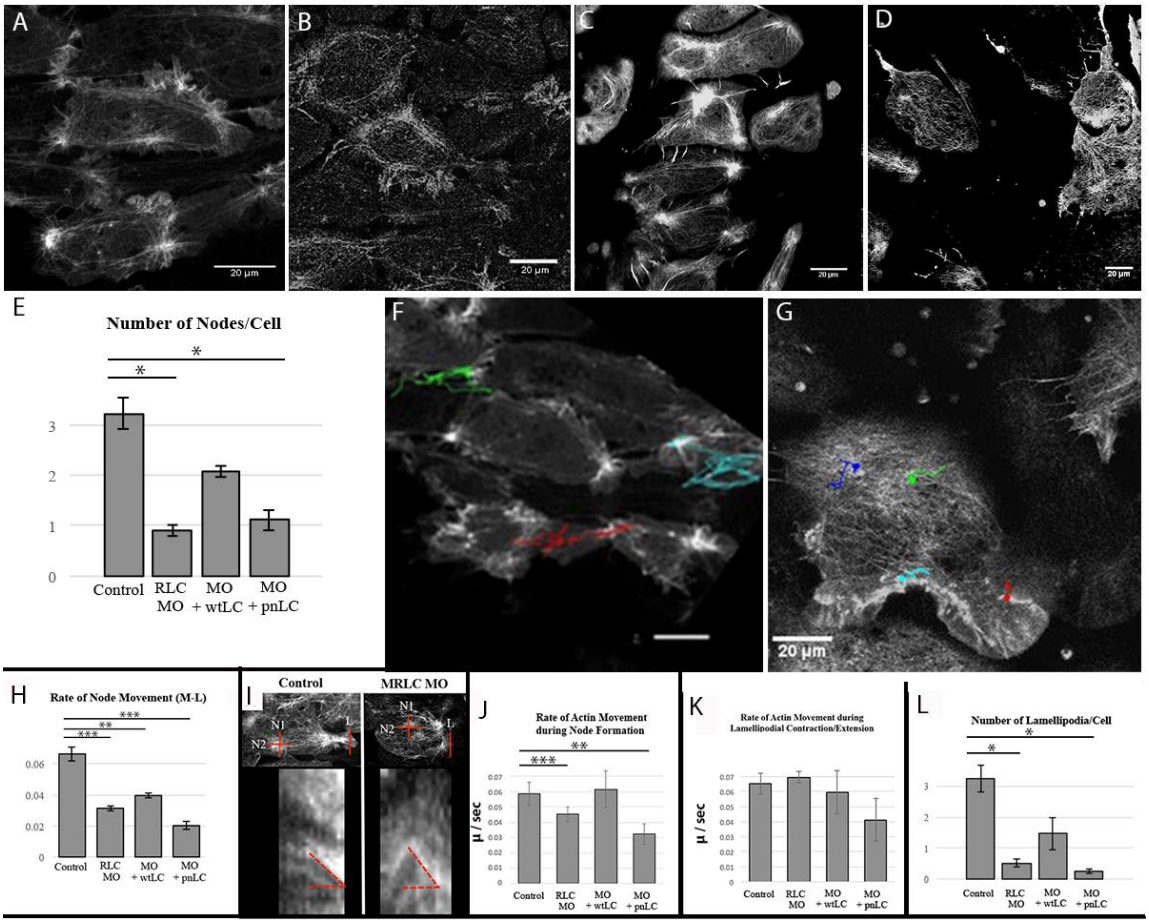
A
B
C
D
20 µm
E
Number of Nodes/Cell
*
*
3
2
1
0
Control
RLC MO
MO + wtLC
MO + pnLC
F
G
20 µm
H
Rate of Node Movement (M-L)
***
**
***
0.06
0.04
0.02
0
Control
RLC MO
MO + wtLC
MO + pnLC
I
Control
MRLC MO
N1
N2
L
J
Rate of Actin Movement during Node Formation
**
***
µ / sec
0.07
0.06
0.05
0.04
0.03
0.02
0.01
0
Control
RLC MO
MO + wtLC
MO + pnLC
K
Rate of Actin Movement during Lamellipodial Contraction/Extension
µ / sec
0.07
0.06
0.05
0.04
0.03
0.02
0.01
0
Control
RLC MO
MO + wtLC
MO + pnLC
L
Number of Lamellipodia/Cell
*
*
3
2
1
0
Control
RLC MO
MO + wtLC
MO + pnLC

Figure 5: Co-localization and Interdependencies of Transcellular Array Components

Imaging of F-actin with moe-GFP (A) and RLC with wtRLC-mCherry (A') shows co-localization (A'') in both node and cable structures with the same relative concentrations in both (B; n = 8 regions of interest). Using both Myosin heavy chain IIB (red) and mono-phosphorylated RLC (green) (S19-P) antibodies, both RLC-P and MHC are localized to cell cortices in St 13 explants (C). Levels of both are reduced in RLC morphants (D), and rescued by expression of wtRLC (E), while pnRLC expression rescues heavy chain IIB but not RLC-P levels (F). At both St 10 (5G, H) and St. 12 (I, J), C-Cadherin localization by immunostaining is perturbed in RLC morphant cells (H). Expression of red (K) and green (L) labeled C-Cadherin in neighboring cells reveals they co-localize at the membrane (yellow in M), as expected if they are serving a role in adhesion.

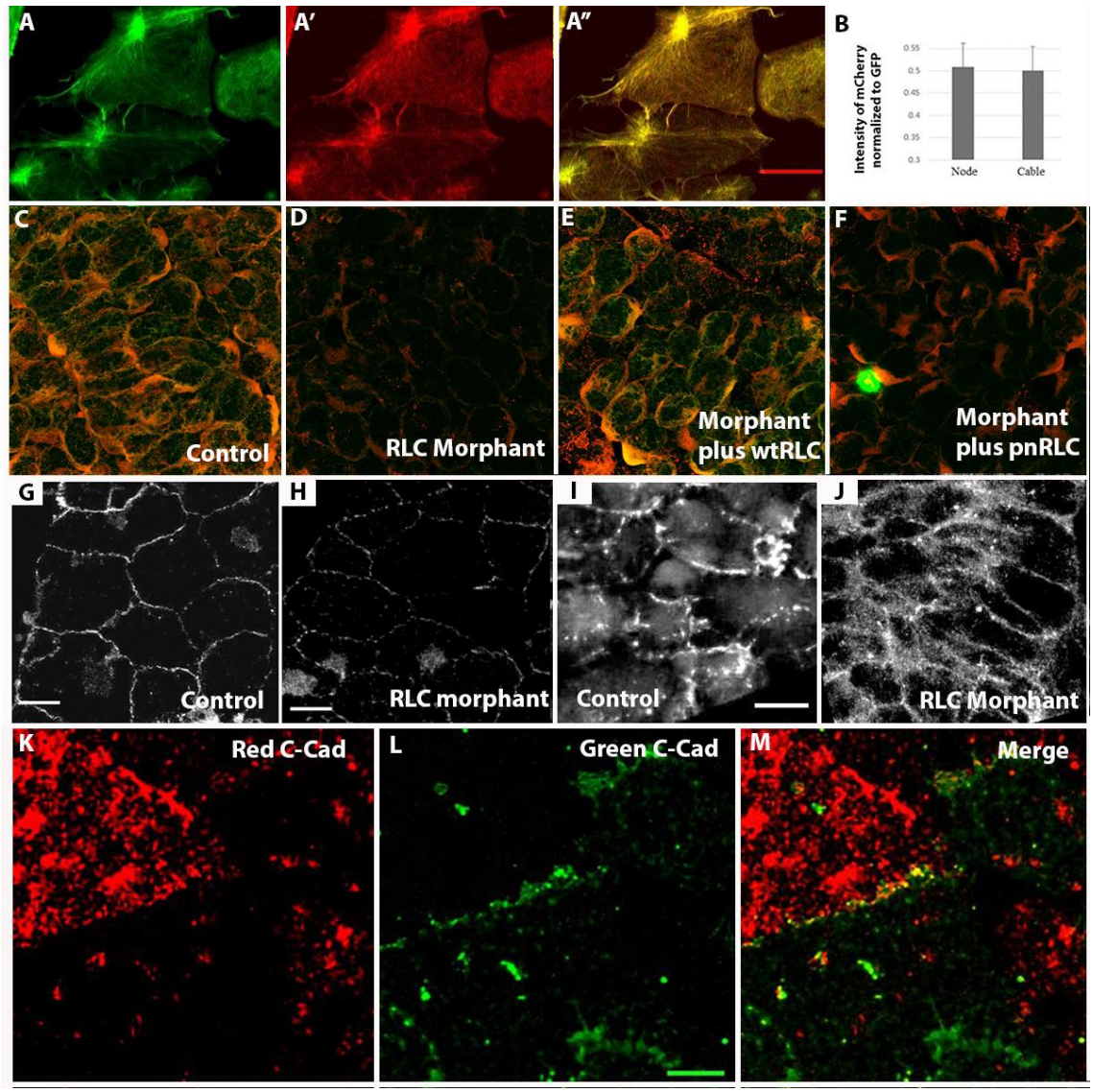
A
A′
A″
B
Intensity of mCherry normalized to GFP
0.55
0.5
0.45
0.4
0.35
0.3
Node
Cable
C
Control
D
RLC Morphant
E
Morphant plus wtRLC
F
Morphant plus pnRLC
G
Control
H
RLC morphant
I
Control
J
RLC Morphant
K
Red C-Cad
L
Green C-Cad
M
Merge

Figure 6: C-Cadherin localization on lamellipodia depends on RLC

Actin is labeled in Red and C-Cadherin or caC-Cadherin is in Green. Cadherin forms puncta (arrow) on lamellipodia (A) that resolve into long plaques (arrow), linking actin cables from neighboring cells (B, asterisk). In contrast, lamellipodia on RLC morphant cells maintain a cloud of diffuse C-Cadherin signal (arrow) that does not resolve into puncta (C). Time-lapse microscopy of C-Cadherin dynamics in adjacent control cells labeled singly for actin (left) or C-Cadherin (right) exhibit a natural experiment by displaying adhesions (arrows) that when broken, snap backwards rapidly (asterisk in D), whereas RLC MO treated cells (co-injected with a blue dextran) do not make adhesions with neighboring control cells (E). pnRLC expressing morphant cells display little protrusive activity or adhesion remodeling (arrow in F). Scale bar in A is 20 microns for all images, error bars represent S.E.M.

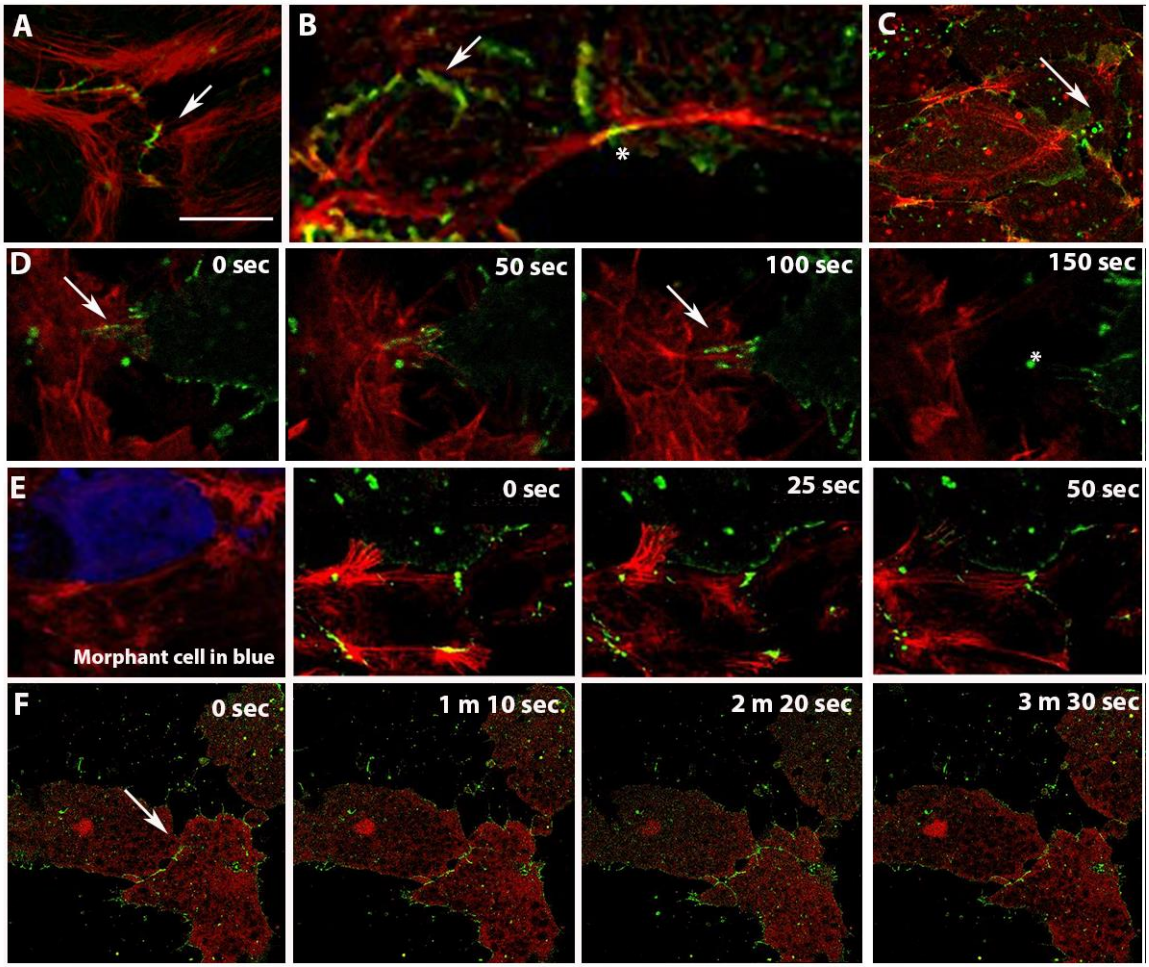
A
B
C
D
0 sec
50 sec
100 sec
150 sec
E
Morphant cell in blue
0 sec
25 sec
50 sec
F
0 sec
1 m 10 sec
2 m 20 sec
3 m 30 sec

Fig. 7 Summary of the roles of Myosin II contractility, actin cytoskeleton and C-Cad dynamics in generating the convergence force driving cell intercalation during CE.

Deep dorsal mesodermal cells extend large filo-lamelliform protrusions in the medial and lateral directions (white arrows, A), a protrusive activity characterized by a diffuse actin network (red crosshatching, A). These attach to neighboring cells by *de novo* formation of small, nascent C-Cadherin puncta (bright green, A). As the actin network undergoes retrograde flow toward the cell body, it coalesces into a series of intersecting arcs, called "proto-nodes" (black arrows, A), which mature into a characteristic "node and cable" actin cytoskeleton spanning the cell body (red cables and intersections A). The node and cable system undergoes a mediolaterally oriented, actomyosin-mediated contraction (blue arrows, A, B), thereby generating tension that shortens the cell, exerts traction on the neighboring cells, drives mediolateral cell intercalation, and generates a tissue-level, tensile convergence force. This mechanism consists of two interlinked and iterated molecular cycles, first an adhesion cycle (A) consisting of nascent, C-Cad plaques arising on polarized lamellipodia, which mature into larger, linear actin containing plaques that link the cytoskeletons of individual cells together in a tissue level system in a contraction-dependent manner, and second, a cytoskeletal cycle (B) consisting of a mediolaterally oriented tension-generating actomyosin contraction. Both cycles are dependent on a contractile myosin II complex (blue arrows in A,B), as the maturation of cadherin puncta into mature adhesion plaques, the maturation of the protrusive cytoskeleton into protonodes and those into the polarized node and cable system, all fail in RLC morphants(C).

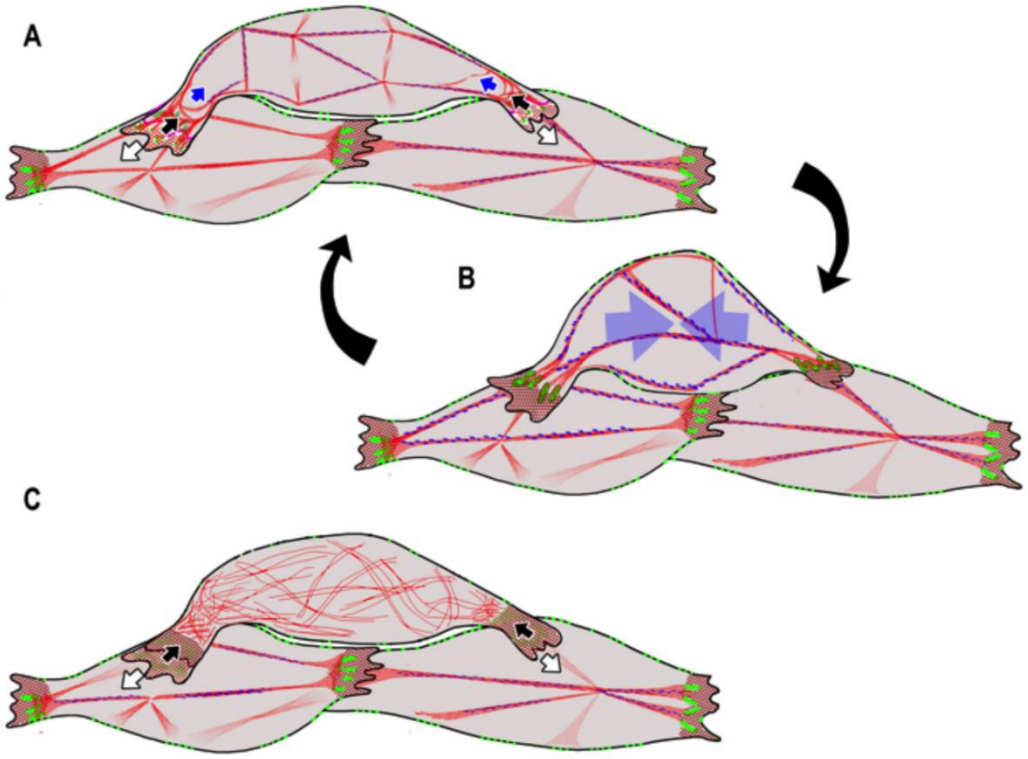
A
B
C

Chapter 2A: Nonmuscle Tropomyosin is required for the Development of the Contractile Cytoskeleton Driving *Xenopus* Convergence and Extension

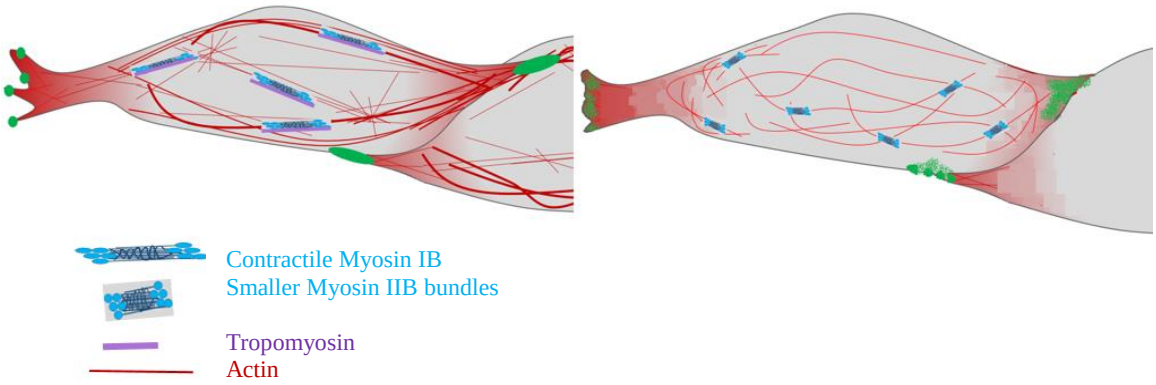

Wild Type **XTm5 MO**

Figure Legend: MIB-expressing cells require a nonmuscle form of tropomyosin, XTm5 to form the contractile NCN, critical for intercalation. When XTm5 protein levels are reduced with a Morpholino, the NCN does not form. The morphant cells retain normal protrusive activity and similar aspect ratio to wild type cells, but the morphant embryos show severe defects in Convergence and Extension.

I performed the experiments in this chapter and wrote the manuscript. The antibodies and Morpholino used for these studies were designed by Dr. Paul Skoglund.

Abstract:

In all vertebrate embryos, gastrulation and elongation of the anterior-posterior axis are critical events in morphogenesis. In *Xenopus laevis* mesenchymal cell intercalation generates a force that narrows and elongates the body plan, a process called Convergence and Extension (CE). Cell intercalation is driven by the dynamics of the contractile actomyosin cytoskeleton comprised of foci of actomyosin (nodes) connected by filament bundles (cables) that I call the Node and Cable Network (NCN). Maturation of the NCN from an isodiametric mesh of F-actin requires phosphorylation on S19 of Myosin Regulatory Light Chain (MRLC) (see previous chapter). Here I show that the development on the NCN is dependent on the *Xenopus* Tropomyosin isoform XTm5. When I knockdown the levels of XTm5 during CE, the intercalating cells adopt the normal bipolar shape of stage matched controls, but they lack a NCN and show whole embryo elongations defects. I hypothesize that XTm5 is essential to form contractile filament bundles and thus in the knockdown of XTm5, the cells fail to develop sufficient contractile force despite their normal shape. This is consistent with the hypothesis that XTm5 behaves similarly to mammalian Tm5 which binds to actin filaments and promotes myosin association, creating a contractile filament bundle.

Introduction:

Convergence and extension (CE) of embryonic tissue is critical in the development of the vertebrate body plan, and in *Xenopus laevis* CE is driven by a process in which cells actively intercalate mediolaterally (with respect to the future body axis). At

the onset of Mediolateral Intercalation Behavior (MIB), cell protrusive activity is confined to the mediolateral axis and the large lamelliform protrusions exert traction on neighboring cells, pulling the cells together and, in the process, driving cell shape change (Shih and Keller, 1992a; Keller et al, 2000). A dynamic, mediolaterally polarized cortical actin cytoskeleton, which I call the Node and Cable Network (NCN), is necessary for cell intercalation in *Xenopus* (Skoglund et al, 2008; Pfister et al., 2016). The characteristic structure and behavior of the NCN, cell intercalation, and the resulting CE in both mesodermal (Skoglund et al, 2008) and neural (Rolo et al, 2009) tissue require myosin IIB.

The cytoskeleton defines cell shape, cell behavior, and interactions with surrounding cells. These characteristics are modulated by actin-binding proteins. For instance, formins promote the formation of linear actin bundles such as those in filopodial protrusions, while Arp 2/3 promotes branched nucleation of new actin filaments resulting in a cross-linked dendritic actin network characteristic of those in lamellipodia (Welch, 1991). Other actin binding proteins further regulate actin filaments and network organization: capping proteins prevent actin polymerization, cofilin promotes actin depolymerization, and crosslinking proteins interconnect filaments into distinct architectures (Blanchoin et al, 2014). The repertoire of actin-binding proteins governs the formation and dynamics of different filament networks involved in cell movements. Here I examine the interaction of F-Actin with nonmuscle tropomyosin during *Xenopus* cell intercalation.

The tropomyosin family of actin-binding proteins consists of a number of isoforms, several of which promote association of myosin II with filaments and prevent cofilin binding (for example, mammalian Tm5). Other isoforms promote actin turnover with binding of ADF (actin depolymerizing factors), resulting in filament disassembly at the leading edge (mammalian Tm3) (Gunning et al, 2008). Regional localization of different tropomyosin isoforms results in specific and local effects on actin networks. In some cases the spatiotemporal distributions of tropomyosin isoforms create kinetically and functionally distinct networks in a single cell (Ponti et al, 2004). Perturbing the ratio of tropomyosin isoforms in a cell changes the mechanism of movement (i.e. lamellipodial, lobopodial, or filopodial protrusive activity), highlighting the influence of tropomyosin on local actin networks (Gupton et al, 2005).

I have previously shown that the node and cable network (NCN) in MIB-expressing cells functions in both contractility and formation of new adhesions on neighboring cells (Pfister et al, 2016). The combination of cross-linked actin filaments in the mediolateral lamellipodia and the cables of actin filaments in the tensile oscillatory actomyosin node and cable network (NCN) suggests local regulation of actin behavior. In this study I examine the function of the *Xenopus* non-muscle orthologue of Tm5 (XTm5) in the formation of the force-generating NCN during cell intercalation. (Hardy et al, 1991; Pfister et al, 2016).

Results:

Non-Muscle Tropomyosin Is Expressed in Mesodermal Cells during CE:

To investigate the role of *Xenopus* Tropomyosin (XTm5) in Convergence and Extension (CE), I imaged antibody staining specific for XTm5 and found that XTm5 localized to both the somitic tissue (from which muscle, cartilage and bone tissue develop) the notochordal cells, and the notochord somite boundary (Fig 1A). Within the cells, I saw filamentous signal of both actin and XTm5 across the cortex of notochordal cells (Fig 1 B-Phalloidin, XTm5, and Merge). I used the "skeletonize" function in ImageJ to increase the contrast of explants co-stained for actin and XTm5 (Fig 1B with blue cell outlines). This localization data is consistent with the hypothesis that XTm5 is expressed during cell intercalation of mesodermal cells.

XTm5 Morpholino results in CE defects

We designed a sequence specific Morpholino (MO) to examine the phenotype of XTm5 depleted cells during CE. A 5μM and 10 μM dose of the MO resulted in a 40% and 50% depletion of XTm5 protein, respectively (Fig 2A) and a corresponding dose-dependent delay in blastopore closure and axial elongation which is indicative of CE defects (Fig 2B, C). Isolating the presumptive notochordal, somitic, and neural tissue in a "giant sandwich" explant (see graphic Fig 2D) showed that the somitic and notochordal extension was defective in XTm5 morphant explants (orange line in Fig 2D) compared to controls (blue lines in Fig 2D). The mature explants of the XTm5 morphants showed defects in both mesodermal and neural extension (Fig 2 E, E').

I imaged the dynamics of XTm5 morphant cells during intercalation and found no significant alterations in the aspect ratio and no difference in the mediolateral bias of protrusive activity compared to controls (Fig 3A, A', quantified in Fig 3B). I examined the effect of XTm5 MO on the structure of the node and cable cortical actin network (NCN). Surprisingly, at 10 μM doses of Morpholino there were no F-Actin rich structures observed in these cells, even when two different fluorescent actin probes were used (Fig 3C'). At a lower (2μM) dose of MO, the F-Actin cytoskeleton mimicked an early stage of NCN development (Fig 3C'', diagrammed in Fig 3D-modified from Pfister et al, 2016). From these experiments, I suggest that XTm5 is involved in the organization of the cytoskeleton during CE, and subsequent defects in axial elongation.

Xenopus Tropomyosin and Myosin IIB operate in the same pathway during CE

To assess if the lack of NCN in XTm5 morphant cells is a result of less myosin activation, I assayed the phenotypes of embryos morphant for both myosin IIB and XTm5. A low dose of both XTm5MO and Myosin IIB MO or XTm5MO and MRLC MO resulted in axial elongation defects similar to those with XTm5 MO alone (Fig 4A). Additionally, there was no significant change in the levels of total myosin protein (Fig 4B) or active MRLC (S19-P) with increasing doses of XTm5 MO (Fig 4C). Co-injected XTm5 MO with Fluorescein dextran and stained with a phospho-specific antibody for MRLC showed colocalization of S19-P in the notochord cells and the notochord somite boundary (Fig 4D). Within the cell, distinct puncta of phosphorylated MRLC are seen on the cortex of the cells, reminiscent of normal localization shown in Chapter 2 (Fig 4E).

From these preliminary experiments, I suggest that XTm5 knockdown prevents normal NCN development without affecting the total levels of active myosin protein.

Discussion:

Embryonic development requires spatially and temporally patterned actomyosin regulation to locally deform tissue shapes. During *Xenopus* mesodermal cell intercalation, the formation of the Node and Cable Network requires nonmuscle tropomyosin (XTm5) association with actin filaments. Embryos with depleted XTm5 show axial elongation defects which I suggest are a result of decreased actomyosin cables. The total level of active myosin protein is unchanged in XTm5 morphants, which is consistent with the hypothesis that the formation of the NCN is critical for *Xenopus* CE.

XTm5 is required for development of the Node and Cable Network

I propose that XTm5-bound actin is required for formation of the NCN. Depletion of 40% of the *Xenopus* orthologue of Tm5 disrupts CE. Additionally, the NCN of intercalating cells is completely ablated with very little actin signal detected in cells of morphant explants. If less XTm5 is depleted, a finely cross-linked structure reminiscent of early MIB-expressing cells is detectable. Interestingly, the polarity of protrusive activity and the aspect ratio of the cells are similar in XTm5 knockdowns and controls. Zygotic XTm5 is reported to increase its expression after NF St. 12, which is the time that the NCN structures first appear (Pfister et al, 2016). Thus I suggest that the CE defects in XTm5 morphant embryos result from loss of NCN.

While the question of direct interaction between MRLC and XTm5 in *Xenopus* remains unanswered, my preliminary experiments suggest a role for XTm5 in the recruitment of myosin thick filaments to the cytoskeleton. In the previous chapter, I showed that myosin levels decrease significantly when the MRLC subunit is depleted, however depletion of XTm5 does not affect the level of myosin protein or its phosphorylation. These results in combination with the defects in CE show that normal intercalation requires more than normal levels of myosin protein. Myosin activation and force generation depend on the organization of the NCN. I propose that the correlation of NCN development and normal axial elongation is evidence for the critical role of the NCN in tissue force generation.

Autonomous force generation in *Xenopus* tissue requires the cells to both generate tension and withstand forces from neighboring cells. Early in MIB, (NF St. 10.5) MIB-expressing cells restrict tractive lamelliform protrusions mediolaterally, and there is no significant delay at this stage in XTm5 morphant embryos. Quantification of force generation during MIB shows that at this stage the tissue is producing about 20% of the force it does when the NCN is detectable (Shook, in preparation). Defects in MIB are seen in XTm5 morphant embryos as CE progresses: the blastopore fails to close, the axes are shorter, and scattered morphant cells in a wild-type background are extruded from the notochord at NF St. 17 (~ 8 hours after St. 10.5). From these observations, I suggest that the fine meshwork of actomyosin seen in early gastrulation is capable of withstanding force up to a threshold value. After this threshold, the NCN organization of the

cytoskeleton is required to produce force and to provide a stiff cortical substrate for lamellipodial protrusions.

This study, while preliminary, suggests that the structure of the NCN is initiated and maintained in the presence of Tropomyosin and without XTm5 the NCN does not form well, the myosin activity acts on smaller bundles of F-Actin, and CE is delayed. In future we should examine direct localization between XTm5 and Myosin IIB, and observe the effect of XTm5 on myosin thick filament formation and maintenance.

Materials and Methods:

Embryos and manipulations

Performed as described in Chapter 2 Materials and Methods

Morpholino and Fluorescent RNA Injections

Embryo injections were performed as described in Chapter 2. The XTm5MO was generated from Gene Tools Inc: 5'CCTCCAAAGAAGTTATTCCGGCCAT 3'. Final concentrations of MO were 5-10 μM, mRNA was 1-2 ng/embryo equivalent, and fluorescent dextran was at 1-2 ug/embryo equivalent in the injected cell.

Live Imaging

Performed as described in Chapter 2. Briefly, embryos were injected with either Moesin ABD: GFP or LifeAct:mCherry in either 1 of 2cell, or dorsally targeted at 32-cell stage. Imaging was performed on a Zeiss 510Meta or Zeiss 780, using the 63x objective. Time lapse images were taken at a 5 second interval and analysis was performed using ImageJ.

Whole-mount immunohistochemistry and Western Blotting

Lysates were generated as described in Chapter 2. The XTm5 antibodies were created at ThermoFisher from specific antigens, given the sequence from Hardy et al. 1991. MRLC-P antibody is the same used in Chapter 2, used at 1:500 for western blots, and 1:200 for whole-mount immunohistochemistry.

Figure 1: XTm5 localizes to actin filaments during CE

Tropomyosin localization using an antibody specific to *Xenopus* nonmuscle XTm5 shows signal in Mediolateral Intercalation Behavior –expressing cells. Fluorescent antibody staining of XTm5 (red) in Dorsal Marginal Zone explants co-localizes with Phalloidin staining (green), suggesting an interaction *in vivo* (A, Zstack of 6µm). Increasing the contrast of these explants and compressing slices further from the surface of the explant shows filaments within the cell, both of actin (green), and XTm5 (red). Merge panels show mostly colocalized signal, demonstrated using the skeletonized function of ImageJ, the cell outlines are marked in blue (B, Z stack of 2.5µm). Images taken at 63x with scale bars of 20µm.

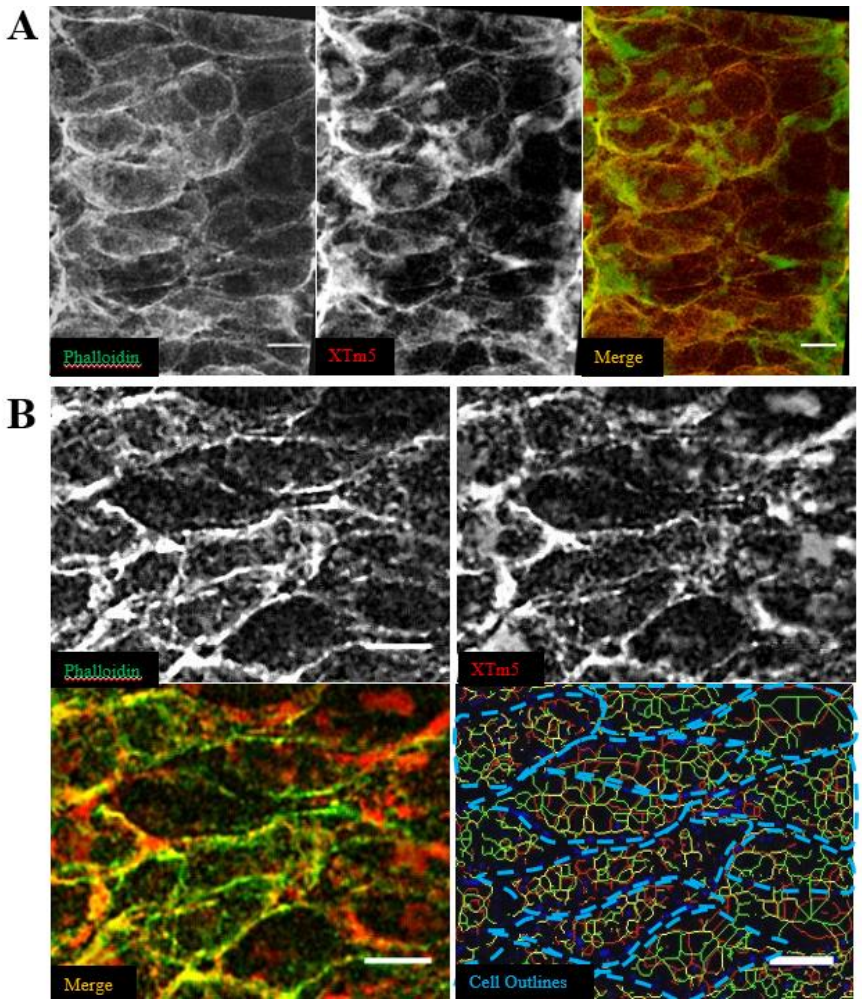
A
Phalloidin
XTm5
Merge
B
Phalloidin
XTm5
Merge
Cell Outlines

Figure 1

Figure 2: XTm5 Morphant embryos show defects in CE

Sequence-specific Morpholino of XTm5 (MO), results in a 40-50% reduction in protein levels when applied at 5 and 10μM concentrations (A). Embryos at tailbud stage show significant reductions in axial extension, and reduced blastopore closure, as compared to control embryos (B, C). Explanting the involuting marginal zone of two embryos and placing them together to make a "giant sandwich" (D, diagram from R. Keller) shows specifically decreased elongation of the mesodermal tissue. Cutting the explants at Stage 10, I saw the rate of elongation over the course of 5hours of CE, compared to control embryos (blue lines), XTm5 morphants (orange line) elongate more slowly. The sandwich explants one day after being made again demonstrate defects in elongation of both the mesodermal and neural extension in morphant embryos compared to controls (E, E') Error bars represent S.E.M.

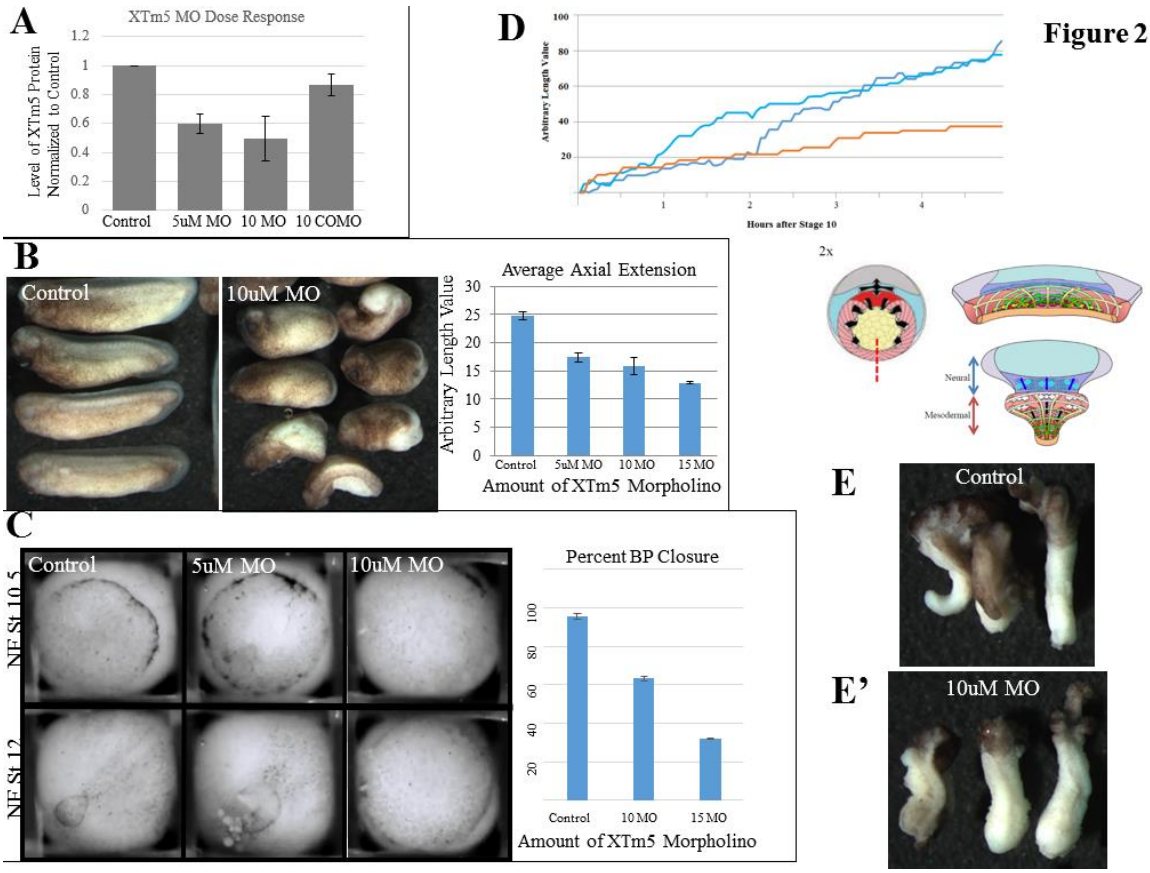
A
XTm5 MO Dose Response
Level of XTm5 Protein Normalized to Control
1.2
1
0.8
0.6
0.4
0.2
0
Control
5uM MO
10 MO
10 COMO
D
Arbitrary Length Value
100
80
60
40
20
1
2
3
4
Hours after Stage 10
B
Control
10uM MO
Average Axial Extension
Arbitrary Length Value
30
25
20
15
10
5
0
Control
5uM MO
10 MO
15 MO
Amount of XTm5 Morpholino
C
Control
5uM MO
10uM MO
NF St 10.5
NF St 12
Percent BP Closure
100
80
60
40
20
Control
10 MO
15 MO
Amount of XTm5 Morpholino
2x
Neural
Mesodermal
E
Control
E'
10uM MO

Figure 2

Figure 3: XTm5 is required for Node and Cable Network Maturation

Decreased XTm5 levels do not affect mediolateral biased protrusive activity or elongated aspect ratio of MIB-expressing cells. The aspect ratio of both control and 10µM XTm5MO explants were measured by dividing the long axis of the cell, correlating to the M-L axis of the embryo, by the short axis, correlated to the A-P axis of the embryo. There was no significant decrease in stage matched controls (labeled with MoesinABD: GFP) and morphants (labeled with green membrane) (A, A', quantified in B). Additionally, mediolaterally biased protrusions are seen in both explants (A' is an overlay of two optical Z-sections in XTm5MO explants, one right at the surface of the explant (red) and one 5µm deeper in the cell (green)). The Node and Cable Network is detected by MoesinABD: GFP at NF St. 12 (C), but is not detectable in stage-matched morphant embryos using both the MoesinABD: GFP (not shown) and UtrophinABD: RFP (C'). At a lower dose of Morpholino an F-Actin cytoskeleton is detected using MoesinABD: GFP (C'') but the structure resembles an earlier phase of NCN development, consistent with the idea that the NCN maturation shows a dose-dependent response to XTm5MO concentration. D is a modified version of the model presented in Chapter 2, suggesting the prevention of NCN maturation.

Figure 3

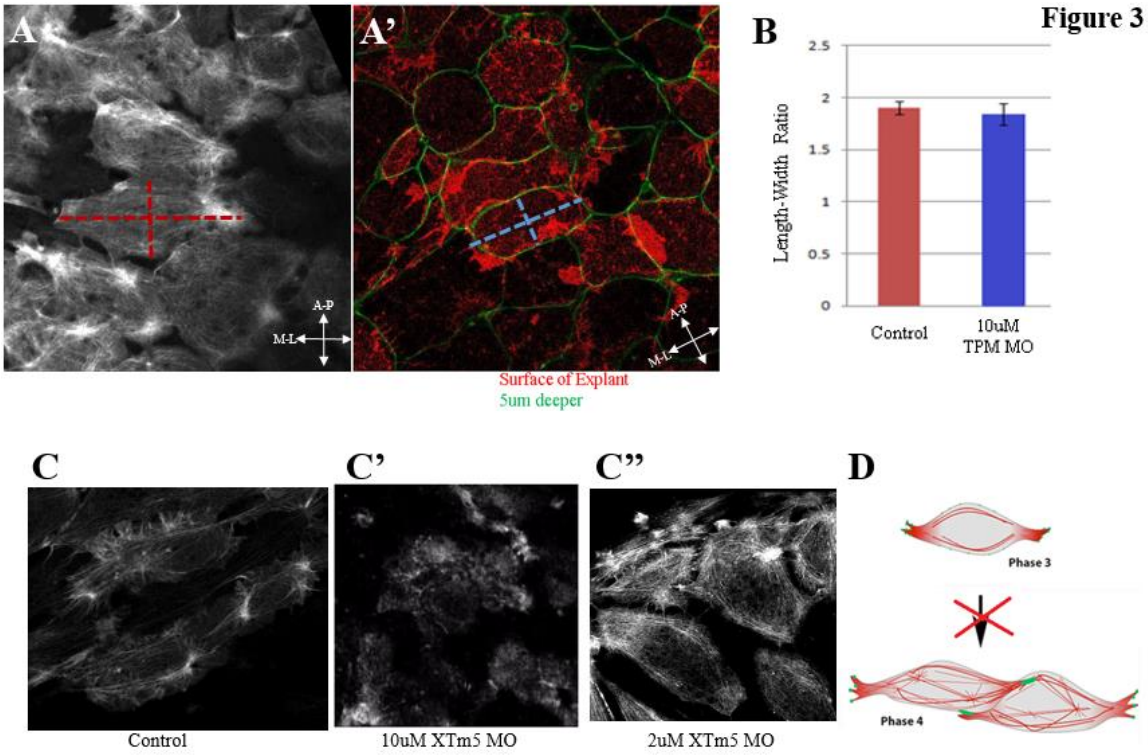
A
A'
A-P
M-L
Surface of Explant
5um deeper
B
Length-Width Ratio
2.5
2
1.5
1
0.5
0
Control
10uM
TPM MO
C
C'
C''
Control
10uM XTm5 MO
2uM XTm5 MO
D
Phase 3
Phase 4

Figure 4: XTm5 does not affect total MRLC levels or S19-P

Tropomyosin and Myosin IIB Morpholino-mediated knockdown results in similar axial extension defects as the XTm5 MO alone (A), suggesting there is no additive affect. Additionally, quantification of the total MRLC protein level assayed through western blot shows that XTm5 reduction does not cause MRLC reduction (B), and similarly the levels of phosphorylated Myosin Regulatory Light Chain- indicative of contractile myosin does not change with increasing XTm5 MO concentration (C). Whole-mount antibody staining of embryos that are half morphant (XTm5MO co-injected with a Fluorescein dextran), show similar amount and localization of phosphorylated MRLC (D, E). The blue arrows in E show puncta of localized MRLC-P on the cortex of the cells, and the red arrows show similar localization on the XTm5 morphant half. Error bars represent S.E.M. Scale bar in D=50µm of a 15µm Z Projection, taken at 25x at NF St. 13. Scale bar in E=20µm of a 5µm Z Projection, Merged panel shown at the left, just MRLC-P staining (red) shown in right panel.

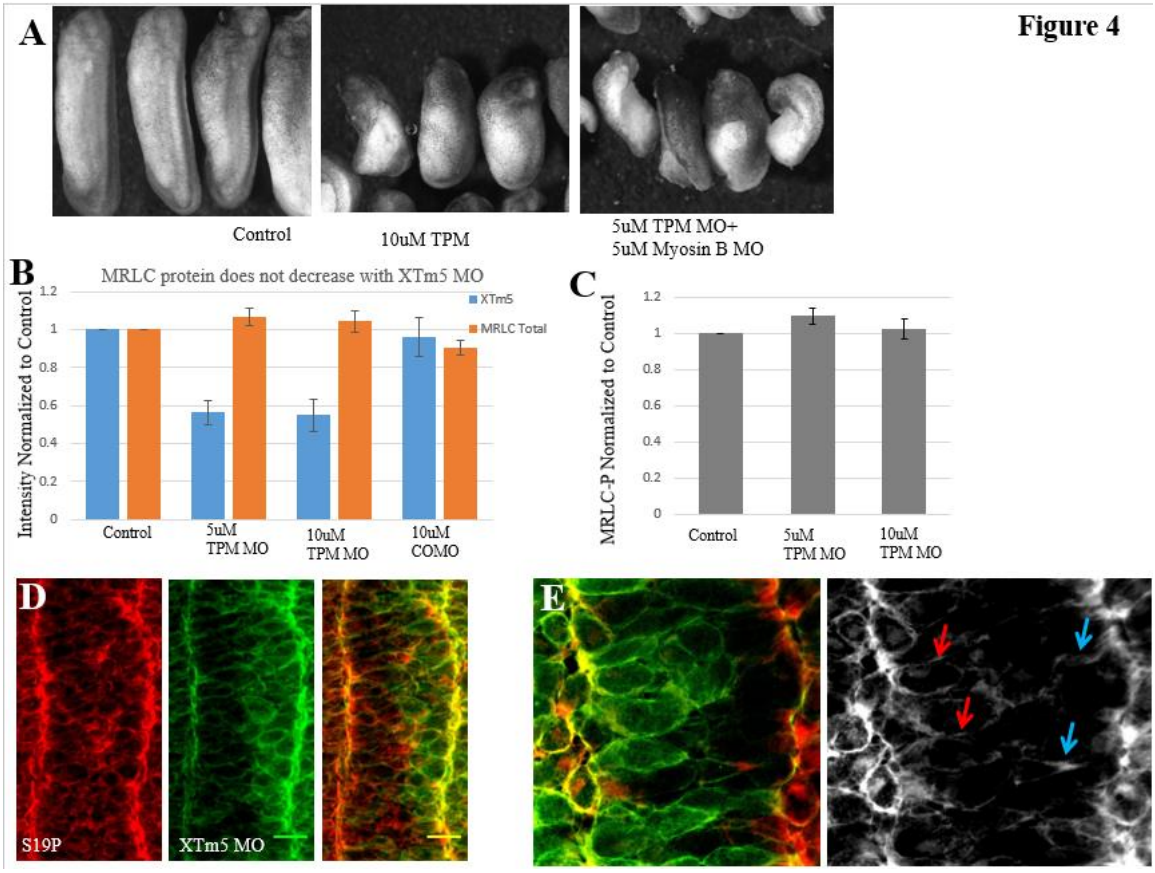
A
Control
10uM TPM
5uM TPM MO+
5uM Myosin B MO
B
MRLC protein does not decrease with XTm5 MO
Intensity Normalized to Control
XTm5
MRLC Total
Control
5uM TPM MO
10uM TPM MO
10uM COMO
C
MRLC-P Normalized to Control
Control
5uM TPM MO
10uM TPM MO
D
S19P
XTm5 MO
E

Figure 4

Chapter 3: A Second Actin Cytoskeleton is Independently Regulated in Force Producing Cells during *Xenopus* Convergence and Extension

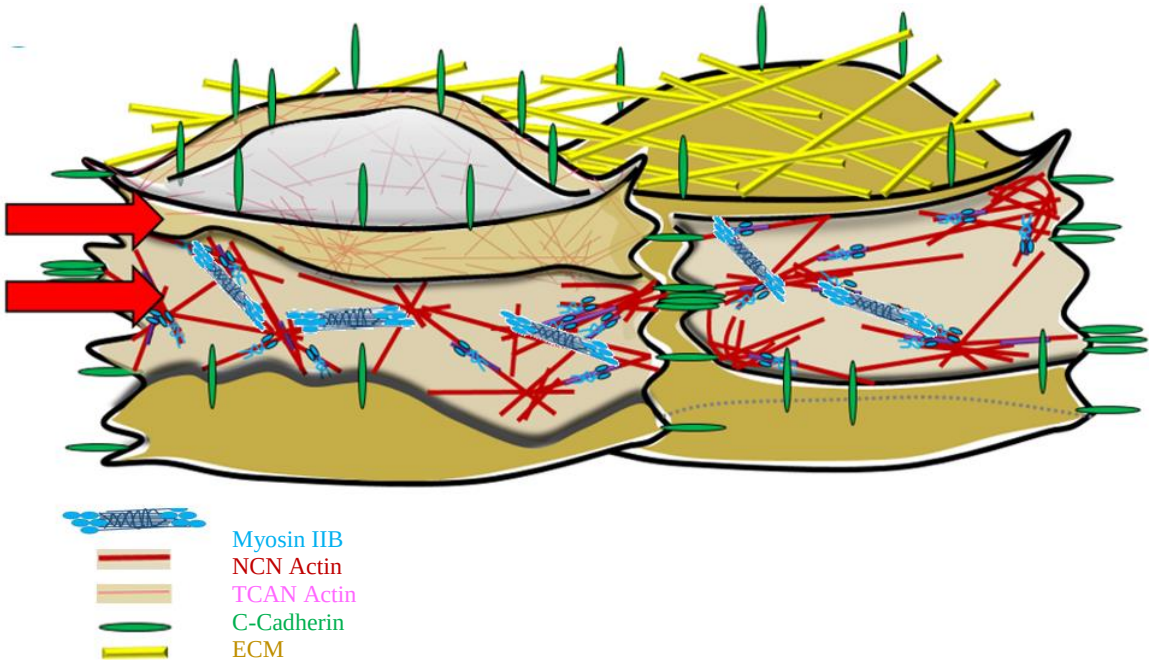

Figure Legend: MIB-expressing cells require the F-Actin network referred to here as the NCN. Active nonmuscle myosin IIB forms contractile bundles with the F-Actin in the NCN and the iterative local contractions and relaxation events cause the NCN to oscillate in the mediolateral direction (left-right in the above diagram). Forces caused by the contraction are transmitted throughout the tissue via C-Cadherin adhesions. A second, cortical F-Actin network lies between the membrane and the NCN. This cytoskeleton does not require active myosin contraction, and flows in an unbiased direction with respect to the embryonic axes.

I performed the experiments in this chapter, and wrote the manuscript with assistance from Dr. Ray Keller

Abstract:

Vertebrate embryo elongation requires active Convergence and Extension (CE), which in *Xenopus* embryos occurs via a contractility-dependent intercalation of mesenchymal cells. In dorsal mesodermal tissues undergoing CE, a Node and Cable Network (NCN) develops coincidentally with increasing force in mesodermal tissues. In this study, I used Total Internal Reflection Fluorescence (TIRF) of explanted *Xenopus* tissue to reveal a second cortical actin cytoskeleton superficial to the NCN. The presence of this actin network redefines the NCN as a *subcortical* actin network but more importantly raises the question of the functional differences between these two cytoskeletons so close in proximity. I present evidence that: 1) The TIRF-imaged Cortical Actin Net (TCAN) is separate from the NCN; 2) unlike the NCN, the TCAN exists in all cells of the developing embryo; 3) the TCAN is independently regulated, being less dependent on the level of contractile Myosin II and more dependent on actin polymerization, compared to the NCN.

Introduction:

Elongation of the body plan in all vertebrate embryos involves an active convergence (narrowing) of tissue which results in extension (lengthening), a process called Convergence and Extension (CE). The mechanism of tissue CE by cell intercalation varies with the type of tissue involved (i.e. epithelial or mesenchymal) (Bertet et al, 2004; Blankenship et al, 2006; Keller et al, 1989; Shih and Keller, 1992; Elul and Keller, 2000; Sepich et al, 2005). During *Xenopus* gastrulation, the deep

mesodermal cells intercalate by expression of Mediolateral Intercalation Behavior (MIB). MIB-expressing cells are defined by extension of mediolaterally biased lamellipodia onto neighboring cells followed by myosin-dependent contractions, which pull the cells between one another. Traction forces from cycles of extending lamellipodia and cell body contraction reinforce the adhesions with neighbors, and mediolaterally oriented tensile forces are generated by the contraction of the cortical actomyosin network consisting of transient foci ("nodes") connected by actin filament bundles ("cables"). The tensile forces are transmitted throughout the tissue by C-Cadherin based adhesions (Pfister et al, 2016).

In this study, I used a combination of high resolution Total Internal Reflection Fluorescence Microscopy (TIRFM) and Laser Scanning Confocal Microscopy (LSCM) to characterize two types of dynamic actin filament networks during CE: the Node and Cable Network (NCN) and the TIRFM-Imaged Cortical Actin Net (TCAN). I show that these actin networks are spatially close to one another but are functionally different and independently regulated.

Results:

Imaging with TIRFM Reveals a Second Cortical Cytoskeleton Different from the Node and Cable in Morphology and Dynamics

To visualize the live actin dynamics during intercalation, I explanted the dorsal lip of early-gastrula stage embryos (NF St. 10) that were scatter-labelled with fluorescent Actin Binding Protein (LifeAct:mCherry). These explants are similar to the explants made in previous live imaging studies with LSCM that revealed the NCN actin

cytoskeleton within a few micrometers of the plasma membrane (Skoglund et al, 2008). To obtain a view of the cortical cytoskeleton, I used a Total Internal Reflection Fluorescence Microscope (TIRFM). By TIRFM, I detected a cortical actin meshwork that is dramatically different from the Node and Cable Network (NCN). Unlike the NCN which consists of thick, mediolaterally oriented actomyosin cables (Fig 1A), the TIRFM-imaged Cortical Actin Net (TCAN) is made up of thinner actin filament bundles (Fig 1A') with little apparent bias in the orientation of actin movement with respect to the embryonic axis (Fig 1B, B'). The actin bundles of the TCAN flow parallel to the TIRF field, and less often (~1/5min) flow towards a common point in the cell cortex where they disappear from the TIRF field, whereas the NCN displays iterative contraction and relaxation biased in the mediolateral direction (C). To quantify these observations, I recorded the number of times local actin movement switched direction in the mediolateral axis of the cell (i.e. from left to right along the long axis of the cell) during a 10min time-lapse recording with a five second framing interval (Fig1D). Measurement of the rate of actin flow showed a significant difference between the TCAN (1-2um/min) and NCN (10μm/min) (Fig 1E).

Unlike the NCN, the TCAN is not unique to *Xenopus* mesodermal cells expressing MIB. TIRFM imaging of *Xenopus* neural plate, mesendodermal, and epithelial cells showed a cytoskeleton similar in structure and rate of movement to the mesodermal TCAN (Fig1F, F'). I conclude that the TCAN is found in other cells and may be a ubiquitous cellular cortical actin network. I conclude from these results that the TCAN is spatially close to the NCN, within 900nm, but has different dynamics.

Changes in Substrate Coating do not Affect TCAN Dynamics

The TCAN and the NCN differ in their response to different substrates. The characteristic structure and behavior of the NCN occurs when the explants are cultured in a medium containing BSA, which prevents strong adhesions to the glass substrate (see Shih and Keller, 1992; Davidson et al, 2004; Skoglund et al, 2008). When cultured in the same media but on glass substrates pre-coated with molecular fibronectin, the MIB-expressing cells stick to the glass and adopt an aspect ratio of 4:1 as opposed to the *in vivo* ratio of 2.5:1 observed in embryos (Fig 2C). Under these conditions, the NCN is reorganized into thick, linear bundles of actomyosin (Fig 2 A, A'). When the MIB-expressing cells are presented with high levels of fibronectin on an undeformable glass substrate, bipolar cells cannot exert balanced tractional forces and therefore intercalate poorly or not at all (Davidson et al, 2004). In contrast, the formation and rate of flow of the TCAN is the same on both BSA and FN-coated glass (Fig 2B). I conclude that the TCAN dynamics do not depend on specific types of cell-substrate adhesions.

Lattice Light Sheet Imaging of Dorsal Explants Allows Coincident Imaging of both the TCAN and NCN

To eliminate the possibility that the differences between the TCAN and NCN are a property of the imaging technique, I imaged both simultaneously with a specialized Bessel Beam Lattice Light Sheet Microscope. Using this approach, I imaged deeper into the mesodermal tissue without the high background signal typically obtained using standard confocal imaging (Chen et al, 2014). Time-lapse, lattice light sheet imaging

revealed concurrent actin network dynamics characteristic of both the TCAN and NCN (Fig 2E). The insets (Figure 2F) show an example of actin bundles flowing out of a single point in the cortex (yellow arrows) at a similar rate of movement to the TCAN. In the same cell, I saw an example of two node structures moving towards and then away from each other in the mediolateral direction (pair of yellow arrows Fig 2F'). Additionally, kymograph analysis of the events seen in Fig 2F and F' showed a different rate of actin movement as evidenced by the slope of the actin line (white lines in Fig 2G, G') These observations support the hypothesis that the TCAN and NCN are different structures that work in concert during MIB, as well as in other types of cell motility during gastrulation.

Disruptions of the TCAN and the NCN Reveal Different Regulation

To determine if the TCAN movement is as dependent on myosin activity, I examined TCAN flow after decreasing actomyosin contractility with a Morpholino knock down of MRLC (myosin regulatory light chain), which I have previously shown prevents development of the NCN (Fig 3A, B' and see Ch 2). Surprisingly, the same dose of MRLC Morpholino did not affect the structural organization or rate of TCAN flow (Fig 3A, C'). Additionally, acute application of Blebbistatin, which inhibits myosin activity, also did not perturb the TCAN (Fig 3 A, B, C). These results suggest that the TCAN is not sensitive to decreased myosin function or assembly. In contrast, Latrunculin B, an inhibitor of actin polymerization, significantly decreased the rate of movement of the TCAN (Fig 3A, D), and the TCAN actin filaments appeared dispersed and had disappeared from the TIRF field before the cells in these explants rounded up (Fig 3D,

D'). Latrunculin-induced depolymerization resulted in a similar cessation of normal movement and eventual dissolution of the NCN structure (data not shown). I conclude that the TCAN and the NCN both depend on actin polymerization, but unlike the NCN, TCAN formation and dynamics are independent of myosin contractility.

Crosslinking Interactions between the TCAN and NCN

To determine if the F-actin filaments of the NCN and TCAN are cross-linked, indicative of indirect interaction, I did preliminary experiments knocking down the expression of α-actinin. A low dose of a *Xenopus* α-actinin-specific Morpholino decreased actinin levels by 10% (Fig 4A), higher doses were lethal after the onset of CE (not shown). At the low dose, I noted a significant increase in embryo deformability when subjected to negative pressure from a microcapillary tube (Fig 4B-C) (see Materials and Methods). The slight depletion of α-actinin protein resulted in mediolateral lamellipodial protrusions that recoiled rapidly after extension, and mediolateral node excursions were exaggerated in the NCN (Fig 4D-E). Imaging the TCAN using TIRFM did not show any major reorganization in explants, however the embryo deformability and the effect on the NCN mentioned above is consistent with a decrease in cortical tension. Further investigations are needed to determine if the lack of detectable phenotype in the TCAN is a function of the explants being viewed through glass on an inverted scope. I propose more imaging using the Lattice Light Sheet microscope will detect any surface abnormalities suggesting lack of cortical tension in alpha-actinin knockdown embryos.

Discussion:

The cell intercalation underlying CE occurs by a cell-on-cell traction that requires cells to actively contract while also serving as substrates for movement. Neighboring cells crawl on and wedge between one another, suggesting a critical role for the actin cytoskeleton and myosin activity (Levayer and Lecuit, 2012). The Node and Cable Network (NCN) of *Xenopus* mesodermal cells is necessary for cell intercalation (Pfister 2016). In this study, live imaging of the same tissue with Total Internal Reflection Fluorescence Microscopy (TIRFM) revealed a new F-actin network never seen before in *Xenopus* cells. This TIRFM-imaged Cortical Actin Net (TCAN) was visualized 100nm or less from the glass substrate and does not, to a first approximation, include actin bundles involved in the NCN. The experiments described here raise the question of how two cytoskeletal assemblies are related in space and time and what the function of the TCAN might be.

Active Cytoskeletal Rearrangements are Necessary for Convergence and Extension

The cortical actin network of intercalating cells is critical for changing cell shape, orientation, and adhesions with neighboring cells. In the current *Xenopus* model of mesenchymal cell intercalation, individual cells extend lamellipodia to neighboring cells, and autonomously contract the actomyosin cytoskeleton (NCN) to pull the cells closer together. If these contraction events only occurred in a few cells throughout the tissue, or only occurred once per cell, it is possible one could see a “substrate cell” with a highly cross-linked and stabilized cytoskeleton, and a “contractile cell” with a dynamic

contractile cytoskeleton crawling on the neighbor. In *Xenopus* however, the same cells perform both roles simultaneously. Therefore multiple types of actin organization support these roles. I suggest that the two cytoskeletal organizations described in this study (NCN and TCAN) cooperate during MIB, driving CE.

The TIRF-imaged Cortical Actin Net (TCAN) is Different from the NCN

Analysis of the rate of movement and organization of F-actin in the TCAN were significantly different from those of the previously described Node and Cable Network (NCN) (Skoglund et al, 2008; Pfister et al, 2016). The mesh-like TCAN displays an unbiased flow of actin bundles while the NCN actin structures oscillate mediolaterally and generates tensile stress. Inhibitors of myosin contraction affect the two cytoskeletons differently, suggesting differential regulation. Additionally, the NCN cannot be seen in the TIRF field, suggesting the two are spatially separated. These data led us to conclude that the TCAN is a cortical actin cytoskeleton, separate from the now redefined "subcortical" NCN. The TCAN is not specific to intercalating cells, and its presence in *Xenopus* neural, epithelial, and migratory cells suggest that it is a ubiquitous property of embryonic cells in general. The presence of two actin assemblies displaying different behavior and regulation in close spatial proximity (900nm) raises questions of whether and how actin networks are compartmentalized within a single cell and work synergistically to support MIB.

Possible Roles for TCAN during CE

The movement of actin is a major contributor to defining the physical properties of the cell cortex. Cytoskeletal rearrangements driven by active agents can resist passive rearrangements from the cellular environment. In the case of the NCN, the active agent is the recruitment of myosin proteins and activation of contractility. The preliminary experiments presented in this study do not provide a clear answer for the driving force of the TCAN movement, but nevertheless, the observations are consistent with the idea that one does exist. The rapid oscillatory behavior of the NCN would theoretically cause horizontal shear lines in any passive cortical actin network, however the TCAN persistently displays the flowing movement shown in Figure 1. I suggest that actin polymerization plays a large part in the movement of the TCAN, but to resist deformation by the TCAN, multiple actin-binding protein partners may be required as well. There may also be interaction between transmembrane proteins and the TCAN actin bundles, but as of yet there is no evidence to support this idea. In fact, the lack of effect that substrate coating had on the TCAN movements raises the interesting question of how the subcortical NCN can be so greatly affected by surface conditions, while the cortical TCAN flows around presumptive substrate adhesions, seemingly independent of NCN affinity and behavior. Additional studies of different substrate coatings will hopefully provide an answer for how this cortical actin and the transmembrane adhesion proteins interact.

Given the proximity but disparate movements of the NCN and TCAN, I hypothesize that a shear force is generated and serves to maintain cortical integrity during MIB. While I have not determined a way to detect this force, spending more of the experiments visualizing the differences, the generation of shear stress through exposure to flowing movement is not undocumented. Mechanotransduction studies in developing vascular epithelial cells suggest that shear force from blood flow can strengthen the integrin/ECM adhesions, and in turn stiffen the cytoskeletal cortex (Parsons et al, 2010; Keller et al, 2008). The flowing movements of the TCAN actin bundles are not laminar, however the rapidity of displacement of the subcortical oscillations would provide a mechanical challenge to the flow of the TCAN.

It seems intuitive that some cortical stiffness is essential for both force production and maintenance of cell shape and polarity, and that less cortically stiff cells could not produce as much tensile force as stiffer ones. The actyomyosin force-generation machinery is only able to generate as much force as the weakest component can withstand. If cortical F-Actin is prevented from forming more and larger bundles, the force required to break the filaments is less. I suggest that the exaggerated node excursions of the NCN requires another cytoskeletal assembly to maintain cortical integrity during MIB and reinforcing the “substrate” role of the intercalating cells as neighbors attach to and pull on them. My working hypothesis from the limited experimentation on function presented here is that the TCAN serves as this second cytoskeletal assembly. It is possible that this role is also filled by the microtubule and

intermediate filaments present in *Xenopus* mesoderm, but the dynamics of actin microfilaments more closely match the rapidity of movement during intercalation.

The discovery and characterization of the TCAN in this work sets the stage for future experiments to learn if the TCAN is a widespread feature of all vertebrate embryonic cells and to understand its function in embryonic morphogenesis.

Acknowledgements:

I would like to acknowledge Dr. Ammasi Periasamy and the W.M. Keck Center for Cellular Imaging staff (UVA), and Dr. Wesley Legant and Dr. Eric Betzig at Janelia Farms Research Campus for imaging assistance.

Materials and Methods:

Embryos and manipulations

Performed as described in Chapter 2 Materials and Methods. Explants made by peeling off the endodermal epithelium and placing the exposed deep mesoderm face down onto a #1.5 cover glass-bottomed dish in media containing BSA. FN substrates were prepared by incubating coverslips in either 20ug/mL molecular FN at 4°C overnight and then washed in PBS before placing the explants on the coverslip. The explants were allowed to adhere to the substrate for 1hour before imaging. The Lattice Light Sheet microscope requires no interference from any material between the objective and the tissue of interest. To accommodate this, I removed the superficial epithelium on the neural side of the explant, and placed the explants neural-side down on a fibronectin coated glass. I consistently did not see any defects in CE of the explants made in this manner, as the MIB-expressing mesodermal cells are at least 4 cell layers away from the exogenous fibronectin and the mesodermal tissue extended normally.

Morpholino and Fluorescent RNA Injections

Embryo injections were performed as described in Chapter 2. The α-actinin MO was generated at Gene Tools Inc: 5’ TATTCTGGGAATCATAATGATCCAT 3’

Final concentrations of MO were 5-10 µM, mRNA was 1-2 ng/embryo equivalent, and fluorescent dextran was at 1-2µg/embryo equivalent in the injected cell.

Live Imaging

LSCM: Performed as described in Chapter 2.

TIRF: Embryos were injected and explants cut as described in Chapter 2. Samples were mounted on a #1.5 coverslip-bottomed chamber suspended in Danilchick's for Amy Solution (DFA-see Chapter 2). Time-lapses were taken at a 5sec interval, with an average exposure time of 100-500ms on a modified Olympus IX-70 with a 60x TIRF objective (1.45NA). The TIRF scope had two independent TIRF illuminators for simultaneous Argon and HeNe imaging, images captured on a Hamamatsu cMOS CCD using the Metamorph Software

Lattice Light Sheet: Embryos were injected as described in Chapter 2. Explants were cut at St. 12 in DFA, small lateral cuts were made in the epithelial layer of the neural tissue and the explants were mounted onto a coverslip coated with molecular fibronectin, with the neural side down and the mesodermal side free in the DFA solution. Imaging was performed as described in Chen B-C et al. Lattice Light Sheet Microscopy: Imaging Molecules to Embryos at High Spatiotemporal Resolution (2014). Science 346:6208.

Whole-mount immunohistochemistry and Western Blotting

Lysates were generated as described in Chapter 2. The α-actinin antibody was obtained from Developmental Studies Hybridoma Bank (Iowa City, IA) and used at 1:500 for Western Blots.

Drug treatments:

Application of drugs for the TIRFM regulation studies were performed during imaging. Explants were in 1mL of DFA in an imaging chamber and acute injections of 50μM Blebbistatin, 0.1μM Cytochalaisin-D, 0.6μM Latrunculin B into the medium. MRLC MO

(sequence in Chapter 2 Materials and Methods) was injected at 2-cell stage at a dose of 10µM.

Embryo Strain

The suction machine consists of a DFA bath containing a 0.33mm microcapillary tube (Drummond) connected by tubing to a syringe, whose height relative to the bath was varied using a micromanipulator. Embryos were placed against the capillary tube opening and slowly pulled into the capillary by applying negative pressure of 2 mm H2O (equal to 19.6 Pa). The amount of strain chosen resulted in a pulling speed of 0.4 mm/hour, occurred over a 4 hour period to mimic the duration of gastrulation, and caused epithelial cells in the explants to elongate along the axis of strain to a LWR of around 1.3.

Figure 1: The NCN and TCAN are different F-Actin organizations

Live imaging of explants labeled with MoesinABD: GFP shows the structure of the cortical actin cytoskeleton during MIB. The difference in structure is clearly seen when explants are imaged with Laser Scanning Confocal Microscopy (A-scale bar 20um) and Total Internal Reflection Fluorescence Microscopy (A'-scale bar 10um). I refer to these structures as the Node and Cable Network (NCN) and TIRFM-imaged Cortical Actin Net (TCAN) respectively. Behavior of the actin during the timelapse is schematized by tracing fiduciary points over time, by watching the tracks made from the original starting point (time expressed in min:sec). The NCN can be seen to oscillate in the mediolateral direction (B) whereas the TCAN displays an unbiased flowing movement (B'). The bias of movement is quantified in C and confirmed by the quantification of the number of direction changes per minute (D). The rate of movement is significantly different between the NCN and TCAN, quantified in um/min in (E). The TCAN structure can be seen in multiple other cell types with no significant changes in rate of movement (F) between the mesodermal cells (F'i) and the epithelial (F'ii), mesendodermal (F'iii), and neural cells (F'iv) (scale bars are 10um, error bars represent S.E.M)

Figure 1

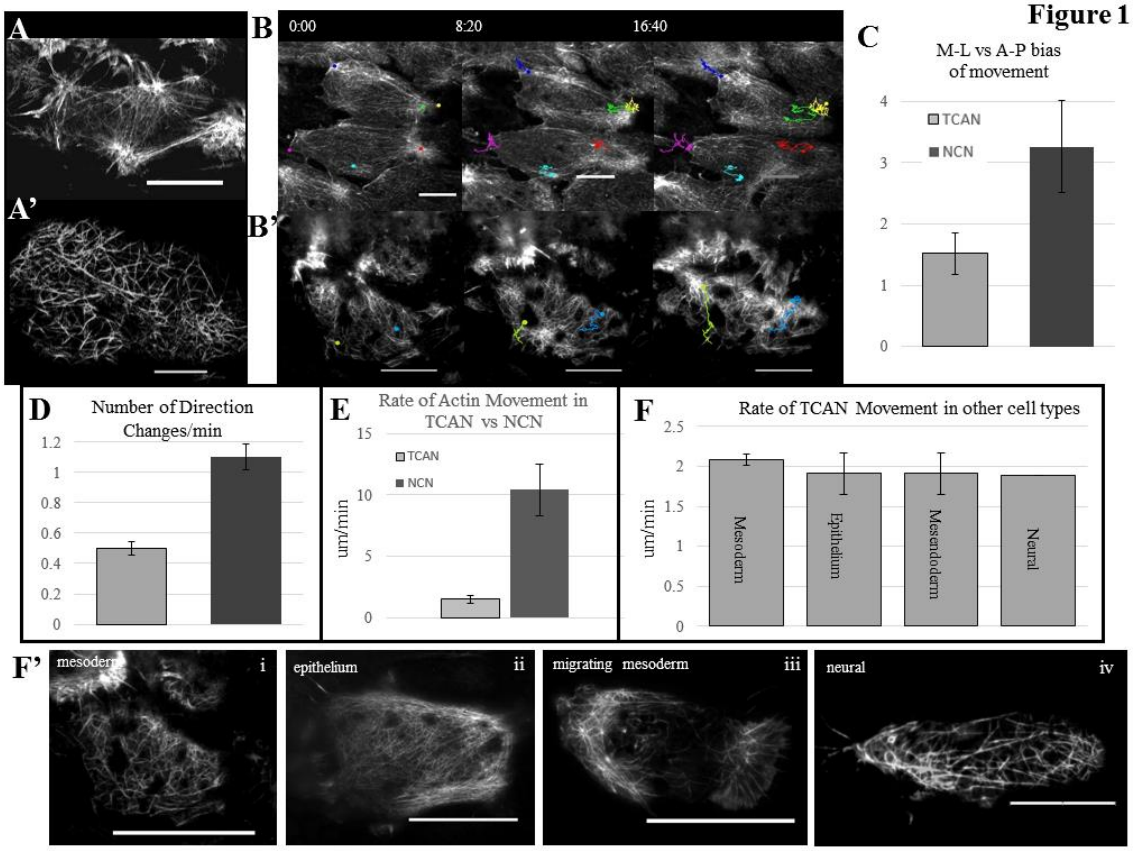
A
A'
B
B'
0:00
8:20
16:40
C
M-L vs A-P bias of movement
TCAN
NCN
D
Number of Direction Changes/min
E
Rate of Actin Movement in TCAN vs NCN
um/min
F
Rate of TCAN Movement in other cell types
Mesoderm
Epithelium
Mesendoderm
Neural
F'
mesoderm
i
epithelium
ii
migrating mesoderm
iii
neural
iv

Figure 2: F-Actin organization and movement characteristic of both TCAN and NCN are visualized simultaneously with the Lattice Light Sheet

The structure and rate of movement of the TCAN is not altered by substrate coating, whereas the NCN is (A, A', B). The aspect ratio of cells on exogenous fibronectin is significantly increased, changing the dynamics of the NCN, but the TCAN movement is unperturbed even under conditions of dramatic cell shape change and intercalation behavior (C). To visualize the coincident movement of the TCAN and NCN, I imaged explants with the Bessel Beam Lattice Light Sheet (Chen et al, 2014). The explant prep for imaging with this microscope is slightly different than that of the inverted LSCM or TIRFM (D). The dorsal blastopore lip (black circle) is excised, including both the mesodermal (purple) and neural (blue) tissue, and the endodermal epithelium is removed. Rather than placing the mesodermal side down on glass and sandwiching the explant with a coverslip, I placed the neural side down leaving the mesodermal surface open to the media. To keep the explant fixed onto the coverslip to prevent rounding up I made cuts in the neural epithelium and placed the explants (neural-side down) on exogenous fibronectin substrate (black cross-hatching). Movies of the free mesodermal surface show TCAN and NCN movement in the same cell (E). From the blue inset in (F) I saw actin bundles flow from one point (yellow arrow) out to other areas of the cell cortex (yellow arrows in subsequent frames). In contrast the green inset (F') shows node-like structures in the cortex (yellow arrows) that subsequently contract closer together and oscillate away from each other (yellow arrows in subsequent frames). Kymographs of F-Actin

movement within the insets in (E) show different rates and directions of movement, the TCAN showed a slower uni-directional flow for a longer time (G) and the NCN showed rapid oscillations (G'). I conclude from this imaging that the NCN and TCAN co-exist in the same cells during MIB.

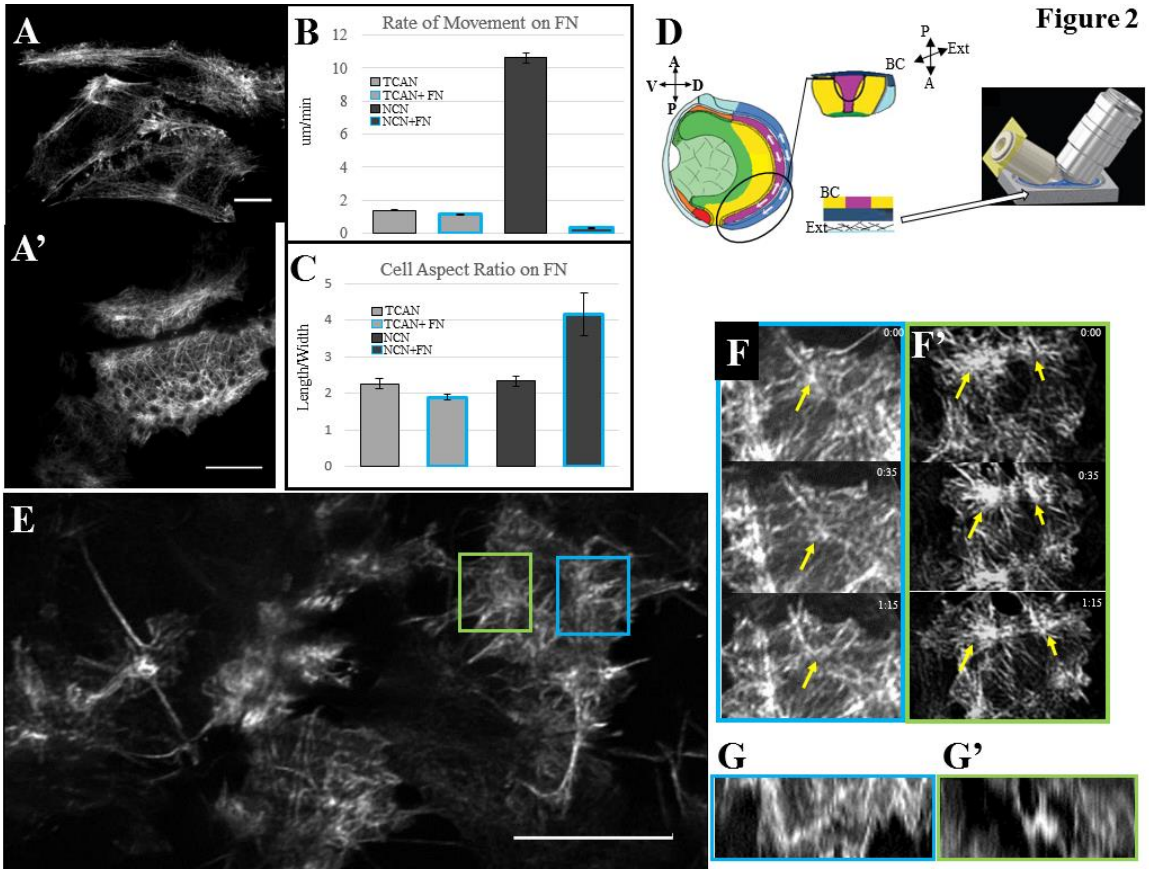
A
A'
B
Rate of Movement on FN
um/min
TCAN
TCAN+ FN
NCN
NCN+FN
C
Cell Aspect Ratio on FN
Length/Width
D
BC
Ext
E
F
F'
G
G'
0:00
0:35
1:15

Figure 2

Figure 3: TCAN movement is regulated by actin polymerization, not myosin contractility

The TCAN movement is not dependent on contractility of myosin. Previous work by Pfister et al (2016) showed the decrease in rate of movement and structural changes of the NCN when myosin contractility is reduced through a Myosin Regulatory Light Chain Morpholino (LC MO) (A, B, and B'). This treatment does not have the same effects when visualizing the TCAN (C, C'). The rate of TCAN movement is not significantly changed between the control and LC MO or Blebbistatin treated embryos (A). The movement is disrupted when acute applications of Latrunculin is applied. A table summarizing the results from these perturbations and the effect on the NCN or TCAN is presented in D. These experiments show the different regulation of the TCAN and NCN and I suggest that the movement of the TCAN is not dependent on actomyosin contractility.

Figure 3

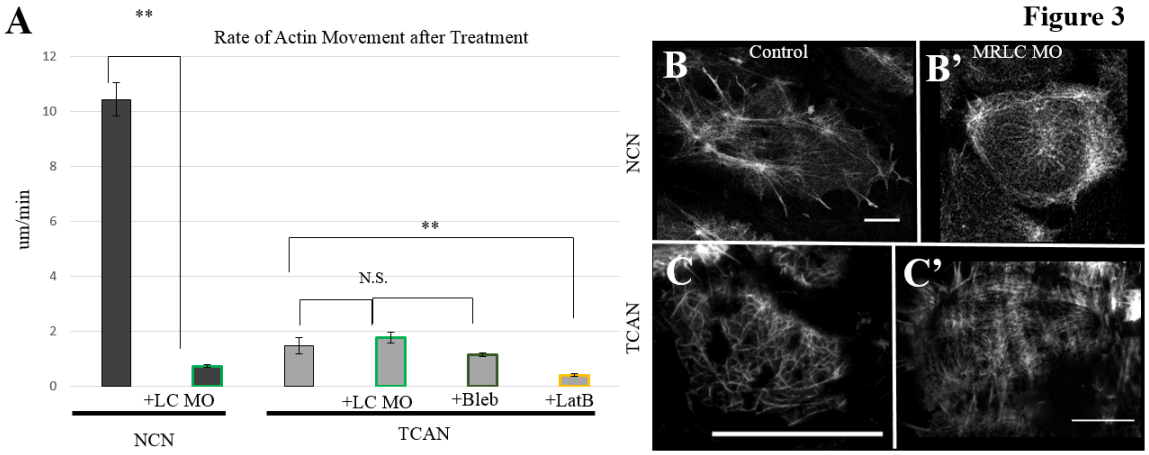

D

Treatment	Effect on NCN	Effect on TCAN	Notes
MRLC MO	Yes	No	Fewer nodes, less tissue force
Blebbistatin	Yes	No	Fewer nodes, less tissue force
Latrunculin	Yes	Yes	Actin depolymerizes as cell rounds up
Cytochalaisin	Yes	Yes	Actin depolymerizes as cell rounds up
FN-substrate	Yes	No	Aspect Ratio is larger, nodes don't oscillate

Figure 4: Alpha-Actinin knockdown results in cortical blebbing

A Morpholino knockdown of α-actinin results in a 10% decrease in protein level compared to controls (A). The morphant embryos are seen to be more deformable than controls as evidenced by the larger amount of tissue pulled into the micropipette when subjected to negative pressure (B, B') and quantified in (C). The NCN is seen to oscillate over greater distances as compared to controls (D-E'). Error bars represent S.E.M. scale bars are 20um

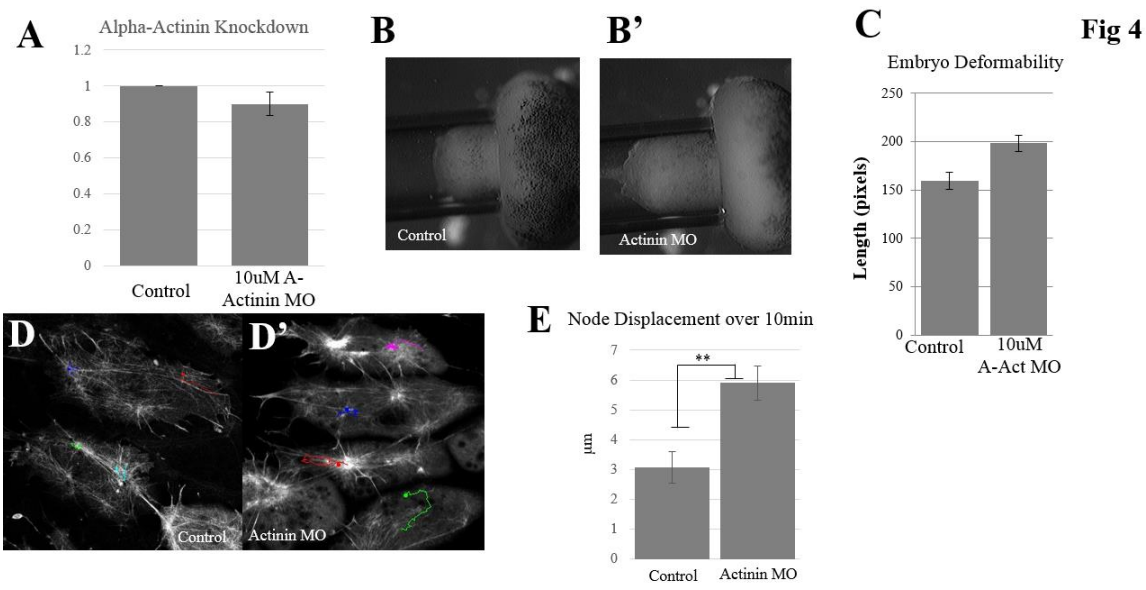
A
Alpha-Actinin Knockdown
1.2
1
0.8
0.6
0.4
0.2
0
Control
10uM A-Actinin MO
B
B'
Control
Actinin MO
C
Embryo Deformability
Length (pixels)
250
200
150
100
50
0
Control
10uM A-Act MO
D
D'
Control
Actinin MO
E
Node Displacement over 10min
μm
7
6
5
4
3
2
1
0
**
Control
Actinin MO

Fig 4

Appendix to Chapter 3: The Turnover of C-Cadherin Adhesions is Necessary for Convergence and Extension in *Xenopus*

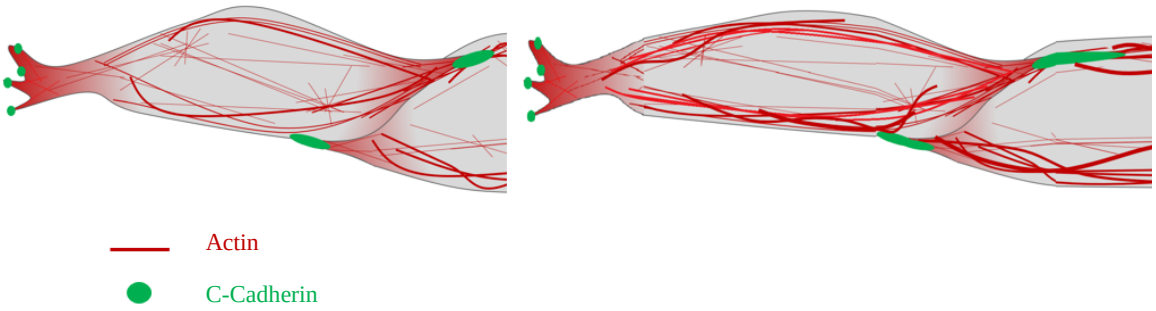

Wild Type **caC-Cad**

Figure Legend: The movement of contractile actomyosin oscillations of the NCN has a visible effect on the size and orientation of C-Cadherin plaques in intercalating *Xenopus* cells, consistent with the idea that these adhesions are part of the mechanical linkage between cells. C-Cadherin turnover is required for the cells to crawl between neighboring cells and undergo multiple rounds of intercalation. Here we express a molecular variant of C-Cadherin in which the beta-catenin binding domain of the intracellular C-Cadherin tail is removed and alpha-catenin is fused to the remaining C-Cad tail. When expressed in *Xenopus* mesoderm, the cells express a phenotype that suggests this molecular variant of C-Cad is constitutively active (caC-Cad), that is the C-Cad based adhesions do not turn over. Additionally, the NCN becomes thicker and the caC-Cad plaques are larger than wild type C-Cadherin adhesions. These cellular defects are associated with failed blastopore closure, and less Convergence and Extension.

The constitutively active C-Cadherin construct was made by Dr. Chenbei Chang. I performed the experiments with Paul Skoglund. I wrote the manuscript with assistance from Dr. Ray Keller and Dr. Paul Skoglund. Some sections and Figure 4 A-C are from the published version of Pfister et. al. 2016.

Abstract:

Elongation of most vertebrate embryos is driven largely by an active narrowing and lengthening (convergent extension, CE) of the presumptive notochordal and somitic mesoderm and/or the presumptive posterior neural tissue. At the cellular level, CE is driven by an active, mediolaterally oriented cell intercalation, which occurs as cells extend lamellipodial protrusions mediolaterally to make transient, cadherin-mediated adhesions on neighboring cells (see Chapter 2). Subsequent to forming adhesions, cells shorten and exert traction on adjacent cells, thereby pulling them between one another. As this process is repeated, many rounds of cell intercalation gradually lengthen the tissue. These dynamic exchanges in position of neighboring cells occurs as tension is generated in the mediolateral axis to exert a force that extends the tissue along the anterior posterior axis. One question raised by these observations is how adhesion turnover is coordinated with the rate of cell intercalation and the magnitude of force-generation. Here I report preliminary experiments that examine how C-Cad dynamics regulate cell intercalation during CE. When adhesion turnover is decreased by expression of a form of C-Cadherin that is fused to alpha-catenin, cell intercalation and CE are slowed. These findings suggest that this modified C-Cadherin construct may serve as a constitutively active form of the protein, in that the adhesions can't be remodeled. In this study I present preliminary phenotypes of embryos expressing this presumptive constitutively active C-Cadherin (caC-Cad) and discuss the possible mechanism causing these results.

Introduction:

In the course of *Xenopus* embryonic development, force must be generated to deform a round embryo into an elongate tadpole. This process requires distinct patterns of active, oriented cell intercalation that produces narrowing (convergence) and lengthening (extension) of embryonic tissues (convergence and extension, CE) without significant cell division or growth (Keller et al., 2000). Similar modes of cell intercalation also elongate embryos, in zebrafish (Melby et al, 1996; Glickman et al., 2003), mouse (Yen et al., 2009) and the ascidian (Cloney, 1966; Miyamoto et al, 1985), among the chordates. Cell intercalation also occurs during CE of the germband (Bertet et al, 2004; Blankenship et al, 2006), the appendages (Fristrom et al., 1975; Taylor et al, 2008), and the hindgut of *Drosophila* (Lengyel et al, 2002), during CE of the dorsal hypodermal cells of the nematode (Williams-Mason, 1998), and during CE of the echinoderm archenteron (Ettensohn, 1984; Hardin et al, 1986), as well as other tissue movements of invertebrates and chordates (see Keller et al., 2002). In *Xenopus*, mesodermal cells polarize with large lamelliform protrusive activity at the medial and lateral ends of the cells (Keller et al., 1989; Shih and Keller, 1992). Traction generated as these protrusions interact with adjacent cells pulls the cells between one another, elongating them mediolaterally and collectively forming a narrower, longer tissue (CE) (Shih and Keller, 1992a, b).

The cellular basis for *Xenopus* CE has been previously attributed to myosin based contractility generating tension that is mechanically translated through C-Cadherin based cell-cell adhesions to neighboring cells (Pfister et al, 2016). Fluorescent imaging of actively converging and extending Dorsal Marginal Zone (DMZ) explants shows a

contractile actin filament network organized as transient foci, or “nodes”, connected to one another via actin filament bundles, or “cables”. The components of the Node and Cable Network (NCN) lengthen and shorten in a dynamic pattern predominantly in the long axis of the cell. The formation and characteristic movement of the NCN depends on Myosin IIB contractility (Skoglund et al, 2008; Pfister et al, 2016). Co-imaging of with fluorescently tagged actin and C-Cadherin shows cooperative movement of the NCN and C-Cadherin adhesions during Mediolateral Intercalation Behavior (MIB), suggesting a critical role for C-Cadherin in CE (Pfister et al, 2016).

Cadherins are calcium dependent adhesion molecules. E-, C-, and N-Cadherin are expressed in different ratios during development, in an organism-specific manner. E-Cadherin has been implicated to function in CE of epithelial tissues, i.e. *Drosophila* germband extension, whereas N-Cadherin is predominantly involved in neural CE processes. C-Cadherin (C-Cad) is highly expressed in mesodermal tissue in *Xenopus*, and while the C-Cad protein level remains fairly constant during gastrulation, the activity of C-Cadherin decreases as cells intercalate (Zhong et al, 1999). This finding led us to hypothesize that tissue cohesion during intercalation requires rapid, dynamic regulation of C-Cad distribution and clustering. Here I test this hypothesis by overexpressing a C-Cad protein that is molecularly fused to α-catenin.

C-Cad adhesion complexes consist of the transmembrane cadherin protein, which has multiple extracellular calcium sensitive domains and an intracellular domain associated with β-catenin. B-catenin functions as a nuclear signaling molecule when released from cadherin complexes. B-catenin also forms a complex with α-catenin and F-

Actin. By deleting the β-catenin binding domain on the cytosolic tail of C-Cadherin and replacing it with a permanently bound α-catenin, the C-Cadherin complex binds to actin irreversibly, preventing turnover (Nagafuchi et al, 1994). During MIB, adhesion complexes are short-lived. By expressing the constitutively active C-Cadherin (caC-Cad), I can directly examine the correlation between adhesion turnover and cell intercalation.

Results:

C-Cadherin is dynamic in intensity and position during CE

Low level expression (50pg) of a GFP- tagged C-Cad protein allowed for analysis of its dynamics during MIB without inducing overexpression effects in the embryo (see Chapter 2). Imaging close to the membrane of cells in gastrulation stage explants using Total Internal Reflection Fluorescence Microscopy (TIRFM) showed discrete, dynamic puncta of C-Cad (Figure 1A). The C-Cad puncta moved through the membrane and in and out of the TIRFM plane, suggesting either fluctuations of the membrane in the evanescent wave, or the turnover of C-Cad. In addition, the relative intensity of fluorescence levels varied by 40-50% in a matter of minutes, suggesting that C-Cad puncta were dynamically associated as clusters during MIB (Fig 1B).

I used embryos mosaically expressing either RFP or GFP-tagged C-Cadherin to test that C-Cad adhesions involve both neighboring cells. Examination of a shared adhesion showed several instances of colocalized red and green cadherin, suggesting both cells contribute to the C-Cad adhesions (Fig 1C-E). Fluorescence Recovery After Photobleaching (FRAP) analysis on pairs of cells in which one expressed RFP: C-Cad

and the neighbor expressed GFP: C-Cad, showed that both cells contribute equally to the restoration of labeled C-Cad (outlined in Fig1F). Additionally, I observed that C-Cad fluorescence was recovered by movement of C-Cad puncta within the membrane (magenta dots in Fig 1F, F') and transverse movement associated with exocytosis (white, cyan dots in Fig 1F, F'), calculated by tracking the appearing puncta through the timelapse. These data highlight the dynamic behavior of C-Cadherin puncta during MIB.

C-Cadherin Substrates Decrease Cell Mobility and Mediolateral Intercalation Behavior

Given the dynamic behavior of C-Cad during CE, I examined cell behaviors when C-Cad is situated as a physical substrate during MIB, compared with behaviors when cells are plated on fibronectin (FN). Dorsal Marginal Zone (DMZ) explants were placed mesoderm face down on coverslips coated with either the extracellular domain of C-Cad or molecular FN. These explants and stage-matched control explants (placed on BSA-coated glass substrates) exhibited elongated cell shapes (Fig 2A-A''). The rate of actin flow within the cell cortex (light gray bars) and in the protrusions (dark gray bars) was significantly decreased in cells of explants plated on FN and C-Cad (Fig 2B).

Cell protrusive activity differed markedly in explants plated on FN or C-Cad. Cells in control explants send out protrusions that are retracted and remodeled on a second-to-second basis. Cells in explants plated on FN-coated glass extended protrusions on the medial and lateral ends of the cell but these protrusions fail to retract in most case suggesting that more protrusions adhered to the glass substrate (Davidson 2006). Cells in explants plated on C-Cad-coated substrates extended one large protrusion, usually uni-

directionally in the M-L axis (yellow arrows, Fig 2C). These protrusions persisted for upwards of 20min; during this time they continued to lengthen while the cell body remained stationary in the tissue. More control experiments must be done to confirm these preliminary results, however I suggest that modification of the biochemical nature of the extracellular environment *ex vivo* changes the behavior of MIB expressing cells.

caC-Cad Perturbs CE

A molecular fusion of the cytosolic tail of C-Cadherin and α-catenin (caC-Cad) creates a C-Cad molecule that can link directly to the cortical actin cytoskeleton (Nagafuchi et al, 1994). Expression of this construct, hereafter referred to as "constitively active C-Cadherin (caC-Cad), in *Xenopus* embryos led to severe axial defects in tailbud stage embryos (Fig. 2 D, D'). The notochordal sheath in the caC-Cad expressing embryos deflected dorsally, or was split (Fig 2E'). caC-Cad expressing embryos also failed to internalize vegetal tissue during gastrulation, frequently resulting in failure of blastopore closure (Fig 2F). This phenotype is often seen in embryos defective in force generation, they are unable to generate the force required to close over a large yolk plug and instead extended around either one or both sides of the blastopore, creating a ring embryo (Keller et al, 2008). These results suggest that transient C-Cad association with the cytoskeleton is necessary for CE, probably due to the requirement of dynamic adhesions to mediate multiple neighbor exchanges during cell intercalation.

caC-Cadherin overexpression results in defects consistent with loss of adhesion dynamics

Embryos and explants overexpressing various amounts of caC-Cad were examined further for cellular defects that might explain the whole embryo phenotypes. Endogenous C-Cad levels were assayed in “low” (50pg) or “high” (100pg) caC-Cad expressing marginal zone explants. In both western blot (Fig 3A, A’) and whole mount staining (Fig 3B, B’, B’’) I noted a dose dependent decrease in the level of endogenous C-Cad when caC-Cad was expressed. While preliminary, these data are consistent with the hypothesis that caC-Cad competes with endogenous C-Cad for expression sites on the membrane. The aspect ratio of the caC-Cad cells was significantly greater than stage matched controls (Fig 3C). In normal CE, mesodermal cells elongate from a 1:1 to 3:1 aspect ratio by the time the blastopore has closed. The caC-Cadherin expressing cells, by contrast, start at a 1:1 ratio, but as more caC-Cad is translated, cells reach a 4:1 aspect ratio (Fig 3D). I suggest that caC-Cad expressing cells become mediolaterally polarized, but protrusions onto neighboring cells create stable adhesions that do not turn over. As the tissue narrows, cells expressing caC-Cad are unable to retract old adhesions, but continue to interdigitate with neighbors, therefore stretching in the mediolateral direction.

caC-Cad expression results in thickening of actomyosin cables

Imaging of caC-Cad -GFP and fluorescent actin in live cells of explants undergoing cell intercalation shows localization of caC-Cad at cell-cell adhesions, and connected to the NCN (Pfister, 2016). These caC-Cad puncta remain relatively stationary throughout the timelapse, consistent with the hypothesis that the adhesions involving

caC-Cad are not turned over as dynamically as the near endogenous C-Cad shown in Figure 1. Other notable differences seen in these explants included an increased aspect ratio (see Fig 3) and significantly wider actomyosin cables in the NCN compared to those seen in control cells (Fig 4A, B, quantified in C). Additionally, FRAP was performed to evaluate the turnover of caC-Cadherin complexes. Over multiple trials, only 40% of the caC-Cad recovered, whereas nearly 80% of C-Cadherin recovered over a 30second time period (Fig 4D). I conclude from the results presented here that expression of caC-Cad reduces normal C-Cad dynamics during CE. I suggest that the larger actomyosin bundles seen in the caC-Cad expressing tissues exert increasing force on the caC-Cad adhesions, but these forces can only act over short distances due to inhibition of neighbor exchanges. I could test this hypothesis by measuring the tension across the tissue by laser ablating adhesions or by loading normal and caC-Cad expressing explants into the tractor pull device (see Pfister et al, 2016) and measuring the force they exert as the tissue undergoes CE.

Discussion:

Mediolateral cell intercalation is driven by the cooperation of cytoskeletal elements and motor proteins within mesoderm cells and the adhesion proteins connecting the cells in a cohesive tissue. The dynamics of adhesion complexes during the cycle of extension, adhesion, contraction, and retraction in MIB expressing cells is poorly understood. S.E.M of marginal zone cells and live imaging of fluorescently labeled cells first identified the differences between lamellipodial protrusions in the mediolateral axis

and filopodial protrusions on the anterior and posterior faces of intercalating mesodermal cells (Keller, 1980). This study focuses on identifying the phenotypes of intercalating *Xenopus* mesoderm expressing a variant of C-Cadherin that is molecularly fused to the cytoskeleton via alpha-catenin. This study's aim is to understand if this construct functions as a constitutively active adhesion protein, meaning it could be a valuable tool to understand the necessity of adhesion dynamics during CE. *Xenopus* mesodermal cells undergo several rounds of intercalation to elongate the developing axis (Shih and Keller, 1992) while maintaining tissue cohesion during morphogenesis. Cell-cell adhesions must form and break to allow the progressive tissue convergences through intercalation. As the tissue narrows, the cells elongate and the associated stiffness and tension increases necessitating a strengthening in adhesion. C-Cadherin is capable of transmitting this increasing tension, which would contribute to cell intercalation (Pfister et al, 2016).

Constitutively Active C-Cadherin does not disrupt patterns of MIB

Expression of the constitively active C-Cadherin generates an *in vivo* perturbation to the molecular and mechanical environment of the embryo. C-Cadherin has previously been shown to develop in a step-wise pattern during MIB, first appearing as diffuse circumferential signal and progressing through distinct puncta, and then as streaks associated with retracting lamellipodia, and finally in localizing and reinforcing cell-cell adhesions between neighboring node and cable arrays (Pfister et al, 2016). When the tissue expresses caC-Cad, MIB occurs but at a slower rate than controls, suggesting a decrease in neighbor exchange or a biophysical impediment to intercalation. caC-Cad

expressing cells still show protrusive activity and to some extent a “node and cable” array, suggesting that the polarization of the intercalating cells is not severely inhibited under these conditions. The contractile NCN shows a thickening after expression of caC-Cad, which I argue is consistent with increased tension due to higher resistance to neighbor exchange. This hypothesis is based off of the cellular evidence presented in this study but requires confirmation by biophysical measurements. The identification of phenotypes associated with the expression of caC-Cad is a useful tool for investigating the function of this molecular C-Cadherin variant and for examining the role of rapidly remodeled adhesions during CE.

Materials and Methods:

Embryos and manipulations

Performed as described in Chapter 2 Materials and Methods. FN and C-Cadherin substrates were prepared by incubating coverslips in either 20ug/mL molecular FN or 4ug/mL C-Cadherin extracellular domain (from Gumbiner/DeSimone) overnight at 4°C and washed in PBS before the explant is placed on the substrate. The explants were allowed to associate with the substrate for 1 hour before imaging.

Fluorescent RNA Injections

Embryo injections were performed as described in Chapter 2. CaC-Cad: GFP was generated in two steps. caC-Cad was first constructed by ligation of the EcoRI/BamHI N-terminal fragment of C-Cad (with its β-catenin binding domain removed) with the BamHI/XbaI fragment of α-catenin (also without its β-catenin binding domain). The ligation product was inserted into the EcoRI/XbaI sites of pCS105. caC-Cad-GFP was subsequently generated by inserting the GFP sequence in frame at the C-terminal end of caC-Cad, using a PCR-based strategy.

caC-Cad: GFP was generated by Dr. Chenbei Chang. The mRNA was 50-100pg/embryo equivalent.

Live Imaging

Performed as described in Chapter 2 for LSCM, and as described in Chapter 3 for TIRFM.

Fig 1: Normal C-Cadherin Dynamics (A)TIRFM imaging of Actin (red) and C-Cadherin (green) shows membrane expression in a range of small and large clusters across the face of the intercalating cell. These puncta fluctuate in both positions (data not shown) and in relative intensity (B). Only those puncta which are present in the TIRFM field for the entire 2 minutes were measured. Imaging a mosaically labeled explant with either GFP: C-Cad or tdTomato: C-Cad (C), showed that C-Cad puncta from both cells contribute to the cell-cell adhesion. The profile of a line along the adhesion (D), showed adhesions between GFP and tdTomato C-Cad (E). Fluorescence Recovery After Photobleaching experiments show that both cells contribute equally to C-Cadherin based adhesions (F, F'). The yellow box represents the area bleached, the puncta of C-Cad signal were tracked as they appeared in the bleached area. White and magenta dots are puncta that appeared in the C-Cad: tdTmto expressing cell, the cyan, green, and red dots were puncta appearing in the C-Cad: GFP expressing cell. F' shows the relative displacement of these puncta towards the membrane (gray line) from either side. This is one representative tracing, the experiment was repeated 6 times.

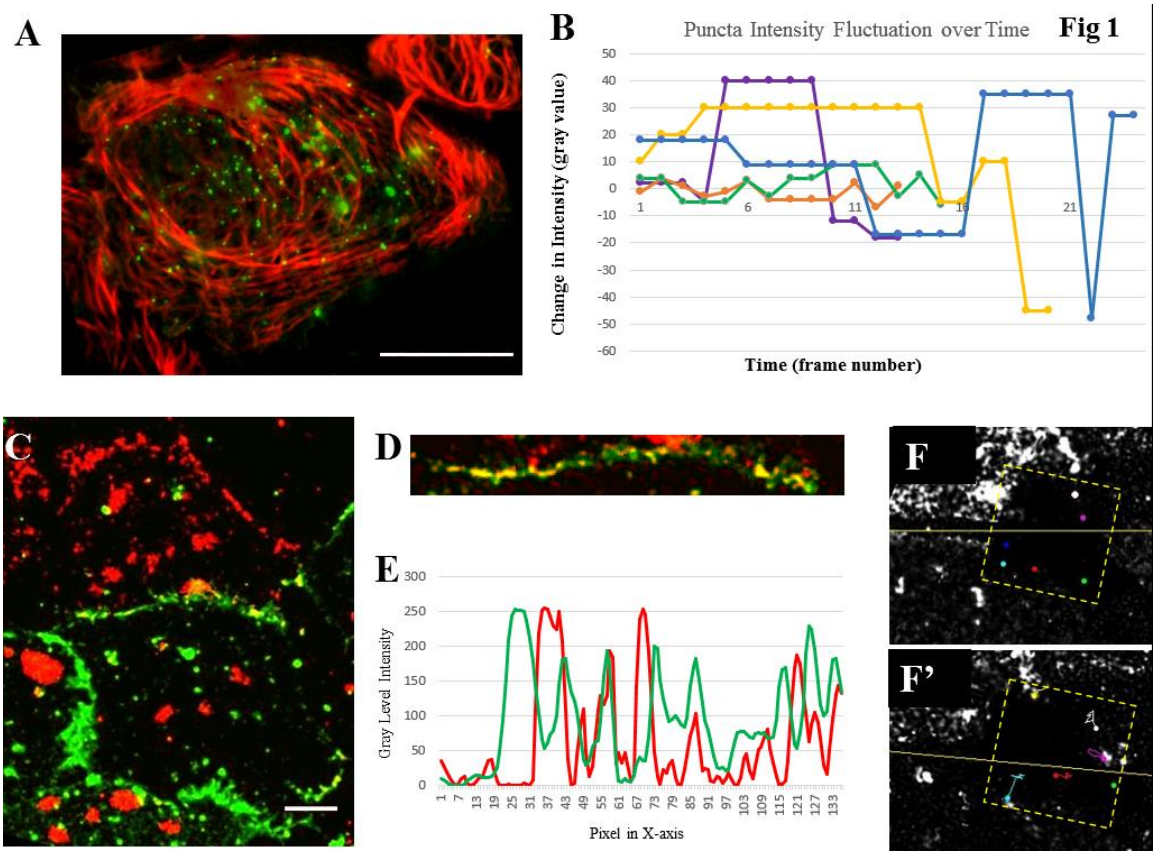
A
B
Puncta Intensity Fluctuation over Time
Fig 1
Change in Intensity (gray value)
Time (frame number)
C
D
E
Gray Level Intensity
Pixel in X-axis
F
F'

Fig 2: Modifications of C-Cadherin Environment and Behavior (A-A'')

Representative images of stage matched explants injected with a MoesinABD: GFP label in controls (A), explants cultured on exogenous molecular fibronectin coated coverslips (A') or exogenous extracellular domain of C-Cadherin (A''). The control image displays the developing node and cable array that oscillates regularly in the mediolateral direction, as quantified in B. Both the FN and C-Cad substrates display elongated cables of actin (green in A'') and very little movement compared to controls (B). The explants cultured on C-Cadherin substrate often (n=5) formed elongated protrusions of actin in one direction of intercalating cells (arrows in C). A representative time lapse is shown with images from one minute intervals. Injection of a constitutively active C-Cadherin results in defects in CE. 50pg injections result in shortened axes (D') as compared to controls, and split notochordal tissue during neurulation with a roughly 50% penetrance (E). The notochordal tissue is stained with Tor70 (red), labeled with "N" and the surrounding somitic tissue is stained with 12/101 (green), labeled with "S" in a representative Control embryo (E) and a caC-Cad expressing embryo (E'). These origin of these axial defects are seen in gastrulation where failure of the vegetal tissue to be internalized causes the preaxial mesoderm to extend around an open blastopore (F).

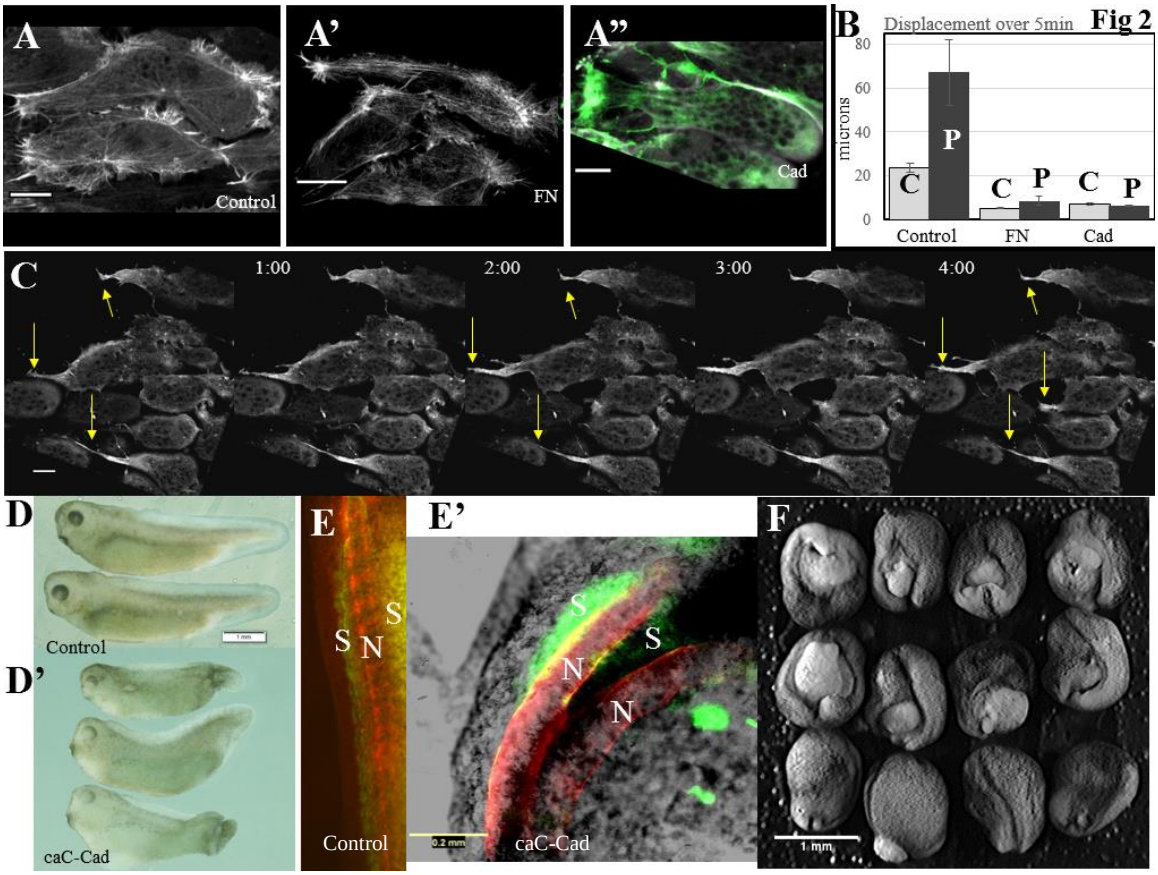
A
Control
A'
FN
A"
Cad
B
Displacement over 5min
Fig 2
microns
80
60
40
20
0
C
P
C
P
C
P
Control
FN
Cad
C
1:00
2:00
3:00
4:00
D
Control
D'
caC-Cad
E
S
S
N
Control
E'
S
S
N
N
caC-Cad
0.2 mm
F
1 mm

Figure 3: Cellular Defects in caC-Cad Expressing Axial Tissue

(A) Western Blot analysis of endogenous C-Cadherin levels in control St 13 embryos (left lane), and those injected with 50 (middle lane) or 100pg of caC-Cad. Note the increased levels of caC-Cad band around 170kDa and the decreasing levels of endogenous C-Cad (100 kDa). α -Actinin loading control. Quantifications of this experiment (n=4) are averaged in A'. Whole mount immunohistochemistry shows the same trend: 15µm Z projection of a control explant (B) 50pg caC-Cad (B') or 100pg caC-Cad (B'') stained for C-Cadherin (green) and Fibronectin (red). The caC-Cad was scatter injected with a Cascade Blue Dextran (blue in B', B''). caC-Cad expressing cells (C') displayed a significantly longer aspect ratio that controls (C), quantification of 3 experiments shown in (D).

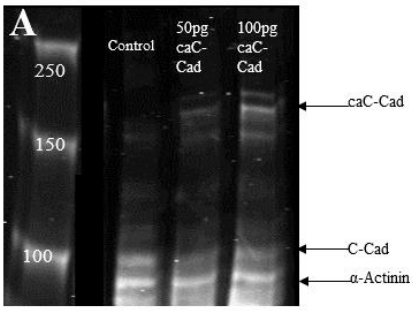
A
Control
50pg caC-Cad
100pg caC-Cad
250
150
100
caC-Cad
C-Cad
α-Actinin

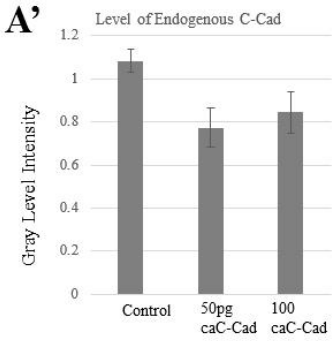
A'
Level of Endogenous C-Cad
Gray Level Intensity
1.2
1
0.8
0.6
0.4
0.2
0
Control
50pg caC-Cad
100 caC-Cad

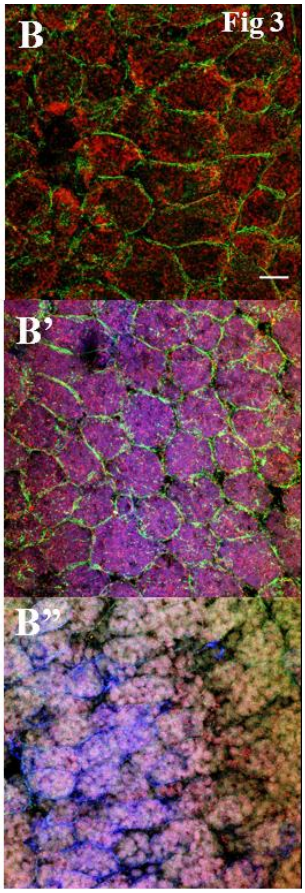
B
Fig 3
B'
B''

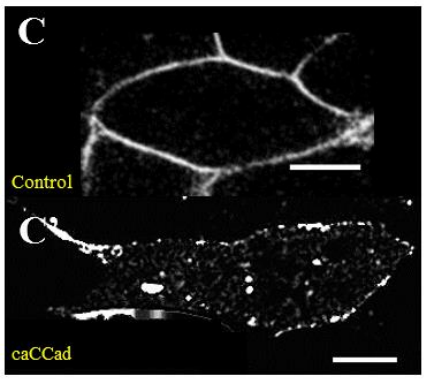
C
Control
C'
caCCad

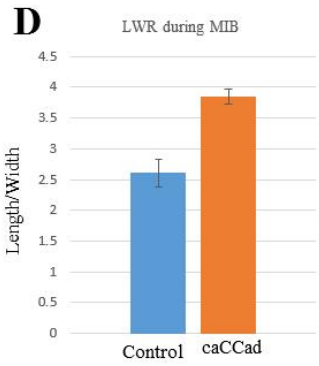
D
LWR during MIB
Length/Width
4.5
4
3.5
3
2.5
2
1.5
1
0.5
0
Control
caCCad

Figure 4: caC-Cad expressing cells display thicker cables in the NCN

caC-Cad expressing intercalating cells show rearrangements in the NCN. In addition to the longer aspect ratio, the actomyosin cables (labeled with mCherry:LifeAct), as well as the cell-cell adhesions (labeled with either GFP:C-Cad or GFP:caC-Cad) are larger in the same Z-section as controls, both structures are highlighted by white arrows (A-B). The quantification of the width of the actomyosin cables was significantly greater than those found in control cells (C). Additionally, to show the lack of dynamic movement within the membrane of caC-Cad, I performed a FRAP assay and found that the caC-Cad signal did not recover as quickly or as much as the control C-Cad (D). Error bars represent S.E.M. Figure A-B is a modified version of a figure from Pfister, 2016.

Fig 4

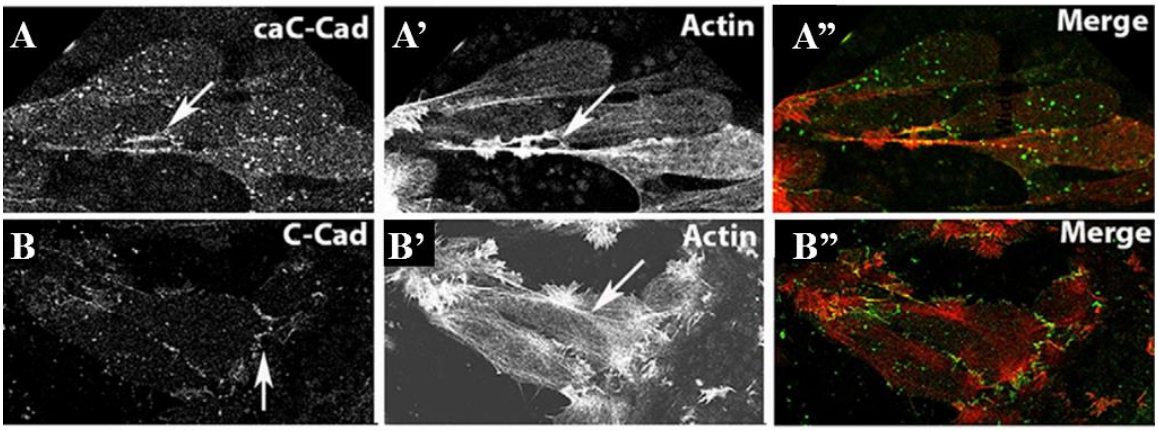
A
caC-Cad
A'
Actin
A"
Merge
B
C-Cad
B'
Actin
B"
Merge

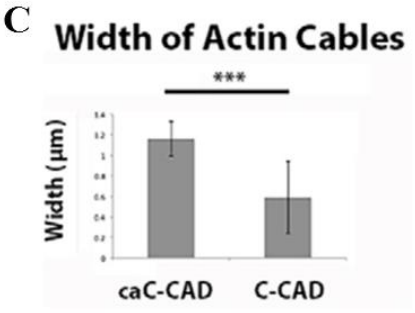
C
Width of Actin Cables
***
Width (µm)
caC-CAD
C-CAD

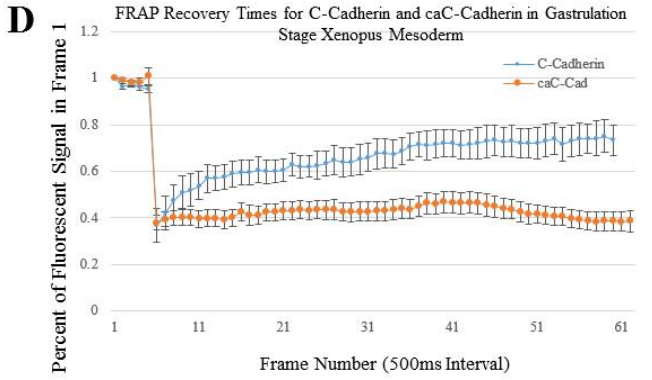
D
FRAP Recovery Times for C-Cadherin and caC-Cadherin in Gastrulation Stage Xenopus Mesoderm
C-Cadherin
caC-Cad
Percent of Fluorescent Signal in Frame 1
1.2
1
0.8
0.6
0.4
0.2
0
1
11
21
31
41
51
61
Frame Number (500ms Interval)

Chapter 4: Conclusions and Further Questions

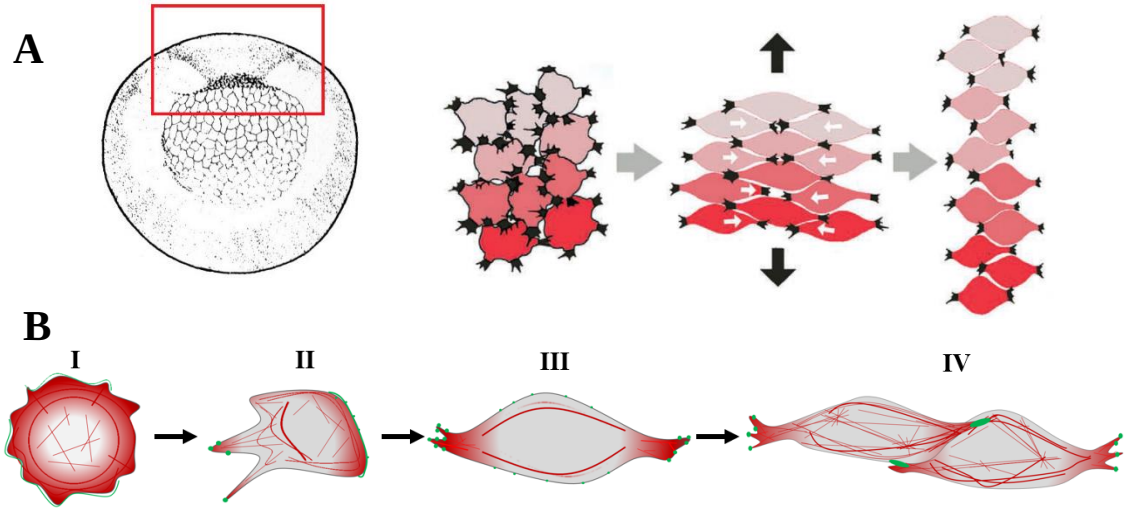

Model Legend: Gastrula cells on the dorsal lip of the embryo are isolated in a dorsal marginal zone explant, which exposes the mesodermal axial and paraxial tissue with the neural tissue on the opposing face. The previously known progression of CE is shown in (A) (modified from R. Keller). My work on the details of this morphogenic movement is shown in (B). Presumptive axial and paraxial cells at St. 10 have an actin cytoskeleton similar to all other cells in the embryo, and display lamellipodial protrusions flowing rearward into a lamellar basket (Phase I). As the cells receive polarity signals, this cytoskeleton rearranges membrane proteins, namely C-Cadherin (green), to bias protrusive activity in the mediolateral axis (Phase II). Expression of a *Xenopus* nonmuscle tropomyosin (Xtm5) and increased Myosin Regulatory Light Chain (MRLC) phosphorylation occurs as the subcortical cytoskeletal structure -the Node and Cable Network (NCN) internal to the TIRF-imaged Cortical Actin Net (TCAN). As convergence force rises in the tissue, MRLC activity increases and the NCN becomes more defined, consisting of transient foci joined by thick bundles of actomyosin (Phase III). The NCN oscillates in the mediolateral direction as lamellipodia extend onto and adhere to neighboring cells, C-Cadherin clusters mature, and the actomyosin machinery contracts, generating mediolaterally oriented tension (Phase IV). In their role as substrates, the cortices of neighboring cells stiffen in response to lamellipodial contact, C-Cadherin adherence and applied tension. Then the cycle repeats with another lamellipodia extending in a different area of the cortex to wedge neighboring cells between each other, causing tissue convergence. While surrounding matrix proteins restrict thickening, the axial tissue extends anterior-posteriorly deforming the round embryo into a tadpole.

The over-arching purpose of my research has been to describe the transition of isodiametric cells of the notochordal mesoderm of the early gastrula into the mediolaterally elongated, contractile cells that actively crawl on and wedge between their neighbors while simultaneously acting as a substrate for neighboring cell crawling. To understand the mechanism of this behavior, known collectively as Mediolateral Intercalation Behavior (MIB), I have focused on three proteins: nonmuscle myosin II (MII), F-actin, and C-Cadherin (C-Cad). I will discuss the major conclusions, present questions they raise, and provide my hypotheses for my working model of CE driven by cell intercalation in *Xenopus laevis*.

I: Myosin Regulation during Convergence and Extension

As discussed in Chapter 2, regulation of myosin is critical for morphogenesis. In *Xenopus*, I studied the nonmuscle MII complex which consists of two heavy chains, two essential light chains and two regulatory light chains. During gastrulation, Myosin Regulatory Light Chain (MRLC) regulates the amount of MII available for CE in two ways- by stabilizing the whole complex and by regulating contractility and force generation.

A. MRLC Controls the Amount of Myosin IIB Available during MIB

Previous work describing the Node and Cable Network (NCN) in *Xenopus* showed that nonmuscle myosin II (MII) is essential for its development and for CE (Skoglund et al, 2008; Kim et al, 2010). However, cells in MII morphants lose cortical integrity and adhesion to their neighbors. As MIB is being established, tissue integrity is

lost as the cells dissociate from one another, as expected from previous work showing that MII functions in cell adhesion (Shewan et al, 2005; Smutny et al, 2010). Therefore MII clearly has several functions, potentially including contractility, organization of adhesion, and organization (cross-linking) of the cytoskeleton, and these experiments (which often led to embryo lethality, Skoglund et al, 2008) did not distinguish between these roles of MII.

I have teased apart MII functions by depleting only one subunit of MII, the MRLC. Biochemically, knockdown of MRLC results in decrease of Myosin II similar to direct knockdown of MII, the cellular and embryonic phenotypes are markedly different. MRLC knockdown results in blastopore closure delay (rather than failure), no loss of cortical integrity, and adhesion to neighboring cells is maintained as the cells do not dissociate from the tissue. I suggest that the lack of MRLC results in a labile MII that fails to promote the maturation of the NCN, and is quickly degraded by the cell if it is not involved in crosslinking and adhesion. From this study, I conclude the cellular levels of MRLC regulates the amount of functional contractile MII present.

Additionally, I observed that exogenous expression of wtRLC mostly rescued the morpholino knockdown, but also had subtle differences than the wild type control embryos. After knockdown of MRLC and rescue with near endogenous expression of wtRLC, higher levels of MII were detected through western blot and immunohistochemistry. However, the wtRLC expressing tissue showed a reduction in the change of force values over time, and the oscillations of the NCN were slower than controls. I propose that when the cells are presented with exogenous wtRLC there is a

change in the assembly of the myosin complex. Extra MRLC message could promote the formation of more MII than controls, or "rescue" of any labile MII resulting from MRLC knockdown. Given the scope of this study, I am unable to determine the exact structure of MII resulting from these perturbations, however the idea that additional myosin expression does not result in increased contractility, highlights an additional level of regulation during CE. The tissue is undoubtedly constantly regulating force production as the mechanical environment changes during CE. It is possible that there is an endogenous pool of myosin protein poised for activation should the tissue require it. I propose that the *Xenopus* embryo endogenously downregulates MII activity during CE, and overexpression of MII results in defects due to the perturbation of the *in vivo* regulation.

B. Myosin Contractility is required for the Maturation of the NCN

Embryonic morphogenesis is driven by spatially and temporally patterned, region-specific cell behaviors that deform local tissue domains (Gerhart and Keller, 1986). Mechanical integration of the forces generated by these domains changes the shape of the embryo. The variety of embryo architectures requires different modes of force generation, different patterns of forces, and different mechanical coupling between cells. CE is a commonly used, regionally autonomous, active force-producing process, and in the *Xenopus* embryo, CE of presumptive axial and paraxial mesoderm is not dependent on a substrate or on forces developed elsewhere (Shih and Keller, 1992; Keller and Danilchick, 1988). Because CE can operate in a tissue-autonomous manner, its

component cells must simultaneously or iteratively generate force, and serve as a substrate upon which that force, generated by other cells, can act.

Due to the rapid oscillations of the NCN, there must be a level of MRLC regulation that is more rapid and dynamic than translation of proteins. MII activity is governed by phosphorylation of the S-19 residue of MRLC (Somlyo and Somlyo, 2003). Multiple kinases have been shown to phosphorylate this residue making kinase targeting an experiment worth investigating in the future (Bresnick, 1999). In this study, I expressed an MRLC that is incapable of being phosphorylated on S19 and thus acts as a phosphonull version of MRLC (pnRLC). In addition to adhesion plaque and cytoskeletal organization defects, the pnRLC-expressing tissue showed decreased force generation. This critical result has led to a correlation between phosphorylation of a single residue with force values. I then focused on correlating the cytoskeletal structure with decreased tissue force to establish an array of cellular phenotypes indicative of decrease in the ability to produce force. The next step to understanding the cellular basis of force production during CE is to measure force at the cellular level, i.e. to place explants on Traction Force Microscopy substrates, or perform Fluorescent Speckle Microscopy on intercalating cells at different stages of CE. Correlations of regional force values with specific F-Actin networks quantify embryonic cell forces to a level previously reached only in isolated cells.

II: Two Cortical Cytoskeletons are Present in Intercalating Cells

I examined the dynamics and organization of the actin cytoskeleton under different perturbations and correlated those changes with alterations in force production and CE.

A: The NCN Structure and Function

I characterized the NCN and classified its development and maturation into four distinct phases, describing the step-wise reorganization of the actin cytoskeleton during MIB. Once matured, the NCN is composed of transient foci of actin (nodes) connected by thicker filament bundles (cables). These cables are contractile and therefore the nodes they connect oscillate in the mediolateral direction as the cells intercalate. These oscillations reflect local disparities in the contractile strength and geometries of the NCN cables, as these cables shorten and generate mediolaterally oriented tensile forces that pull the cells between one another in the "power stroke" of cell intercalation. The iterated extension of protrusions mediolaterally reflects the "reset" phase, in which the cells "get a new grip".

In *Xenopus*, the structure of the NCN is unique to intercalating cells involved in CE and therefore must be linked to the mechanism of force generation. MIB-expressing cells elongate in the mediolateral direction, and thus intercalate between neighbors along the long axis of the cell and contribute to extension in the short axis. From a physical standpoint, this mechanism does not seem to be the most effective or parsimonious way to rapidly narrow and lengthen an array of units, however it is a program that has been

evolutionarily conserved in many vertebrate embryos (Keller, 2002). As the cells crawl between one another, they experience compressive forces in the anterior-posterior axis. Protrusions that extend mediolaterally (as opposed to anterior-posteriorly) therefore have more area to crawl on cell "substrate" and to counteract the compressive forces. The combination of these forces results in shape change as mediated by the actin cytoskeleton. As the MIB-expressing cells confine their lamellipodial protrusions to one axis, the cytoskeleton remodels into tangential arcs on the anterior and posterior faces, limiting protrusive activity in this axis and creating a stiffer area on which neighboring cells can crawl (Kolega, 1986; Katsumi et al, 2002) Why does tension rearrange the cables into the NCN pattern, rather than the linear stress-fiber-like bundles which have been correlated in culture with increased force (Burridge and Wittchen, 2013; Beningo et al, 2001; Lo et al, 2004; Vicente-Manzares et al 2007).

Unlike cultured fibroblasts, which have more or less linear contractile cables between leading edge adhesions and trailing edge adhesions to the substratum, intercalating cells have multiple attachment sites, some at the lamellar regions behind the lamellipodia, acting as tractional devices, and some along the anterior and posterior sides, acting as substrates. At any given point, a MIB-expressing cell may be shortening as contraction wedges it between neighbors or elongating to extend protrusions. The cells must serve as both a substrate and an active agent of elongation. To accommodate all of these activities in one cell, the cortical actin network must consist of multiple local compartments. The NCN cables connecting nodes integrates the tractional and substrate functions of the cytoskeleton. I propose that the nodes represent a local collection of

forces, stiffening that particular area while another area of the cell consists of more protrusive actin. In this way, a single cell has both regions of contractility and extension. If the actin was organized as linear bundles from one end to the other, this would limit the dynamic capability of a cell to respond, as a substrate, to neighboring cells at various angles. By expressing an NCN, contractile actin is compartmentalized and can accommodate multiple behaviors simultaneously.

Previous studies have identified the NCN as a necessary structure for *Xenopus* CE (Skoglund et al, 2008; Kim et al, 2010), but I have begun to understand how and why this structure is necessary. In addition to the correlations with force values mentioned above, a key experiment in my studies was the total ablation of the NCN by knocking down the structural protein XTm5. This experiment did not result in loss of myosin protein or phosphorylation of MRLC, however it did result in severe defects in CE. These results highlight the importance of the presence of the NCN without perturbing myosin levels directly. The cellular perturbations were subtle, XTm5 morphant cells do not show changes in bipolar protrusive activity, size, or adhesion within the tissue, but nevertheless do not extend to the same extent as controls. My results indicate that Tm5 is necessary to promote myosin function and that force generation requires more than just cellular expression of MRLC-P.

B: The Structure and Possible Functions of the TCAN

In Chapter 3, I described the structure, movement, and regulation of a second actin cytoskeleton viewed using Total Internal Reflection Fluorescence Microscopy (TIRFM). As opposed to the NCN which only appears in intercalating cells, the TIRF-imaged Cortical Actin Net (TCAN) is, to a first approximation, ubiquitously expressed in the *Xenopus* embryo. The NCN is a rapidly remodeled and active F-actin network used to produce sufficient force to physically change the shape of a major part of the embryo. In theory, the rapid movements and large displacements of actin structures during intercalation would result in areas of a cell that are stiff and some that are less stiff. I suggest that the TCAN is maintained to ensure cortical integrity and stiffness required to prevent cell rupture. From my perspective, it seems odd that the embryonic cells would maintain two actin organizations that are spatially close but significantly different in both behavior and regulation. I propose that the NCN serves a highly specialized function in force generation while the TCAN is present to promote tissue cohesion and cortical integrity. In Chapter 3 I suggested functions for the TCAN, including this role of cortical integrity and surface tension.

Additional possibilities for the function of the flowing movement of the TCAN are that it functions to rearrange Planar Cell Polarity (PCP) proteins, some of which have been reported to be polarized (Yin et al, 2008). Preliminary experiments involving knockdown of PCP proteins shows a cessation of TCAN movement, but continued embryonic development (Vangl MO in collaboration with Dr. Ann Sutherland and Dr. Ray Keller). In addition to examining the movements of the TCAN in the absence of PCP

proteins, it is important to look at the movement of the TCAN, if it is present, in isolated cells to test if the TCAN can promote cell motility in the absence of the NCN.

III: C-Cadherin Transmits Actomyosin-generated Forces, Driving CE

In concordance with the model of cell-on-cell traction driving intercalation, I showed that C-Cadherin acts as the adhesion complex that translates contractile force between cells during *Xenopus* CE. While both integrin-matrix adhesions and other cell-cell adhesions play a role in intercalation, C-Cad dynamics are influenced by and respond to actomyosin forces. From this I conclude that C-Cad is the dominant protein complex involved in transmitting force from one cell to another. Isolated contractions of the actomyosin network do not by themselves promote intercalation, the cells migrate on a substrate, and in the case of *Xenopus* CE the substrate is predominantly other cells. Coincident imaging of the actin cytoskeleton and C-Cad dynamics using Laser Scanning Confocal Microscopy (LSCM) (Ch. 2) and Total Internal Reflection Fluorescence Microscopy (TIRFM) (Ch. 3, 3A) show a coordinated and progressive development and localization of F-actin and C-Cad complexes. Isodiametric cells display diffuse C-Cad localization consistent with tissue cohesion, but as cells reorganize their cortical cytoskeleton during MIB, the C-Cad localizes as dense plaques associated with protrusions on neighboring cells. Additionally, C-Cad dynamics are modulated by contractility of cortical myosin; pnRLC-expressing cells maintain small adhesion plaques and minimal rearrangement, coincident with decreased contractility compared to controls.

The key experiment in my studies was expression of a presumably constitutively active form of C-Cadherin (caC-Cad). In these embryos, the thickening of F-Actin cables, the exaggerated elongation of cell shape, and the CE defects provide evidence for the importance of C-Cad dynamics during intercalation. Previous studies have shown a reduction of adhesive activity of C-Cad during gastrulation, but my studies address the kind of phenotypes associated with an adhesion that is not dynamic (Zhong et al, 1999).

As mentioned previously, dynamic fibronectin (FN) and integrin binding is necessary for CE and FN fibrillogenesis increases progressively, coincident with increasing tensile forces in intercalating cells (Davidson et al, 2008). If FN fibrillogenesis is blocked however, there is little effect on CE (Rozario et al, 2009). Integrin signaling is necessary for initial polarization of MIB-expressing cells; blocking integrin activation prevents bipolarity and superactivating integrins with Manganese blocks protrusive activity (Marsden et al, 2006). Additionally, FN deposition at the developing notochord-somite boundary results in embryo lengthening during vacuolization of the fiber-wound hydrostat that is the notochord (Adams et al, 1990). I argue that the integrin-FN adhesions play a role in signaling and tissue separation, rather than force transmission between cells. However, given the data from the caC-Cad expression, a critical future experiment would be to create a constitutively active α5β1 integrin to test if the effects of preventing FN-integrin turnover results in similar cell lengthening and F-actin cable thickening. While placing embryos on a stiff substrate mimics a loss of FN dynamics, the cellular response has yet to be fully characterized. The data from this experiment would

highlight the role of the *in vivo* stiffness, resolving some debated issues about the behavior of explants on BSA-coated glass.

IV: Combined Imaging Techniques Are a Useful Tool for examining *in vivo* Development

All imaging techniques have limitations when it comes to watching live embryo development. That being said, the technology available nowadays has revolutionized imaging development, but it is important for developmental biologists to understand the specified function of each system before designing an experiment. The breakthroughs in superresolution microscopy have generated much excitement for biologists, but not every project calls for high resolution microscopy or even fluorescence, when the question can be answered by focusing on the embryonic movements, rather than the technology.

Vertebrate embryos that develop outside of the mother contain yolk proteins to support development. In both laser-based and arc-lamp-based illumination systems, the presence of paracrystalline arrays of yolk protein results in reflection and refraction, leading to a high background signal. In non-fluorescence studies, this is an advantage. Instead of passing light through the opaque *Xenopus* embryo, low-angle epi-illumination enhances the differences in the topography of the surface of explants and can be filmed with a standard video camera. The low energy of the incandescent light bulb promotes embryo survival and long-time lapse acquisition. The techniques of Differential Interference Contrast Microscopy (DIC) and Phase Microscopy use the principle of

slower light speeds through samples of different refractive indices. Additionally, these microscopy techniques have benefited from the development of EMCCD cameras with 16-bit depths, increasing the dynamic range of signal. As such, one can obtain a clear image of the tissue at a lower magnification and faster acquisition time. These methods have been critical in examining the normal cell behaviors of tissue development and have provided biologists with data to analyze for years (see Shih and Keller, 1992).

Fluorescence microscopy is critical in the sub-cellular resolution of proteins. Antibody-specific labeling, or plasmid expression of fluorescently labeled proteins increases the avidity of the label and allows for study of a single complex within a cell. Due to the ubiquitous expression of many of the proteins I have studied and the thickness of the tissue I study, illumination of the embryo using a standard compound scope does not provide accurate localization data. Microscopic techniques using limited illumination (light sheet microscopy, total internal reflection) or limited detection (confocal microscopy) increase the signal to noise ratio, increasing resolution over fluorescence wide-field imaging. LSCM creates an optical section by removing out of focus light with the pinhole aperture before the detector. However, it is important to remember that this is an optical section, the entire embryo is still subjected to high powered laser light as the system rasters through the field of view which can result in an increased rate of bleaching and phototoxicity in the embryo. The resolution is achieved after excitation of fluorophores rather than before light incidence on the sample.

TIRFM and Light-sheet based systems circumvent these problems by limiting the amount of laser light on the sample. However, light sheets have proved inefficient for

imaging *Xenopus* development due to the opacity of the samples and the limited depth of penetration of the light sheet. TIRFM-imaging is difficult in *Xenopus* due to the constant movement of the tissue, including within the TIRF plane. It becomes hard to distinguish whether movements seen are moving within the cell, or whether the embryo is moving with respect to the objective.

In the case of *Xenopus* development, the size of the embryo and the presence of yolk in all cells (unlike in zebrafish or chick where the zygote develops on top of a yolk filled sac) further limits the depth of imaging. Multiphoton imaging uses a wavelength of light twice as long as standard visible light which means these wavelengths carry more energy and as a result the yolk platelets absorb heat, causing embryo lethality.

Super-resolution systems break the Rayleigh criterion of the resolution of two points of light, allowing for clearer images at higher magnifications. These techniques are revolutionary in the optics field and the mechanism of super-resolution comes in several varieties. Structured Illumination (SIM) systems are a modification of a widefield scope in that a known pattern is placed over the sample and turned slightly during each subsequent image acquisition, and post-imaging, is deconvolved into a single image. This process necessitates illumination of the entire sample and prolonged image acquisition as multiple pictures are taken at the same field of view, not beneficial for imaging the rapid movements of the *Xenopus* cytoskeleton. Stimulated Emission Depletion (STED) microscopy involves excitation of a fluorophore and subsequent bleaching of fluorophores surrounding the desired Region of Interest (ROI). Similar to Multiphoton microscopy, the involvement of high powered long wavelengths of light result in

Xenopus embryo lethality. PALM/STORM microscopy systems function by pulsed activation of specialized fluorophores, which requires a new generation of molecular tools incorporating these fluorophores instead of conventional fluorophores readily available. These microscope advances are important to developmental biology and can produce accurate data, as long as the scope of the experiment and the purpose of these systems is analyzed before imaging.

In addition to multiple modes of image acquisition, I have combined image analysis techniques to glean information about the molecular dynamics during CE. Preliminary FRET-based analysis of proteins associated with both the TCAN and C-Cad provides additional quantitative assessment of the proximity of two proteins rather than standard co-localization. Overall, the current state of imaging technology has much to offer in terms of benefits in spite of several limitations, when it comes to imaging live embryo development. While there is no perfect system for imaging *Xenopus* embryos, I argue that one can get a holistic view of development by applying combinations of imaging, processing, and analysis techniques. The combination of techniques reveals different perspectives and prevents over-interpretation of data. The *Xenopus* embryo offers a system to study a host of different developmental processes but does come with the added challenge of visualizing embryonic movements in a spherical, opaque, and large embryo. I trust that future advances in optics and imaging modalities will further our understanding of the embryonic movements during development.

V: Conclusions

I have elucidated the roles of several ubiquitously expressed and highly conserved proteins during Convergence and Extension: myosin, actin, and C-Cadherin. Myosin contractility generates force during cell intercalation that pulls and wedges neighboring cells between themselves and as a result deforms the overall shape of the embryo. Myosin and actin crosslinking is required to maintain cortical integrity and increase stiffness of cells as they change shape during MIB, and accommodate the iterative cycles of contraction and extension. C-Cadherin is the main protein complex that responds to increasing forces generated during CE and transmits force over several cell diameters. These contractions are coincident with increasing overall tissue stiffness. The cellular behaviors and tissue properties during CE are dynamic and dependent on the combination of many proteins. My research has further teased apart the requirements of actomyosin regulation, organization, and C-Cadherin dynamics during morphogenesis.

References:

Adams, D., Keller, R. E., and Koehl, M. A. R. 1990. The mechanics of notochord elongation, straightening, and stiffening in the embryo of *Xenopus laevis*. *Development* 110, 115-130.

Beningo, K. A., Dembo, M., Kaverina, I., Small, J. V. and Wang, Y. L. 2001. Nascent focal adhesions are responsible for the generation of strong propulsive forces in migrating fibroblasts. *J Cell Biol* 153, 881-888.

Bertet C, Sulak L and Lecuit T. 2004. Myosin-dependent junction remodeling controls planar cell intercalation and axis elongation. *Nature* 429:667-671

Bjerke, M. A., Dzamba, B. J., Wang, C. and DeSimone, D. W. 2014. FAK is required for tension-dependent organization of collective cell movements in Xenopus mesendoderm. *Dev. Biol.* 394, 340-356.

Blanchoin L, Boujemaa-Paterski R, Sykes C, Plastino J. 2014. Actin dynamics, architecture, and mechanics in cell motility. *Physiol. Rev.* 94(1): 235-263

Blankenship J, Backovic S, Weitz J, Zallen J. 2006. Multicellular rosette formation links planar cell polarity to tissue morphogenesis. *Dev. Cell* 11(4):459-470

Bonacci, G., Fletcher, J., Devani, M., Dwivedi, H., Keller, R., and Chang, C. 2012. The cytoplasmic tyrosine kinase Arg regulates gastrulation via the control of actin organization. *Dev. Biol.* 364, 42-55.

Brieher, W. M. and Gumbiner, B. M. 1994. Regulation of C-cadherin function during activin induced morphogenesis of *Xenopus* animal caps. *J. Cell Biol.* 126, 519-527.

Buisson, N., Sirour, C., Moreau, N., Denker, E., Le Bouffant, R., Goullancourt, A., Darribere, T. and Bello, V. 2014. An adhesome comprising laminin, dystroglycan and myosin IIA is required during notochord development in Xenopus laevis. *Development* 141, 4569-4579.

Bresnick A. Molecular mechanisms of nonmuscle myosin-II regulation. 1999. *Curr. Op. Cell Biol.* 11 26-33

Bryce N, Schevzov G, Ferguson V, Percival J, Lin J, Matsumara F, Bamburg J, Jeffrey P, Hardeman E, Gunning P, Weinberger R. 2003. Specification of actin filament function and molecular composition by tropomyosin isoforms. *MBoC* 14:1002-1016.

Bulik D, Wei G, Toyoda H, Kinoshita-Toyoda, A, Waldrip, W.R, Esko, J, Robbins, P., Selleck S. 2000. sqv-3, -7, and -8, a set of genes affecting morphogenesis in *Caenorhabditis elegans*, encode enzymes required for glycosaminoglycan biosynthesis. *PNAS* 97.20: 10838-10843.

Burridge K, Feramisco JR. 1981. Non-muscle α-actinins are calcium-sensitive actin binding proteins. *Nature* 294:565-567

Burridge K, and Wittchen E. 2013. The tension mounts: stress fibers as force-generating mechanotransducers. *JCB.* 200: 9-19

Cai, D., Chen, S. C., Prasad, M., He, L., Wang, X., Choesmel-Cadamuro, V., Sawyer, J. K., Danuser, G. and Montell, D. J. 2014. Mechanical feedback through E cadherin promotes direction sensing during collective cell migration. *Cell* 157, 1146-1159.

Chen B-C, Legant W, Wang K, Shao L, Milkie D, Davidson M, Janetopoulos C, Wu X, Hammer JA, Liu Z, English B, Mimori-Kiyosue Y, Romero D, Ritter A, Lippincott-Schwartz J, Fritz-Laylin L, Mullins RD, Mitchell D, Bembenek J, Reymann A-C, Bohme R, Grill S, Wang J, Seydoux G, Tulu US, Kiehart D, Betzig E. 2014. Lattice Light-sheet microscopy: imaging molecules to embryos at high spatiotemporal resolution. *Science* 346(6208):1257998

Cloney RA. 1966. Cytoplasmic filaments and cell movements: epidermal cells during ascidian metamorphosis. *J Ultrastruct Res* 14(3):300-328

Cote G. 1983. Structural and functional properties of the non-muscle tropomyosins. *Mol Cell Biochem* 57:127-146.

Dale L, Slack JM. 1987. Fate map for the 32-cell stage of *Xenopus* laevis. *Development* 99:527-551

Dalcq AM. Form and Causality in Early Development (1938). Cambridge University Press, Great Britain.

Danuser G, Waterman-Storer CM. 2006. Quantitative fluorescent speckle microscopy of cytoskeleton dynamics. *Ann. Rev. Biophys. Biomol. Struct*. 35:361-387

Davidson, L. and Keller, R. 2007. Measuring forces and mechanical properties of embryonic tissues. In *Cell Mechanics* (Wang, Y.L., and Discher, D. eds.) Elsevier/Academic Press. pp. 425-439.

Davidson, L., and Keller, R. 2001. Basics of a light microscopy imaging system and its application in biology. In *Methods in Cellular Imaging* (Periasamy, A. ed.) Am. Physiol. Soc. Book Series. Oxford University Press, New York.

Davidson, L. A., Keller, R. and DeSimone, D. W. 2004. Assembly and remodeling of the fibrillar fibronectin extracellular matrix during gastrulation and neurulation in *Xenopus laevis*. *Dev Dyn* 231, 888-895.

Davidson, L. A., Marsden, M., Keller, R. and Desimone, D. W. 2006. Integrin α5β1 and fibronectin regulate polarized cell protrusions required for *Xenopus* convergence and extension. *Curr. Biol.* 16, 833-844.

Davidson LA, Dzamba BD, Keller R, Desimone DW. 2008. Live imaging of cell protrusive activity, and extracellular matrix assembly and remodeling during morphogenesis in the frog, *Xenopus laevis*. *Dev Dyn.* 237, 2684-92.

Davidson, L.A., Keller, R. and DeSimone, D.W. 2004. Patterning and tissue movements in a novel explant of the marginal zone of *Xenopus laevis*. *Gene Expr Pat* 4: 457-466.

Davidson, L.A., Keller, R. and DeSimone, D.W. 2004. Assembly and remodeling of fibrillar fibronectin extracellular matrix during gastrulation and neurulation in *Xenopus laevis*. *Dev. Dyn.*, 231, 888-895.

Davidson, L., Hoffstrom, B., Keller, R., and DeSimone, D. 2002. Mesendoderm extension and mantle closure during *Xenopus laevis* gastrulation: combined roles for integrin α5β1, fibronectin and tissue geometry. *Dev. Biol.* 242,109-129.

Delorme V, Machacek M, DerMardirossian C, Anderson KL, Wittmann T, Hanein D, Waterman-Storer C, Danuser G, Bokoch GM. 2007. Cofilin activity downstream of Pak1 regulates cell protrusion efficiency by organizing lamellipodium and lamella actin networks. *Dev Cell* 13(5):646-662

Dzamba B, Jakab K, Marsden M, Schwartz M, DeSimone D. 2009. Cadherin adhesion, tissue tension, and noncanonical Wnt signaling regulate fibronectin matrix organization. *Dev. Cell* 16 421-432

Elul, T. and Keller, R. 2000. Monopolar protrusive activity: a new morphogenic cell behavior in the neural plate dependent on vertical interactions with the mesoderm in *Xenopus Dev. Biol.* 224, *3-19.*

Elul, T., Koehl, M. and Keller, R. 1997. Cellular mechanism underlying neural convergent extension in *Xenopus laevis* embryos. *Dev. Biol.* 191, 243-258.

Ettensohn C. 1984. Primary invagination of the vegetal plate during sea urchin gastrulation. *Am. Zoologist* 24(3):571-588

Fehon R, McClatchey A, Bretscher A. 2010. Organizing the cell cortex: the role of ERM proteins. *Nat. Rev. Mol. Cell. Biol.* 11(4): 276-287

Fernandez-Gonzalez, R. and Zallen, J. A. 2011. Oscillatory behaviors and hierarchical assembly of contractile structures in intercalating cells. *Phys. Biol.* 8, 045005.

Firmino J, Rocancourt D, Saadaoui M, Moreau C, Gros J. 2016. Cell division drives epithelial cell rearrangements during gastrulation in chick. *Dev. Cell* 8;36 (3):249-261

Fristrom D, Fristrom JW. 1975. The mechanism of evagination of imaginal discs of *Drosophila melanogaster* 1: General considerations. *Dev Biol* 43:1, 1-23

Fritzsche M, Lewalle A, Kuke T, Kruse K, Charras G. 2013. Analysis of turnover dynamics of the submembranous actin cortex. *MBoC* 24 757-767

Fulga, T. A. and Rorth, P. 2002. Invasive cell migration is initiated by guided growth of long cellular extensions. *NCB* 4, 715-719.

Gaillard C, Theze N, Hardy S, Allo M-R, Ferrasson E, Thiebaud P. 1998. Alpha tropomyosin gene expression in *Xenopus* laevis: differential promoter usage during development and controlled expression by myogenic factors. *Dev Genes Evol* 207:435-445.

Gally C, Wissler F, Zahreddine H, Quintin S, Landmann F, Labouesse M. 2009. Myosin II regulation during *C.elegans* embryonic elongation: LET-502/ROCK, MRCK 1 and PAK-1, three Kinases with different roles. *Development* 136 3109-3119

Geisbrecht, E. R. and Montell, D. J. 2002. Myosin VI is required for E-cadherin mediated border cell migration. *NCB* 4, 616-620.

Gerhart J, and Keller R. 1986. Region-specific cell activities in amphibian gastrulation. *Ann Rev of Cell Biol* 2.1: 201-229

Glickman, N. S., Kimmel, C. B., Jones, M. A. and Adams, R. J. 2003. Shaping the zebrafish notochord. *Development* 130, 873-887.

Gong Y, Mo C, Fraser S. 2004. Planar cell polarity signaling controls cell division orientation during zebrafish gastrulation. *Nature* 430(7000):689-693

Goto, T. and Keller, R. 2002. The planar cell polarity gene strabismus regulates convergence and extension and neural fold closure in *Xenopus*. *Dev. Biol*. 247, 165-181.

Goto, T., Davidson, L., Asashima, M. and Keller, R. 2005. Planar cell polarity genes regulate polarized extracellular matrix deposition during frog gastrulation. *Curr Biol*. 15, 787-793.

Gottardi C, Wong E, Gumbiner B. 2001. E-cadherin suppresses cellular transformation by inhibiting Beta-catenin signaling in an adhesion-independent manner. *J. Cell. Biol.* 153(5):1049-1060

Gumbiner, BM. 2005. Regulation of cadherin-mediated adhesion in morphogenesis. *Nature Rev. Mol. Cell. Biol.* 6: 622-634

Gunning P, Schevzov G, Kee A, Hardeman E. 2005. Tropomyosin isoforms: divining rods for actin cytoskeletal function. *Trends in Cell Biol.* 15 (6) 333-341

Gunning P, O'Neill G, Hardeman E. 2008. Tropomyosin-based regulation of the actin cytoskeleton in time and space. *Physiol. Rev*. 88: 1-35

Gupton SL, Anderson KL, Kole TP, Fischer RS, Ponti A, Hitchcock-DeGregori SE, Danuser G, Fowler VM, Wirtz D, Hanein D, Waterman-Storer CM. 2005. Cell migration without a lamellipodium- translation of actin dynamics into cell movement mediated by tropomyosin. *J Cell Bio*. 168 (4): 619-631

Hardin J and Chen L. 1986. The mechanisms and mechanics of archenteron elongation during sea urchin gastrulation. *Dev Biol.* 115:490-501

Hardy S, Fiszman M, Osborne B, Theibaud P. 1991. Characterization of muscle and nonmuscle *Xenopus* laevis Tropomyosin mRNAs Transcribed from the Same Gene. *Eur J Biochem*. 202 431-440

Harris, A. K., Wild, P. and Stopak, D. 1980. Silicone rubber substrata: a new wrinkle in the study of cell locomotion. *Science* 208, 177-179.

Hathaway DR, Adelstein RS. 1979 Human platelet myosin light chain kinase requires the calcium-binding protein calmodulin for activity. *PNAS* 76:4, 1653-1657

Hayakawa K, Tatsumi H, Sokabe M. 2007. Actin stress fibers transmit and focus force to activate mechanosensitive channels. *J. Cell. Sci.*121 496-503

He, B., Doubrovinski, K., Polyakov, O. and Wieschaus, E. 2014. Apical constriction drives tissue-scale hydrodynamic flow to mediate cell elongation. *Nature* 508, 392-396.

He, L., Wang, X., Tang, H. L. and Montell, D. J. 2010. Tissue elongation requires oscillating contractions of a basal actomyosin network. Nature cell biology 12, 1133-1142.

Hind, L. E., Dembo, M. and Hammer, D. A. 2015. Macrophage motility is driven by frontal-towing with a force magnitude dependent on substrate stiffness. Integrative biology: quantitative biosciences from nano to macro 7, 447-453.

Holtfreter, J., 1946. Structure, motility and locomotion in isolated embryonic amphibian cells. *J. Morph.*, *79*(1): 27-62.

Holtfreter, J., 1943. A study of the mechanics of gastrulation. Part I. *J. Exp. Zool.*, *94*(3): 261-318.

Ito M, Nakano T, Erdodi F, Hartshorne DJ. 2004. Myosin phosphatase: structure, regulation and function. *Mol Cell Biochem*. 259, 197-209

Jacobson A, Oster G, Odell G, Cheng L. 1986. Neurulation and the cortical tractor model for epithelial folding. *J. Embryol. Exp. Morph*. 96:19-49.

Katsumi A, Milanini J, Kiosses W, del Pozo M, Kaunas R, Chien S, Hahn K, Schwartz M. 2002. Effects of cell tension on the small GTPase Rac. *J Cell Biol* 158(1): 153-164.

Keller, R. 1980. The cellular basis of epiboly: and SEM study of deep-cell rearrangement during gastrulation in *Xenopus laevis. J Embryol Exp Morphol* 60:201-234

Keller, R. E. and Danilchik, M. 1988. Regional expression, pattern and timing of convergence and extension during gastrulation of *Xenopus laevis*. *Development* 103, 193-209.

Keller, R. E. and Tibbetts, P. 1989. Mediolateral cell intercalation in the dorsal axial mesoderm of *Xenopus laevis. Dev. Biol.*, 131, 539-549

Keller, R. E., Cooper, M., Danilchik, M., Tibbetts, P. and Wilson, P. 1989. Cell intercalation during notochord development in *Xenopus laevis*. *J. Exp. Zool.* 251, 134-154.

Keller, R., Shih, J., and Sater, A. 1992. The cellular basis of the convergence and extension of the *Xenopus* neural plate. *Dev. Dyn* 193, 199-217.

Keller, R., Shih, J., Sater, A., and Moreno, C. 1992. Planar induction of convergence and extension of the neural plate by the organizer of *Xenopus. Dev.Dyn.* 193, 218-234.

Keller, R., Shih, J. and Domingo, C. 1992. The patterning and functioning of protrusive activity during convergence and extension of the Xenopus organiser. *Development*, 81-91.

Keller, R., Davidson, R., Edlund, A., Elul, T., Ezin, M., Shook, D., and Skoglund, P. 2000. Mechanisms of convergence and extension by cell intercalation. *Phil. Trans. R. Soc. Lond.* B 355, 897-922.

Keller, R. 2002. Shaping the vertebrate body plan by polarized embryonic cell movements. *Science* 298, 1950-1954.

Keller, R., Davidson, L., and Shook, D. 2003. How we are shaped: the biomechanics of gastrulation. *Differ.*71, 171-205.

Keller, R. 2006. Mechanisms of elongation in embryogenesis. *Development*, 133, 2291-2302.

Keller, R., Shook, D., and Skoglund, P. 2008. The forces that shape the embryo: physical aspects of convergent extension by cell intercalation. *Phys. Biol.* 5, 015007 (23 pp) (E-pub, Apr 9)

Keller, R. and Shook, D. 2011. The bending of cells sheets- from folding to rolling. *BMC Biology* 9, 90.

Keller, R. 2012. Physical biology returns to morphogenesis. *Science* 338, 201-203.

Kim HY and Davidson L. 2010. Punctuated actin contractions during convergent extension and their permissive regulation by the non-canonical Wnt-signaling pathway. *J Cell Sci*. 124 635-646

Kolega J. 1985. The cellular basis of epithelial morphogenesis. *Dev. Biol*. 2:103-143

Kolega J. 1986. Effects of mechanical tension on protrusive activity and microfilament and intermediate filament organization in an epidermal epithelium moving in culture. *J Cell Biol.* 102(4):1400-11

Kwan K and Kirschner M. A 2005. Microtubule-binding Rho-GEF controls cell morphology during convergent extension of *Xenopus laevis*. *Development* 132 4599-4610

Lane, C. and Keller, R. 1997. Microtubule disruption reveals that Spemann's organizer is subdivided into two domains by the vegetal alignment zone. *Development* 124, 895-906.

Laporte D, Ojkic N, Vavylonis D, Wu J-Q. 2012. A-actinin and fimbrin cooperate with myosin II to organize actomyosin bundles during contractile-ring assembly. *MBoC* 23:3094-3110.

Lazarides E. 1976. Actin, a-actinin, and tropomyosin interaction in the structural organization of actin filaments in nonmuscle cells. *J. Cell Biology* 68:202-219

Lee, C. H. and Gumbiner, B. M. 1995. Disruption of gastrulation movements in *Xenopus* by a dominant-negative mutant for C-cadherin. *Dev Biol* 171, 363-373.

Lengyel JA, Iwaki D. 2002. It takes guts: the *Drosophila* hindgut as a model system for organogenesis. *Dev. Biol*. 243(1):1-19

Levayer R, Lecuit T. 2013. Oscillation and polarity of E-cadherin asymmetries control actomyosin flow patterns during morphogenesis. *Dev. Cell* 26 162-175

Levayer R and Lecuit T. 2012. Biomechanical regulation of contractility: spatial control and dynamics. *Trends in cell biology* 22.2: 61-81.

Liu, Z., Tan, J., Cohen D., Yang, M., Yang, M., Sniadeki, N., Ruiz, S., Nelson, C., Chen, C. 2010. Mechanical tugging force regulates the size of cell-cell junctions. *PNAS* 107, 9944-9949.

Lo, C. M., Buxton, D. B., Chua, G. C., Dembo, M., Adelstein, R. S. and Wang, Y. L. 2004. Nonmuscle myosin IIb is involved in the guidance of fibroblast migration. *MBoC* 15, 982-989.

Lo, C. M., Wang, H. B., Dembo, M. and Wang, Y. L. 2000. Cell movement is guided by the rigidity of the substrate. *Biophysical journal* 79, 144-152.

Luther, P. W. B., R.J. 1989. Formaldehyde-amine fixatives for immunocytochemistry of cultured *Xenopus* myocytes. *J of Histo and Cyto* 37, 75-82.

Markova O, Lenne P-F. 2012. Calcium signaling in developing embryos: focus on the regulation of cell shape changes and collective movements. *Semin Cell Dev Biol*

Martin A. 2010. Pulsation and stabilization: contractile forces that underlie morphogenesis. *Dev. Biol*. 341 114-125

Maruthamuthu V, Aratyn-Schaus Y, Gardel M. 2010. Conserved F-actin dynamics and force transmission at cell adhesions. *Curr Op. Cell Biol*. 22 583-588

Melby A, Warga R, Kimmel CB. 1996. Specification of cell fates at the dorsal margin of the zebrafish gastrula. *Development* 122(7):2225-2237

Meyer T, Collins S. 2009. Calcium flickers lighting the way in chemotaxis. *Dev. Cell* 16 160-161

Miyamoto D. 1985. Formation of the notochord in living ascidian embryos. *Development* 86:1-17.

Mizutani T, Haga H, Koyama Y, Takahashi M, Kawabata K. 2006. Diphosphorylation of the myosin regulatory light chain enhances the tension acting on stress fibers in fibroblasts. *J. Cell Phys.* 209:726-731

Moore, S., Keller, R., and Koehl, M. 1995. The dorsal involuting marginal zone stiffens anisotropically during its convergent extension in the gastrula of *Xenopus laevis*. *Development* 121, 3131-3140.

Moore, S. W. 1994. A fiber optic system for measuring dynamic mechanical properties of embryonic tissues. *IEEE Transactions on Biomedical Engineering* 41, 45-50.

Mori M, Monnier N, Daigle N, Bathe M, Ellenberg J, Lenart P. 2011. Intracellular transport by anchored homogenously contracting F-actin meshwork. *Curr. Biol* 21:606-611.

Morgan, T. H. 1894. "The Formation of the Embryo of the Frog." *Anat. Anz* 9.

Munro, E., Nance, J. and Priess, J. R. 2004. Cortical flows powered by asymmetrical contraction transport PAR proteins to establish and maintain anterior-posterior polarity in the early *C. elegans* embryo. *Dev Cell* 7, 413-424.

Nagafuchi A, Ishihara S, Tsukita T. 1994. The roles of catenins in the cadherin-mediated cell adhesion: functional analysis of E-Cadherin- α-catenin fusion molecules. *J. Cell. Biol* 127(1):235-245

Needham J. 1959. A History of Embryology. Issue 374 *CUP Archive* 1-303.

Ohashi T and Erickson H. 2005. Domain unfolding plays a role in superfibronectin formation. *J Biol Chem* 280:39143-51

Ostap E-M. 2008. Tropomyosins as discriminators of myosin function. *Adv Exp Med Biol* 644:273-282

Oster G. 1984. On the crawling of cells. *J. Embryol. Exp. Morph*. 83:329-364

Ostrow B, Chen P, Chisholm R. 1994. Expression of a myosin regulatory light chain phosphorylation site mutant complements the cytokinesis and developmental defects of *Dictyostelium* RMLC null cells. *J. Cell Biol*. 127:6 1945-1955

Otley C, Carpen O. 2004. Alpha-actinin revisited: a fresh look at an old player. *Cell Motility and the Cytoskeleton* 58:104-111

Pare A, Vichas A, Fincher C, Mirman Z, Farrell D, Mainieri A, Zallen J.2014. A positional Toll-receptor code directs convergent extension in *Drosophila*. *Nature* 515:523-527

Park, I., Han, C., Jin, S., Lee, B., Choi, H., Kwon, J. T., Kim, D., Kim, J., Lifirsu, E., Park, W. J., et al. (2011). Myosin regulatory light chains are required to maintain the stability of myosin II and cellular integrity. *The Biochemical journal* 434, 171-180.

Parsons JT, Horwitz AR and Schwartz MA. 2010. Cell adhesion: integrating cytoskeletal dynamics and cellular tension. Nature Rev. *Mol. Cell. Biol*. 11:633-643

Pavalko F, Burridge K. 1991. Disruption of the actin cytoskeleton after microinjection of proteolytic fragments of α-actinin. *JCB* 114:3 481-491.

Periasamy, A., Skoglund, P., Noakes, C., and Keller, R. 1999. An evaluation of two-photon excitation versus confocal and digital deconvolution fluorescence microscopy imaging in *Xenopus* morphogenesis. *Microscopy Research and Technique* 47, 172-181

Pfister K, Shook D, Chang C, Keller R, Skoglund P. 2016. Molecular model for force production and transmission during vertebrate gastrulation. *Development*: 143 (4): 715-727

Pittenger M, Kazzaz J, Helfman D. 1994. Functional properties of non-muscle tropomyosin isoforms. *Curr Biol*. 6:96-104

Ponti A, Machacek M, Gupton SL, Waterman-Storer CM, Danuser G. 2004. Two distinct actin networks drive the protrusion of migrating cells. *Science* 305(5691):1782 1786

Poznanski, A. and Keller, R. 1997. The role of planar and early vertical signaling in patterning the expression of Hoxb-1 in *Xenopus*. *Dev Biol* 184, 351-366.

Rauzi, M., Lenne, P. F. and Lecuit, T. 2010. Planar polarized actomyosin contractile flows control epithelial junction remodelling. *Nature* 468, 1110-1114.

Rolo A, Skoglund P, Keller R. 2009. Morphogenetic movements driving neural tube closure in *Xenopus* require myosin IIB. *Dev Biol*. 327, 327-338.

Rozario, T., Dzamba, B., Weber, G. F., Davidson, L. A. and DeSimone, D. W. 2009. The physical state of fibronectin matrix differentially regulates morphogenetic movements *in vivo*. *Dev Biol* 327, 386-398.

Sabass B, Gardel ML, Waterman CM, Schwarz US. 2008. High resolution traction force microscopy based on experimental and computational advances. *Biophys. J.* 94(1):207-220

Sater, A. K., Steinhardt, R. A. and Keller, R. 1993. Induction of neuronal differentiation by planar signals in Xenopus embryos. *Dev Dyn* 197, 268-280.

Sawyer, J. K., Harris, N. J., Slep, K. C., Gaul, U. and Peifer, M. 2009. The *Drosophila* afadin homologue Canoe regulates linkage of the actin cytoskeleton to adherens junctions during apical constriction. *JCB* 186, 57-73.

Schwartz MA and DeSimone DW. 2008. Cell adhesion receptors in mechanotransduction (2008). *Curr. Opin. Cell Biol.* 20, 551-556

Scott, J. S., A; den Elzen, N; Loureiro, J; Gertler, F; Yap; A. 2006. Ena/VASP proteins can regulate distinct modes of actin organization at cadherin-adhesive contacts. *MBoC* 17, 1085-1095.

Sellers, J. R. 1985. Mechanism of the phosphorylation-dependent regulation of smooth muscle heavy meromyosin. *J Biol Chem* 260, 15815-15819.

Sellers, J.R. 1991. Regulation of cytoplasmic and smooth muscle myosin. *Curr Opin Cell Biol.* 3, 98-104.

Sepich DS, Calmelet C, Kiskowski M, Solnica-Krezel L. 2005. Initiation of convergence and extension movements of lateral mesoderm during zebrafish gastrulation. *Dev. Dyn.* 234(2): 279-292

Shewan A, Maddugoda M, Kraemer A, Stehbens S, Verma S, Kovacs E, Yap A. 2005. Myosin 2 is a key Rho Kinase target necessary for the local concentration of E Cadherin at cell-cell contacts. *MBoC* 16: 4531-4542

Shih, J. and Keller, R. 1992a. Patterns of cell motility in the organizer and dorsal mesoderm of *Xenopus laevis*. *Development* 116, 915-930.

Shih, J. and Keller R. 1992b. Cell motility driving mediolateral intercalation in explants of Xenopus laevis. *Development* 116, 901-914.

Shih, J. and Keller, R. 1992c. The epithelium of the dorsal marginal zone of *Xenopus* has organizer properties. *Development* 116, 887-899.

Shindo, A. and Wallingford, J. B. 2014. PCP and septins compartmentalize cortical actomyosin to direct collective cell movement. *Science* 343, 649-652.

Simoes S, Blakenship J, Weitz O, Farrell D, Tamada M, Fernandez-Gonzalez R, Zallen J. 2010. Rho-kinase directs Bazooka/Par-3 planar polarity during *Drosophila* axis elongation. *Dev Cell* 19(3):377-388.

Sjoblom B, Salmazo A, Djinovic-Carugo K. 2008. Alpha-actinin structure and regulation. *Cell. Mol. Life Sci.* 65:2688-2701

Skoglund, P., Dzamba, B., Coffman, C. R., Harris, W. A. and Keller, R. 2006. *Xenopus* fibrillin is expressed in the organizer and is the earliest component of matrix at the developing notochord-somite boundary. *Dev Dyn* 235, 1974-1983.

Skoglund, P. and Keller, R. 2007. Xenopus fibrillin regulates directed convergence and extension. Developmental biology 301, 404-416.

Skoglund, P. and Keller, R. 2010. Integration of planar cell polarity and ECM signaling in elongation of the vertebrate body plan. *Curr. Opin Cell Biol*. 5, 589-596.

Skoglund, P., Rolo, A., Chen, X., Gumbiner, B. and Keller, R. 2008. Convergence and extension at gastrulation requires a myosin IIB dependent cortical actin network. *Development* 135: 2435-2444.

Smutny, M., Cox, H.L., Leerberg, J.M., Kovacs, E.M., Conti, M.A., Ferguson, C., Hamilton, N.A., Parton, R.G., Adelstein, R.S. and Yap, A.S., 2010. Myosin II isoforms identify distinct functional modules that support integrity of the epithelial zonula adherens. *Nature cell biology*, *12*(7): 696-702.

Solnica-Krezel, L. and Sepich, D. S. 2012. Gastrulation: making and shaping germ layers. *An. Rev. Cell Dev. Biol.* 28, 687-717.

Somlyo AP and Somlyo AV. 2003. Ca2+ sensitivity of smooth muscle and nonmuscle Myosin II: modulated by G proteins, kinases and myosin phosphatase. *Physiol. Rev.* 83 1325-1358

Somlyo AP and Somlyo AV. 2000 Signal transduction by G-Proteins, Rho-Kinase and protein phosphatase to smooth muscle and non-muscle Myosin II. *J Physiol*. 522:2 177-185

Stukenberg, P. T., Lustig, K. D., McGarry, T. J., King, R. W., Kuang, J. and Kirschner, M. W. 1997. Systematic identification of mitotic phosphoproteins. *Curr Biol* 7, 338-348.

Sulik K, Dehart D, Inagaki T, Carson J, Vrablic T, Gesteland K, Schoenwolf GC. (1994) Morphogenesis of the murine node and notochordal plate. *Dev. Dyn.* 201 (3): 260-278

Tahinci E and Symes K. 2003. Distinct functions of Rho and Rac are required for convergent extension during *Xenopus* gastrulation. *Dev. Biol.* 259 318-335

Taylor J, Adler PN. 2008. Cell rearrangement and cell division during the tissue level morphogenesis of evaginating *Drosophila* imaginal discs. *Dev. Biol* 313(2):739-751

Tepass U. 2009. FERM Proteins in Animal Morphogenesis. *Curr. Op. Gen. Dev.* 19 357-367

Townes, P.L. and Holtfreter, J., 1955. Directed movements and selective adhesion of embryonic amphibian cells. *J. Exp Zool*,*128*(1): 53-120.

Trinkaus JP. 1969. Cells into Organs. The Forces that Shape the Embryo. Prentice-Hall, Englewood Cliffs, N. J.

Trybus, K. M. 1989. Filamentous smooth muscle myosin is regulated by phosphorylation. *JCB* 109, 2887-2894.

Tsai F-C and Meyer T. 2012. Ca2+ Pulses control local cycles of lamellipodia retraction and adhesion along the front of migrating cells. *Curr. Biol*. 22 837-842.

Vasquez, C. G., Tworoger, M. and Martin, A. C. 2014. Dynamic myosin phosphorylation regulates contractile pulses and tissue integrity during epithelial morphogenesis. *JCB* 206, 435-450.

Vincente-Manzanares M, Zareno J, Whitmore L, Choi C, Horwitz A. 2007. Regulation of protrusion, adhesion dynamics, and polarity by myosins IIA and IIB in migrating cells. *JCB*. 176(5): 573-580

Vicente-Manzanares, M., Ma, X., Adelstein, R. S. and Horwitz, A. R. 2009. Non-muscle myosin II takes centre stage in cell adhesion and migration. *Nat Rev Mol Cell Biol.* 10, 778-790.

Wallingford, J., Goto, T., Keller, R. and Harland, R. 2002 Cloning and expression of *Xenopus* prickle, an orthologue of a *Drosophila* planar cell polarity gene. *Mech. Dev.* 116, 183-186.

Wallingford, J. B., Rowning, B. A., Vogeli, K. M., Rothbacher, U., Fraser, S. E. and Harland, R. M. 2000. Dishevelled controls cell polarity during *Xenopus* gastrulation. *Nature* 405, 81-85.

Wallraff E, Schleicher M, Modersitzki M, Rieger D, Isenberg G, Gerisch G. 1986. Selection of the *Dictyostelium* mutants defective in cytoskeletal proteins: use of an antibody that binds to the ends of α-actinin rods. *EMBO J* 5:1, 61-67.

Wang, A., Ma, X., Conti, M. A. and Adelstein, R. S. 2011. Distinct and redundant roles of the non-muscle myosin II isoforms and functional domains. *Biochemical Society transactions* 39, 1131-1135.

Warrick H and Spudich J. 1987. Myosin structure and function in cell motility. *Ann Rev. Cell Biol* 3 379-421

Wei C, Wang X, Chen M, Ouyang K, Song LS, Cheng H. 2009. Calcium flickers steer cell migration. *Nature* 457:901-905

Wei Y, Mikawa T. 2000. Formation of the avian primitive streak from spatially restricted blastoderm: evidence for polarized cell division in the elongating streak. *Development* 127: 87-96.

Welch MD. 1999. The world according to Arp: regulation of actin nucleation by the Arp2/3 complex. *Trends Cell Biol*.9 (11):423-427

Wendt, T., Taylor, D., Trybus, K. M. and Taylor, K. 2001. Three-dimensional image reconstruction of dephosphorylated smooth muscle heavy meromyosin reveals asymmetry in the interaction between myosin heads and placement of subfragment 2. *PNAS* 98, 4361-4366.

Williams, M., Yen, W., Lu, X. and Sutherland, A. 2014. Distinct apical and basolateral mechanisms drive planar cell polarity-dependent convergent extension of the mouse neural plate. *Dev Cell* 29, 34-46.

Williams-Masson E, Heid P, Lavin C, Hardin J. 1998. The cellular mechanism of epithelial rearrangement during morphogenesis of the *Caenorhabditis elegans* dorsal hypodermis. *Dev Biol* 204(1):263-276

Wilson, P. and Keller, R. 1991. Cell rearrangement during gastrulation of *Xenopus*: Direct observation of cultured explants. *Development* 112, 289-300.

Wilson, P., Oster, G. and Keller, R. E. 1989. Cell rearrangement and segmentation in *Xenopus*: Direct observation of cultured explants. *Development* 105, 155-166.

Winklbauer, R. and Keller, R. 1996. Fibronectin, mesoderm migration, and gastrulation in *Xenopus*. Develop. Biol., 177, 413, 426

Yamashiro S, Totsukawa G, Yamakita Y, Sasaki Y, Madaule P, Ishizaki T, Narumiya S, Matsumura F. 2003. Citron Kinase, a Rho-dependent kinase, induces di phosphorylation of regulatory light chain of myosin II. *MBoC* 14:1745-1756

Yap A, Brieher W, Gumbiner B. 1997. Molecular and functional analysis of cadherin based adherens junctions. *Ann. Rev. Cell Dev. Biol.* 13:119-146.

Yen WW, Williams M, Periasamy A, Conaway M, Burdsal C, Keller R, Lu X, Sutherland A. 2009. PTK7 is essential for polarized cell motility and convergent extension during mouse gastrulation. *Development* 136:2039-2048

Yin, C., Kiskowski, M., Pouille, P.A., Farge, E. and Solnica-Krezel, L., 2008. Cooperation of polarized cell intercalations drives convergence and extension of presomitic mesoderm during zebrafish gastrulation. *JCB, 180*(1): 221-232.

Zhong Y, Brieher WM, Gumbiner BM. 1999. Analysis of C-Cadherin regulation during tissue morphogenesis with an activating antibody. *JCB* 144(2): 351- 359.

Zhou, J., Kim, H. Y. and Davidson, L. A. 2009. Actomyosin stiffens the vertebrate embryo during crucial stages of elongation and neural tube closure. *Development* 136, 677-688.

Zhou, J., Pal, S., Maiti, S. and Davidson, L. A. 2015. Force production and mechanical accommodation during convergent extension. *Development* 142, 692-701.